

NORTHWESTERN UNIVERISTY

Environmental Interfaces Studied by Second Harmonic Generation

A DISSERTATION

SUBMITTED TO THE GRADUATE SCHOOL
IN PARTIAL FULFILLMENT OF THE REQUIREMENTS

for the degree

DOCTOR OF PHILOSOPHY

Field of Physical Chemistry

by

Christopher Konek

EVANSTON, ILLINOIS

December 2007

© 2007 Christopher Thomas Konek
All rights reserved

Abstract

Interfaces and surfaces are ubiquitous in the environment. Heterogeneous binding events and reactions control the transport and speciation of dissolved pollutants in groundwater. Many heterogeneous processes occur at mineral oxide/water interfaces, and can be controlled either by the mineral oxide, or organic molecules bound to the surface. The prevalent natural organic molecules humic and fulvic acid contain carboxylic acid functional groups, which can chelate aqueous metal ions - a critical step in controlling the phase of metals in the environment. This work uses the nonlinear optical technique second harmonic generation (SHG) to study two common pollutants and organic adlayers at the interface between water and the most abundant mineral oxide, silica.

SHG laser spectroscopy is well-suited for studying environmentally relevant interfaces. SHG allows for highly sensitive measurements under environmentally relevant temperatures and solute concentrations. By simultaneously employing complimentary techniques to probe the bulk, bulk concentration and surface coverage are correlated, allowing for the determination of kinetic, thermodynamic and structural information.

In this work, SHG has been used to study the interaction of the agricultural antibiotic morantel with the silica/water interface. Isotherm measurements result in a ΔG_{ads} of -42(3) kJ/mol at pH 7, consistent with a hydrogen-bonding interaction. Real-time tracking of morantel binding shows that the events are fully reversible, consistent with its high mobility in silica-rich soil environments.

Additionally, SHG studies were carried out to characterize a carboxylic acid-functionalized silica/water interface between pH 2 and 12. Two acid-base equilibria are observed, and the high sensitivity of SHG to interfacial potential, surface charge density, and

surface free energy density was demonstrated. The experimental methodology provides quantitative thermodynamic information necessary for understanding how solvated species interact with organic adlayers.

SHG was used to follow the interaction of dissolved Mn(II) with carboxylic acid groups at a silica/water interface. Similarly to the morantel experiments, an isotherm was constructed showing a ΔG_{ads} of -27.8(3) kJ/mol at pH 7 and fully reversible binding events. This work demonstrates the ability of SHG to probe pollutants that do not have an electronic transition in the UV-vis.

Professor Franz M. Geiger

Research Advisor

Acknowledgements

I would like to thank my advisor, Professor Franz Geiger, who has been a willing and able mentor over the years. In addition to teaching me how to be a good laboratory scientist, he has provided many opportunities for me to expand my skill set and interact with other scientists at conferences, meetings and symposia.

I would like to thank my committee members, Professor Tamar Seideman, Professor Eric Weitz and Professor James Ibers for helpful and constructive critiques of my research during my oral exams. Professor SonBinh Nguyen and Professor Jean-Francois Gaillard provided insight and helpful discussions our collaborations.

The staff in the department office and the graduate assistants that have worked in the chemistry department over the course of my time here have lent invaluable assistance, especially Jim Lord, Beth Ludwig.

I must also express my appreciation to the people in the Geiger Group – Amanda, Andrea, Michael, Catherine, Faith, Grace, Patrick, Juli, Dave, Hind, Avi, Jessica and Jen with whom I have worked over the years. Your patience and understanding has been invaluable, and I appreciate all the time you've spent critiquing my research, writing and presentations. Special thanks to Catherine, who has spent a large amount of her time proofreading my writing, and to Michael, with whom I have had many fruitful collaborations.

I would like to thank the people at Cornell who influenced me and shared their love of chemistry with me: Prof. Stephen Lee and Prof. Paullette Clancy, who had very important input on my decision to pursue research in chemistry, and Professor David Collum and Dr. Anne J. McNeil, who led an amazing organic chemistry class. Additionally, Dr. Joshua Schmidt and Dr. Daniel Fredrickson were great coworkers who gave me very good advice on graduate school.

Lastly, I would like to thank my friends and family – without your support and understanding, this would not have been possible. Thanks.

To Jill

Table of Contents

Abstract		3
Acknowledgements		5
List of Figures		12
List of Tables		19
Chapter 1	Introduction to Environmental Interfaces in Geochemistry	20
1.1	Introduction to Environmental Interfaces	21
1.2	Common Methods for Studying Environmental Interfaces	22
1.3	Goals and Organization	24
Chapter 2	Introduction to Second Harmonic Generation	26
2.1	Second Harmonic Generation	27
2.1.1	Second harmonic generation theory	27
2.1.2	Application of Second Harmonic Generation to Environmental Systems	31
2.2	Laser and Detection System	33
2.3	Flow System and Experimental Setup	34
2.4	Experimental Protocols and Methods	37
2.4.1	Charge screening experiments	37
2.4.2	Titration of the interface	38
2.4.2.1	Preparing the solutions	38

2.4.2.2	Data collection	39
2.4.2.3	Exposure of the organic adlayers to basic conditions	40
2.5	Summary	42
Chapter 3	Characterization of Carboxylic Acid Groups Tethered to Silica	43
3.1	Introduction to Organics in the Environment	44
3.2	Model Systems	47
3.3	Deposition of Organic Adlayers	51
3.4	Contact Angle Measurements	53
3.5	Atomic Force Microscopy	53
3.6	Ellipsometry	55
3.7	Time-of-Flight Secondary Ion Mass Spectrometry	55
3.8	Vibrational Sum Frequency Generation Experiments	57
3.9	Conclusions	59
Chapter 4	Acid-Base Chemistry at the Carboxylic Acid-Functionalized Silica/Water Interface	60
4.1	Carboxylic Acids in the Environment	61
4.2	Interfacial Charge Screening Experiments	63
4.3	Titration of Carboxylic Acids at the Silica/Water Interface	67
4.4	Full Thermodynamic State Information	70
4.5	Environmental Implications and Conclusions	76
Chapter 5	Manganese Interacting with Carboxylic Acid Groups at the	80

	Silica/Water Interface	
5.1	Manganese in the Environment	81
5.2	Manganese Mobility	82
5.3	Manganese Isotherm	85
5.4	Interfacial Charge Screening Experiment	87
5.5	Conclusions	91
Chapter 6	The Agricultural Antibiotic Morantel at the Silica/Water Interface	92
	Interface	
6.1	Morantel in the Environment	93
6.2	UV-vis Spectroscopy	96
6.3	Second Harmonic Generation Spectroscopy	99
6.4	Mobility	100
6.5	Adsorption Isotherm	102
6.6	Orientation Studies	104
6.7	Environmental Implications	108
6.8	Conclusion	109
Chapter 7	Conclusions and Future Directions	110
7.1	Conclusions	111
7.2	Environmental Implications: Carboxylic Acids at the Silica/Water Interface	111
7.3	Environmental Implications: Manganese Interacting with Carboxylic Acids	113

7.4	Environmental Implications: Morantel	113
7.5	Future Directions	114
References.....		119
About the Author.....		142

List of Figures

Chapter 2

Figure 2.1 28

Energy level diagram showing the second harmonic generation process. Two photons at frequency ω are converted into a single photon with twice the frequency via virtual states (dotted lines). If one of the virtual states is close in energy to an electronic transition in the molecule (solid line), resonance enhancement occurs.

Figure 2.2 35

Diagram of the custom-built Teflon flow cell used in these experiments. This diagram indicates the basic measurements needed to machine the cell, more detail can be found in the Geiger Group Machine Shop lab notebook.

Figure 2.3 36

Setup for the second harmonic generation experiments. See text for details.

Figure 2.4 41

Second harmonic signal as a function of time for a carboxylic acid-functionalized silica/water water interface. Bulk solution is at pH 12. Note the instability in the signal which occurs around 100 minutes into the experiment.

Chapter 3

Figure 3.1 45

A model structure for humic acid, from reference 6. Note the prevalence of the carboxylic acid functional group.

Figure 3.2 46

Humic acid adsorption trace at the silica/water interface. Humic acid concentration is 26 mg/L and the solution pH is 7.53.

Figure 3.3 49

A schematic of the top piece of the custom-built Teflon reaction chamber. More detail can be found in the Geiger group machine shop lab notebook.

Figure 3.4 50

A schematic of the bottom piece of the custom-built Teflon reaction chamber. More detail can be found in the Geiger group machine shop lab notebook.

Figure 3.5 52

A schematic representing the deposition process. The trichlorosilane molecule in a 1%v/v solution with toluene is deposited in a custom-built Teflon chamber for one hour. After excessive washing with dry toluene, toluene and methanol, the sample is annealed for an hour to promote cross-linking at the surface. Finally, the hydrolysis of the methyl ester to the carboxylic acid is performed at 85° C in 2.4 M HCl for two hours.

Figure 3.6	14
	54

(a) Phase mode atomic force microscopy image of the organic adlayer deposited on a flat silicon wafer with a native oxide layer. (b) A line section, taken along the black line in part (a) of the figure, shows that the drop in height from the adlayer to a hole is a drop of about 10 angstroms, which is consistent with a well-formed and slightly tilted 10 carbon chain at the surface.

Figure 3.7	56
-------------------------	----

Time of flight secondary ion mass spectrometry images. (a) shows an image of fluorinated methyl ester groups, where lighter colors indicate a higher density of fluorine signal (b) shows a similar sample after hydrolysis, which indicates that there is a high degree of conversion of the fluorinated ester to the carboxylic acid.

Figure 3.8	58
-------------------------	----

Sum frequency generation spectra indicate that upon hydrolysis, the CH_3 symmetric stretch associated with the methyl ester group disappears, indicating a high degree of conversion from the methyl ester to the carboxylic acid.

Chapter 4

Figure 4.1	66
-------------------------	----

Second harmonic signal as a function of bulk ion concentration in solution flowing across the interface at pH 6.5. The solid line is a fit to the data based on the Gouy-Chapman model. The error bar is representative of the uncertainty in all data points and is taken from the standard

deviation of 300 data points. Inset: Ion concentration dependence experiment performed for pH 11.2.

Figure 4.2 68

Second harmonic E-field from carboxylic acid functionalized silica as a function of the bulk solution pH flowing across the interface. The fit to the data is shown in black lines. Data shown is average of three separate runs, and the error bars show one standard deviation in the raw data, propagated through the data analysis.

Figure 4.3 71

Absolute number of deprotonated carboxylic acid groups as a function of bulk solution pH. Note the logarithmic scale on the y-axis.

Figure 4.4 73

Interfacial potential as a function of bulk pH. Note the logarithmic scale on the y-axis.

Figure 4.5 75

Surface free energy density as a function of bulk pH as calculated from the Lippmann equation. Note the logarithmic scale on the y-axis.

Figure 4.6 77

A schematic showing carboxylic acid groups involved in a hydrogen bonding network, which are thought to be responsible for the more basic pK_a value, and carboxylic acid groups not

involved in a hydrogen bonding network, thought to be responsible for the more acidic pK_a value.

Figure 4.7 79

A schematic showing that for a constant bulk pH, a mineral oxide particle coated with an organic adlayer may contain some regimes containing protonated carboxylic acids and other regimes containing deprotonated carboxylic acid groups.

Chapter 5

Figure 5.1 84

SHG E-field as a function of time for a carboxylic acid-functionalized fused quartz/water interface exposed to manganese (II) solution at pH 7. The horizontal bars show the time periods for manganese and water flow.

Figure 5.2 86

SHG E-field obtained from a carboxylic acid-functionalized fused quartz/water interface as a function of manganese concentration in bulk solution at pH 7. The solid line is a fit of data based on the Langmuir-modified Gouy-Chapman model.

Figure 5.3 90

SHG E-field from a carboxylic acid-functionalized fused quartz/water interface as exposed to 1.0 mM manganese (II) solution as a function of increasing NaCl concentration. The solid line is a fit of the Gouy-Chapman model to the data.

Chapter 6**Figure 6.1** 94

UV-vis spectra of morantel at pH 7 and increasing morantel concentration. Insets: Absorbance at 318 nm as a function of morantel concentration, structure of morantel.

Figure 6.2 98

SHG spectrum of morantel adsorbed at the silica/water interface maintained at pH 7 (filled circles, right axis) and bulk UV-vis spectrum at the same pH (solid line, left axis).

Figure 6.3 101

(a) SHG E-field versus time trace recorded while turning the morantel flow on and off while flowing background aqueous solution. The morantel concentrations are given in italics. The horizontal dashed lines indicate the baseline level. (b) UV-vis absorbance of morantel at concentrations corresponding to the on-off experiments.

Figure 6.4 103

Isotherm for morantel adsorption at the silica/water interface maintained at pH 7 and room temperature (filled circles). The solid line is a fit to the Langmuir adsorption model according to $\theta = KC / (1 + KC)$, where θ is the relative surface coverage, K is the equilibrium adsorption constant, and C is the morantel concentration in solution.

Figure 6.5. 105

SHG signal intensity as a function of polarizer analyzer angle in the presence of a

saturated surface of adsorbed morantel at the silica/water interface. The filled circles represent the SHG polarization response while probing with p-polarized input light, and the empty circles represent the SHG polarization response while probing with 45-polarized input light.

Figure 6.6 107

A polar graph, with the D parameter plotted with the molecular tilt angle. The black line shows the calculated value of D for morantel at the silica/water interface (0.528). The grey curves are possible values of D for each calculated distribution.

Figure 7.1 116

An experimental setup for performing second harmonic generation experiments at opaque oxide/water interfaces.

List of Tables

Table 4.1	62
------------------------	----

Select results from the literature of pK_a values for carboxylic acid groups at interfaces.

Chapter 1

Introduction to Environmental Interfaces in Geochemistry

Portions of this chapter are reproduced in part with permission from:

Konek C.T.; Illg K.D.; Al-Abadleh H.A.; Voges A.B.; Yin G.; Musorrafiti M.J.; Schmidt C.M.; Geiger F.M. “Nonlinear optical studies of the agricultural antibiotic morantel interacting with silica/water interfaces.” *Journal of the American Chemical Society*, **2005**, 127 (45), 15771-15777. Copyright 2005, American Chemical Society.

Konek C.T.; Musorrafiti M.J.; Voges A.B.; Geiger F.M. “Tracking the interaction of transition metal ions with environmental interfaces using second harmonic generation.” *Adsorption of Metals by Geomedia II* Ed. Mark Barnett and Douglass Kent. Elsevier series Developments in Earth and Environmental Sciences, **2007**, Copyright 2007, Elsevier.

Konek C.T.; Musorrafiti M.J.; Al-Abadleh H.A.; Bertin P.A.; Nguyen S.T.; Geiger F.M. “Interfacial acidities, charge densities, potentials, and energies of carboxylic acid-functionalized silica/water interfaces determined by second harmonic generation.” *Journal of the American Chemical Society*, **2004**, 126 (38), 11754-11755. Copyright 2004, American Chemical Society.

1. Introduction to Environmental Interfaces

Surfaces and interfaces are ubiquitous in the environment,^{1,2} and range from liquid/solid interfaces in soil to solid/gas interfaces associated with atmospheric particulate matter. The bioavailability, speciation, and cycling of many environmentally important species are dominated or controlled exclusively by heterogeneous processes. In groundwater, the transport and mobility of dissolved pollutants are controlled by pollutant binding events and reactions that occur at mineral oxide/water interfaces. Mineral oxide surfaces, in turn, are commonly coated or partially coated with complex organic molecules such as humic acids, which can further mediate pollutant binding. A molecular understanding of pollutant transport and fate in such complex geochemical environments, therefore, must be informed by surface studies of (1) properties of organic adlayers at mineral oxide/water (2) the interaction of pollutants with organic adlayers at mineral oxide/water interfaces and (3) the interaction of pollutants with mineral oxide/water interfaces.

While chemical binding and speciation in soils are generally governed by interfacial mechanisms, chemical transport models commonly rely on pollutant-to-soil binding constants that are derived from bulk measurements.³⁻⁷ Incorporating surface-specific binding measurements into these models is expected to provide increased accuracy when predicting pollutant transport. By developing a molecular-level description of pollutant binding events to interfaces, and of the environmental interfaces themselves, we can improve the quality of computer simulations that model geochemically important processes such as pore diffusion, oxidation-reduction reactions, and bacterial metabolism.

The work presented in this thesis addresses three scientific questions:

(1) How do acid-base properties of organic molecules change when tethered to an interface?

(2) How do aqueous species interact with the silica/water interface? and

(3) How do aqueous species interact with organic molecules at the silica/water interface?

Specifically, by investigating three different chemical systems, we are in the unique position to significantly increase the level of scientific understanding regarding the factors that control environmental pollutant transport. The motivation for studying each of these systems will be discussed in more detail in individual chapters; however, it should be clear that together, the systems studied in this work combine critical elements of complex environmental interfaces. We first studied carboxylic-acid terminated organic adlayers at the silica/water interface. For this system, we obtained the full thermodynamic state information, and quantitatively determined how the pK_a values of our carboxylic acids differ from aqueous solution when the acids are tethered to the silica/water interface. Next, we studied the dissolved metal cation, Mn^{2+} , interacting with the carboxylic-acid functionalized interface, again obtaining quantitative thermodynamic information for the binding events. Finally, we studied the agricultural antibiotic morantel interacting with the silica/water interface, obtained thermodynamic, spectroscopic, and structural information about the interaction and linked these results to the emerging threat of antibiotic resistance.

1.2 Common Methods for Studying Environmental Interfaces

The critical role that interfaces play in the environment is well-known, and a variety of techniques have been used to study environmentally relevant heterogeneous processes. The techniques listed below can provide complimentary information to one another and continually

improve our understanding of pollutant binding and transport in the environment. While this list is far from complete, it summarizes the optical and mechanical probes that are commonly used in geochemical laboratory studies of soil samples as well as model interfaces.

X-ray based techniques such as X-ray absorption near-edge structure (XANES) and extended X-ray absorption fine structure (EXAFS) are extremely useful for identifying and characterizing metal-containing adsorbates.⁸⁻¹⁵ By applying physical and chemical models to interpret the data, these techniques can determine atomic distances relevant to the surface complexes formed during adsorption. This information can generally be used to determine whether the adsorption mechanism involves an inner-sphere or outer-sphere complex, or if the complex configuration is monodentate or bidentate or both.

Recent advances in surface spectroscopy have led to the development of a number of other techniques for studying environmental interfaces. These techniques often use electrons in techniques such as low-energy electron diffraction (LEED) and high resolution electron energy loss spectroscopy (HREELS)^{16,17} to obtain structural information and surface morphology. Alternatively, visible and infrared photon sources are used in techniques such as ellipsometry, interferometry, Raman spectroscopy,^{18,19} and attenuated total reflection Fourier transform infrared spectroscopy (ATR-FTIR)²⁰⁻²² to spectroscopically probe the interface. Additionally, imaging techniques such as atomic force microscopy (AFM) and transmission electron microscopy (TEM)^{21,23,24} have been used to characterize interfaces and obtain kinetic information for binding processes. A thorough review of surface science techniques is available in appropriate textbooks.^{23,25,26}

It is important to note that any technique applied to environmental systems will have certain limitations. For example, many of the above mentioned spectroscopic techniques are

significantly curtailed by their inability to probe aqueous/solid interfaces in real time while they are exposed to environmentally representative solute concentrations. This limitation is especially important when considering the nonlinear relationship between aqueous phase concentration and surface coverage^{1,7,25,27,28} for small aqueous phase concentrations,^{27,28} which makes the extrapolation of data obtained with high bulk concentrations to environmentally representative concentrations problematic. Some techniques may be able to probe environmentally relevant concentrations, but require long signal integration times to do so, which limits their ability to access information in real time.⁸ Other limitations may include the need for expensive substrates or extensive chemical and physical models for data interpretation. However, this work contributes to the continual efforts of the environmental science community, while improving techniques and methods, to bridge the gap between model systems used in laboratories and environmentally relevant conditions, an effort to which this work contributes.

1.3 Goals and Organization

This work demonstrates the utility of second harmonic generation (SHG) for studying environmentally relevant interfaces in real time, with surface specificity, under dynamic flow conditions, and at environmentally representative analyte concentrations. The goal of these studies is to obtain quantitative molecular-level insight into the processes which control pollutant binding and transport. We use SHG to obtain quantitative thermodynamic state information for carboxylic-acid terminated organic adlayers at the silica/water interface, and obtain thermodynamic and spectroscopic information for pollutants binding to bare silica and to the carboxylic-acid terminated organic adlayers.

Chapter 2 discusses the unique applicability of second harmonic generation to environmental interfaces, outlines experimental protocols for performing the experiments detailed in subsequent chapters, and gives an overview of the mathematical framework behind the second harmonic generation techniques exploited in this work. Chapter 3 outlines the characterization of the organic adlayers, demonstrating that the deposition of the organic adlayer was carried out with a high degree of surface coverage and that the hydrolysis reaction results in a high degree of conversion to the carboxylic acid group. Surface titration and charge screening experiments for the carboxylic acid functionalized silica/water interface are described in Chapter 4. Chapter 4 also includes a discussion of the quantitative determination of interfacial potential and the use of the Lippmann equation to determine the interfacial free energy density. Chapter 5 incorporates the binding of manganese to the carboxylic acid functionalized silica/water interface described in the Chapter 4. Chapter 5 details the determination of the free energy of adsorption of manganese, and the use of the $\chi^{(3)}$ technique to obtain an absolute surface coverage of manganese ions. Chapter 6 focuses on the agricultural antibiotic morantel binding to the silica/water interface, and discusses orientation studies and free energy of adsorption. Chapter 7 will conclude with environmental implications and possible future directions for this work.

Chapter 2

Introduction to Second Harmonic Generation

Portions of this chapter are reproduced in part with permission from:

Konek C.T.; Illg K.D.; Al-Abadleh H.A.; Voges A.B.; Yin G.; Musorrafiti M.J.; Schmidt C.M.; Geiger F.M. “Nonlinear optical studies of the agricultural antibiotic morantel interacting with silica/water interfaces.” *Journal of the American Chemical Society*, **2005**, 127 (45), 15771-15777. Copyright 2005, American Chemical Society.

2.1 Second Harmonic Generation

This work primarily uses the nonlinear optical technique second harmonic generation (SHG) to probe environmentally important interfaces. However, environmental systems are complex and are best understood by the application of many complimentary techniques. In this work, we use SHG in combination with UV-vis spectroscopy, inductively coupled plasma mass spectrometry (ICP-MS), and conductance measurements to probe the silica/water interface. Combining the surface-specific technique second harmonic generation with other techniques well-suited to studying the bulk allows us to correlate bulk and surface responses. This in turn allows us to obtain thermodynamic and spectroscopic information. Additionally, we employed several surface characterization techniques to understand and characterize the organic adlayers, which will be discussed in more detail in Chapter 3. However, second harmonic generation has unique advantages which make it suitable for studying environmental systems. These advantages, and some of the underlying theory for second harmonic generation, are discussed below.

2.1.1 Second harmonic generation theory

In general, the nonlinear response is given by the nonlinear terms of the perturbation expansion of the polarizability, P , where:¹⁻⁴

$$P = \chi^{(1)}E + \chi^{(2)}EE + \chi^{(3)}EEE + \dots \quad 2.1$$

where $\chi^{(i)}$ is the i^{th} order susceptibility, and E is an electromagnetic field (E-field). The form of Eq. 2.1 is similar to that of a Taylor series expansion, where the linear term ($\chi^{(1)}$) is largest, and the response due to each successive higher-order susceptibility term decreases by orders of magnitude. In second harmonic generation, two photons at frequency ω are converted into a

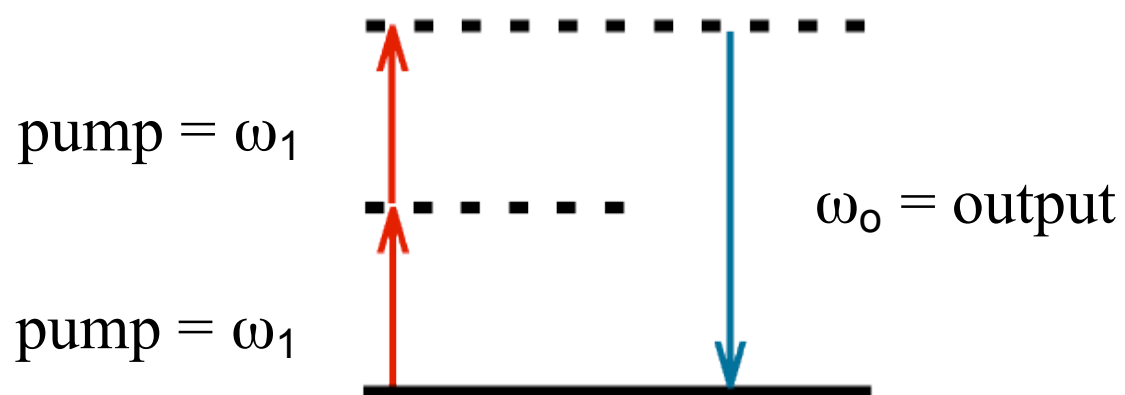


Figure 2.1

single photon at the second harmonic frequency (2ω) (see Fig. 2.1), proportional to the second order nonlinear susceptibility, $\chi^{(2)}$. Therefore, for the case of second harmonic generation, the governing equation is:

$$E_{2\omega} = \sqrt{I_{2\omega}} \propto \chi^{(2)} E_{\omega} E_{\omega} \quad 2.2$$

where $I_{2\omega}$ is the intensity of photons produced at the second harmonic E-field, $\chi^{(2)}$ is the second order susceptibility, and $E_{2\omega}$ is the E-field produced at the second harmonic wavelength. By definition, the E-field is equal to the square root of the intensity of the signal.¹ The $\chi^{(2)}$ tensor contains structural information, similarly to the NMR chemical shift tensor,¹ which can be probed by changing the polarization of the input laser light. The fact that second harmonic generation is proportional to the $\chi^{(2)}$ tensor gives rise to its surface-specificity. It can be shown through symmetry arguments¹ that second harmonic E-fields are generated at locations where centrosymmetry is broken, such as the interface between two bulk isotropic materials. It is important to note that this statement strictly holds only under the electric dipole approximation, which is an appropriate assumption for the insulators studied in this work.

Two classes of surface SHG exist: non-resonant SHG and resonantly enhanced SHG, and both are utilized in this work. Non-resonant SHG is produced when the probe wavelength is far from any electronic resonances that may exist at the interface. Resonantly enhanced SHG, in contrast, occurs when either the probe frequency or the second harmonic frequency matches an electronic transition at the interface. Fundamentally, however, both the non-resonant and resonant effects stem from a single theoretical framework.

As shown in Eq. 2.2, the SHG E-field for either the resonant or non-resonant case is proportional to the second order susceptibility, $\chi^{(2)}$. The second order susceptibility can be

written in terms of a resonant contribution ($\chi^{(2)}_R$) and a non-resonant contribution ($\chi^{(2)}_{NR}$):

$$I_{2\omega} \propto |\chi^{(2)}_{NR} + \chi^{(2)}_R|^2 \quad 2.3$$

In resonantly enhanced SHG, the second order susceptibility can be written in terms of the number of adsorbed species and the molecular hyperpolarizability, β , averaged over all orientations:⁵⁻⁷

$$E_{2\omega} \propto \chi^{(2)} = N_{ads} \langle \beta \rangle \quad 2.4$$

where N_{ads} is the number of adsorbed molecules, and β is the second order molecular hyperpolarizability which contains the resonance enhancement (vide infra), and is the molecular analogue of the macroscopic susceptibility, $\chi^{(2)}$. The second order molecular hyperpolarizability, β , can be expressed as follows:⁸

$$\beta^{(2)}_{ijk} = -\frac{4\pi^2 e^3}{h^2} \sum_{b,c} \frac{\langle a|u_i|b\rangle \langle b|u_j|c\rangle \langle c|u_k|a\rangle}{(\omega - \omega_{ba} + i\Gamma_{ba})(2\omega - \omega_{ca} + i\Gamma_{ca})} + \dots \quad 2.5$$

where μ is the electric dipole transition moment, a, b and c represent the ground, intermediate and final states, respectively (Figure 2.1), h is Plank's constant, ω_{xy} is the frequency associated with the xy electronic transition in the probe molecule, ω is the probe wavelength, and Γ is a damping coefficient associated with the pertinent electronic transition. By matching either the input wavelength (ω) or the second harmonic wavelength (2ω) with the frequency of an electronic transition in the molecule (ω_{ba} or ω_{ca}), the denominator of the fraction approaches zero, leading to an increase in β which leads to an increase in second harmonic signal. As demonstrated by Eq. 2.4, increases in resonantly enhanced SHG can also stem from an increase in the number of adsorbates excited. Resonantly enhanced second harmonic generation directly

tracks the relative amount of an adsorbed species at the interface, and will be applied and discussed in detail in Chapter 6.

In contrast to resonantly enhanced second harmonic generation which requires an electronic transition in the UV-vis to be present at the interface, non-resonant second harmonic signal is inherently present due to the distance-dependent change in the dielectric constant when crossing the interface separating two centrosymmetric bulk materials.^{1,2} Non-resonant second harmonic signals can also be produced from the interaction of two incident photons with a static electric field generating an interfacial potential, Φ , and nonresonant second harmonic generation has therefore been exploited in the past to study charged interfaces.^{9,10} The $\chi^{(3)}$ technique, developed by Eisenthal and coworkers,^{10,11} can be used to directly sample the interfacial potential via a third order term that also produces signal at the second harmonic through the interaction of two oscillating fields with a static field:

$$E_{2\omega} \propto \chi^{(2)} E_{\omega} E_{\omega} + \chi^{(3)} E_{\omega} E_{\omega} \Phi. \quad 2.6$$

SHG can therefore be used to directly track a surface event that produces a change in potential (Φ), such as an acid-base reaction, or bulk ions screening the surface potential. Such applications of nonresonant second harmonic generation to environmentally relevant interfaces will be discussed and applied in Chapter 4 and Chapter 5.

2.1.2 Application of Second Harmonic Generation to Environmental Systems

Environmental systems are complex and pose a host of experimental challenges. Environmentally relevant aqueous pollutant concentrations are generally on the order of micromolar to millimolar, and it can be difficult to study analytes in these concentration regimes. It is important to note that extrapolation of laboratory data at high concentrations to the low

environmentally relevant concentration regime may ignore processes which only occur under low-concentration conditions. In addition, buried interfaces, such as water/solid interfaces, control many of the processes that determine the transport, speciation, and ultimate fate of pollutants in geochemistry. When using a model system in a laboratory, it is important to mimic environmental flow conditions to track interactions in real time.

A surface specific technique such as second harmonic generation (SHG) can be used to address many of the challenges listed above. SHG allows data collection in situ and in real time,¹²⁻¹⁴ and is sensitive enough to probe the interactions between interfaces and analytes at environmentally relevant concentrations.^{15,16} Our data can therefore be used to extract environmentally important thermodynamic, kinetic, and structural information under environmentally relevant conditions. Additionally, our isotherm measurements can provide parameters which can be incorporated into pollutant transport models used by the Environmental Protection Agency (EPA).

Since SHG is a surface-specific technique, it directly probes species adsorbed at the interface without the need for extensive chemical or physical models. SHG additionally allows us to probe buried interfaces, as long as one of the two materials is transparent to both the fundamental and second harmonic wavelength. Additionally, SHG is a non-invasive probe for performing studies in real time and in situ. By collecting photons with a gated single photon counter, kinetic information can be extracted from the system for timescales on the order of a second unless one carries out pump-probe experiments for ultrafast studies.

SHG additionally can be used to probe a wide variety of systems by exploiting intrinsic molecular labels. SHG can be used to track the interfacial potential,^{10,17-20} analytes with ligand-to-metal charge transfer (LMCT) electronic transitions,^{16,21,22} charge transfer to solvent (CTTS)

electronic transitions,²³⁻²⁵ and electronic transitions based on conjugated systems of carbons, including π - π^* transitions²⁶⁻²⁸ and n- π^* transitions.¹⁵ The flexibility of SHG provides a means of studying a wide variety of environmental pollutants with high sensitivity, molecular specificity and under environmentally relevant conditions.

2.2 Laser and Detection System

The laser system used in the SHG work presented here consists of a regeneratively amplified Ti:sapphire laser system (1 kHz, 120 fsec, 1 W, Hurricane, Spectra Physics) pumping an optical parametric amplifier (OPA-CF, Spectra Physics). The full laser system has been described previously.^{16,21,29-33} The OPA contains two β -barium borate (BBO) crystals in an arrangement which enables the laser wavelength to be easily tuned between 550 nm and 800 nm. The output from the Ti:sapphire Hurricane system at 800 nm and 1 W is passed through the first BBO crystal, which generates a signal beam between 1.1 and 1.6 μm and an idler beam between 1.6 and 2.6 μm . The signal beam is then passed through a second BBO crystal which doubles the frequency to the wavelength used in the experiment. Any other wavelengths produced in the OPA are rejected using the appropriate filters and polarizers.

The laser beam is focused onto the aqueous/solid interface at an angle near total internal reflection (60°) to maximize the signal produced at the interface. To avoid sample damage, we typically set the power to less than 1 μJoule in these experiments and regularly verify both the quadratic power dependence of the SHG signal and its proper spectral response. The full width half max of the second harmonic signal was approximately 3 nm, as determined by scanning the wavelength selected by the monochromator while keeping the probe wavelength and the second harmonic center frequency constant. The laser beam spot size at the interface is calculated to be

approximately 50 μm in diameter for the focusing lens used in this work ($D=25.4$ mm, $f=100$ mm). The fundamental laser light is recollimated and the beam is rejected using appropriate filters (Kopp Glass #9863 and #5840). The second harmonic signal is guided through a monochromator (Monospec, TVC) into a photon multiplier tube (Hamamatsu, 0.5 dark counts per second). Photons are counted using a gated Stanford Research Systems photon counter (SRS400). Typical signal intensities are on the order of 2-200 counts per second. We observe a specular reflection from the substrate, indicating a surface roughness below $\lambda/2$, or approximately 300 nm, for the studies described in this work.

2.3 Flow System and Experimental Setup

The experimental setup is shown in Figure 2.2. As in the setup described in the literature,^{16,21} a silica hemispherical lens (ISP optics) is placed on top of a custom-built Teflon flow cell. A seal between the lens and the flow cell is created by using a clamp to keep pressure on a Viton O-ring. The solutions are held in reservoirs until they are pumped into the Teflon flow cell through Tygon tubing at rates ranging from 1 to 5 mL/second. A dual-pump setup, coupled with dual Teflon on/off valves, allows us to quickly switch between flowing pure water and an aqueous pollutant solution. Proper mixing is ensured by combining the two solutions in approximately 1 foot of tubing prior to entering the flow cell. The solution subsequently flows out of the Teflon flow cell to the waste container. By employing complimentary techniques such as UV-vis or ICP-MS to probe the bulk, bulk concentrations are measured and correlated to pollutant surface coverage as measured by SHG. For pollutants with an accessible UV-vis transition, the effluent solution from the flow cell is passed through a quartz cuvette, where UV-vis measurements are taken by an in-line flow cell setup (OceanOpticsUSB4000). For pollutants

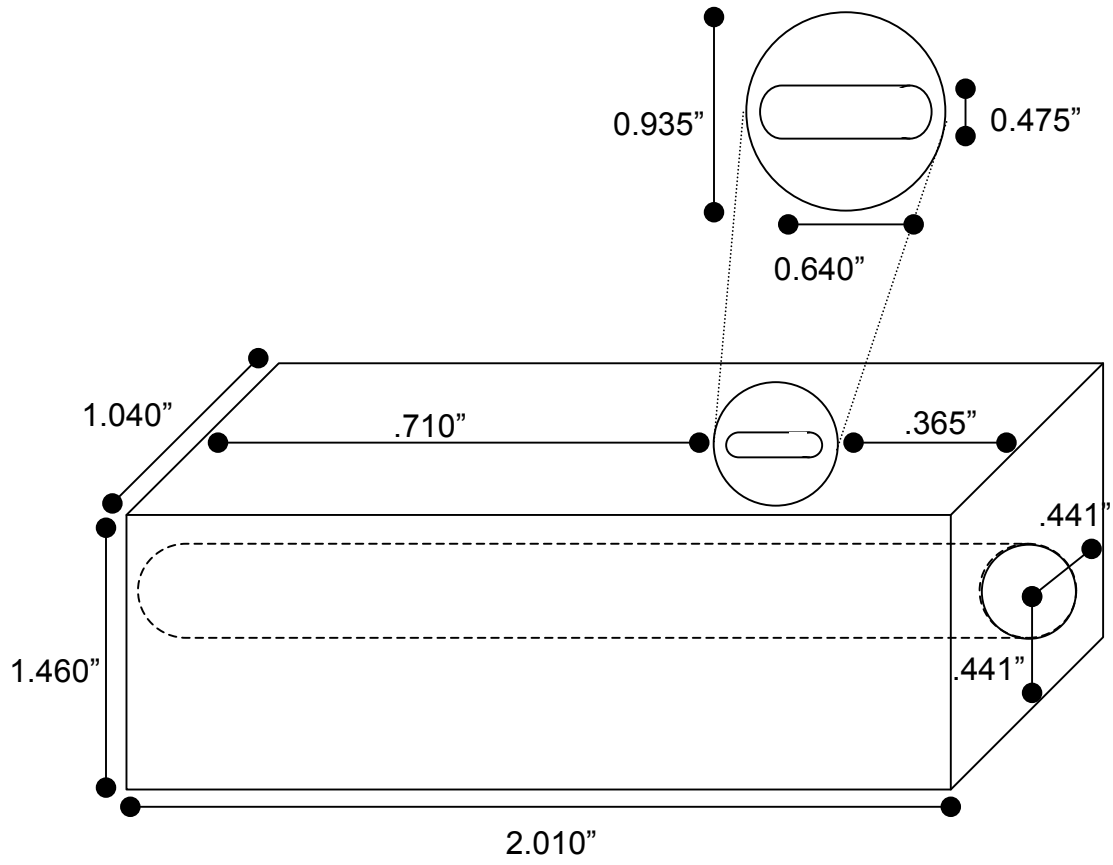


Figure 2.2

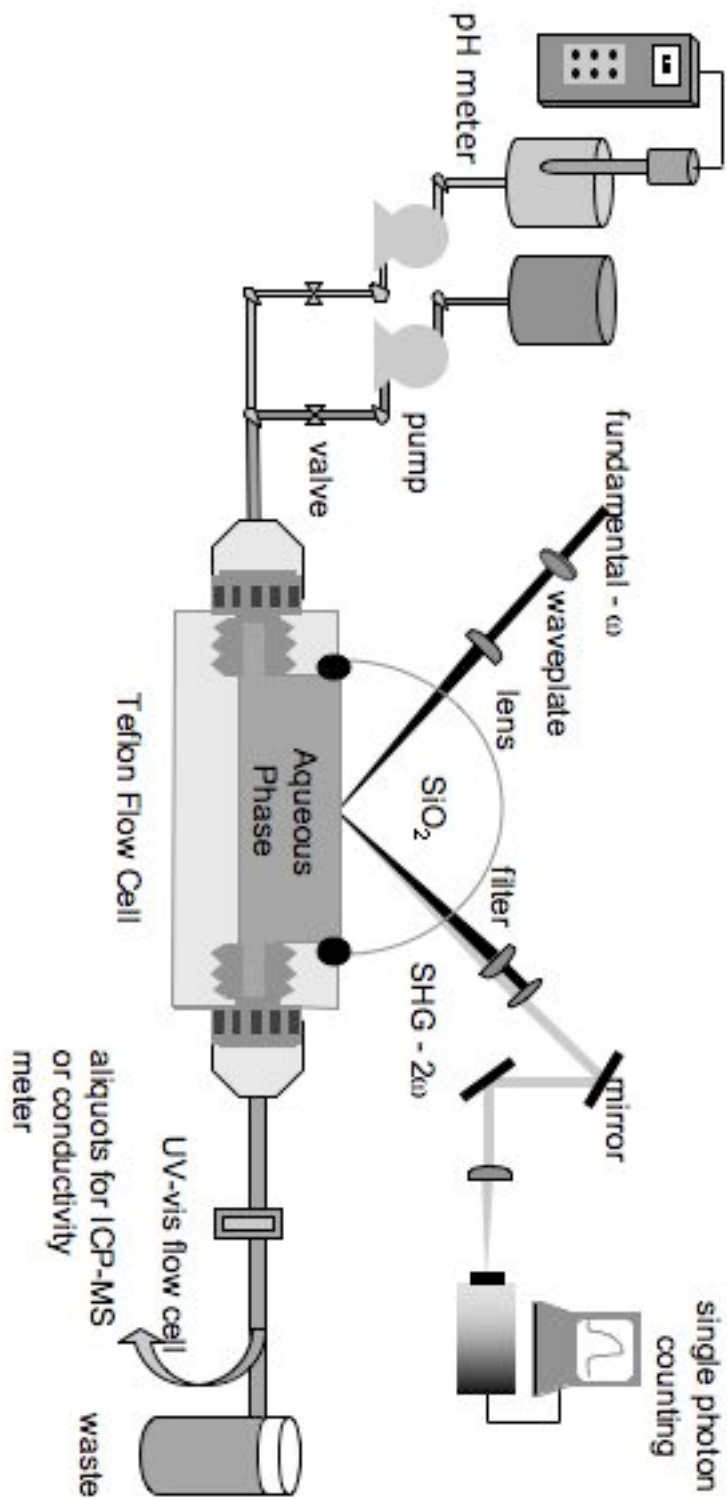


Figure 2.3

without an active UV-vis transion, we perform off-line measurements by taking aliquots of the effluent solution and storing them in glass vials. ICP-MS (Varian) is then used to determine concentration for these analytes, and a conductivity meter (VWR Expanded Range Conductivity Meter) is used to determine ion concentration.

2.4 Experimental Protocols and Methods

2.4.1 Charge screening experiments

Interfacial charge screening experiments are performed by varying the bulk ion concentration flowing over the interface and tracking the second harmonic signal to determine the interfacial charge density. This section briefly details the considerations involved in performing these experiments in the laboratory.

The most critical part of charge screening experiments is to ensure that the system is as clean as possible. Before beginning the charge screening experiments, the entire flow system is purged with Millipore water (18.2 M Ω) for over 2 hours with the peristaltic pumps (Fisher) on the purge setting to ensure the lowest initial ion concentration and a clean flow system. The ion concentration is adjusted in the liquid reservoir, in this case a 2L Erlenmeyer flask, by sequentially adding previously prepared NaCl solutions of increasing concentration. This solution is then pumped across the interface of interest. Observing stable SHG signal on the monitor attached to the computer interfaced to the single photon counter indicates when the system comes to equilibrium. Then, data points are taken for 5 minutes in 1.3 second intervals. Near the end of the 5 minute period, a glass vial, which had previously been thoroughly washed with Millipore water, is rinsed at least 4 times with the effluent solution. The vial is then filled with effluent. The ion concentration meter is then washed with the effluent solution, and placed

into the vial to determine the conductivity of the solution. The vial is subsequently washed thoroughly with Millipore water in preparation for the next data point. This process is repeated for each ion concentration of interest. These experiments are discussed in more detail in Chapter 4 and Chapter 5.

2.4.2 Titration of the interface

Surface titration experiments are performed by varying the bulk pH flowing over the interface and tracking the second harmonic signal to determine the acid-base properties of the interface. This section details the experimental considerations involved in these experiments, focusing on the preparation of solutions, the sequence of the data point collection, and exposure of the organic adlayers to basic conditions. It should be noted that salt is very corrosive, and care must be taken to immediately remove saltwater from the laser table if it overflows any container.

2.4.2.1 Preparing the solutions

Titration experiments are performed by using stock solutions to adjust the pH of the aqueous solution in a reservoir, in this case a two liter Erlenmeyer flask. The pH of the solution in the reservoir is adjusted with one of four stock solutions: pH 1, pH 3, pH 10, and pH 12.5. It is necessary to prepare a wide range of stock solutions to both enable fine control of the reservoir pH when the solution is close to pH 7, and allow us to obtain the more extreme pH values. For the full range of pH values explored in this experiment, see Chapter 4. The solution in the reservoir and the stock solutions contain a background electrolyte concentration of 0.5 M NaCl to ensure that there is not a significant change in electrolyte concentration over the course of the experiment due to ions added while changing the pH. This is an important consideration in the

context of results shown in Chapter 4 which demonstrate the effect that electrolyte concentration has on second harmonic signal.

2.4.2.2 Data collection

Each data point on the graph is the average of 5 minutes of data collection. The solution is pumped out of the reservoir and over the interface while second harmonic signal level is recorded. The second harmonic signal level is again tracked on the computer monitor connected to the single photon counter. After 5 minutes, we block the laser beam with the power meter to record the power, which causes the photon counter to record zero counts. The photon counter continues counting during this interval, which serves to demarcate data taken for different pH values. While the beam is blocked, the reservoir pH is adjusted to the desired value, the power meter is removed from the beam path, and data collection commences again. The second harmonic signal changes to the new equilibrium value corresponding to the new bulk pH. Data is again collected for 5 minutes after the signal comes to equilibrium. This process is repeated for each data point over the course of the experiment.

The collection order of the data points in pH-space is also a consideration. The first data point taken is generally between pH 6 and pH 6.5. Subsequent data points are taken for lower pH values with each data point being lower than the previous one until reaching a pH near 1.5. When the surface titration experiment is performed efficiently and assuming a starting volume of slightly over 2 L, there should be less than 800 mL of aqueous solution left in the 2 liter Erlenmeyer flask at this point. It is now possible to dilute the solution to ~pH 5 by simply adding Millipore water with a background electrolyte concentration of 0.5 M NaCl. This dilution step avoids the buildup of ion concentration over the course of the entire experiment, which may be a factor if it is necessary to neutralize a large volume of pH 1.5 water. The solution is then

adjusted to a pH of 6 before beginning the second half of the experiment. To ensure that signal drift does not occur over the timescale of the experiment, we record a few data points in the second half of the experiment that overlap with the data points from the first half, mainly in the pH 6 – 6.5 region. During the second half of the experiment, the solution is gradually increased to pH 12. Data collection procedures are as previously described.

2.4.3 Exposure of the organic adlayers to basic conditions

A further experimental consideration is the total time that the organic adlayers are exposed to basic conditions. To ensure the stability of the siloxane adlayers studied in this work, it is critical that the second half of the experiment is performed in under 80 minutes to prevent sample degradation. Whitesides and coworkers showed that siloxane adlayer degradation occurred on the timescale of 80 minutes.³⁴ Figure 2.3 shows a sample stability experiment we performed to assess the effect of basic conditions for our carboxylic acid-terminated organic adlayers. Here, the second harmonic signal is plotted as a function of time, while a solution with bulk pH 12 flows over the interface. The second harmonic signal appears to be stable until approximately 100 minutes. This experiment is consistent with a stable organic adlayer for a 100 minute exposure time, and to ensure that we avoid even minor degradation, we conclude the part of the experiment where the adlayer is exposed to basic conditions in less than 80 minutes.

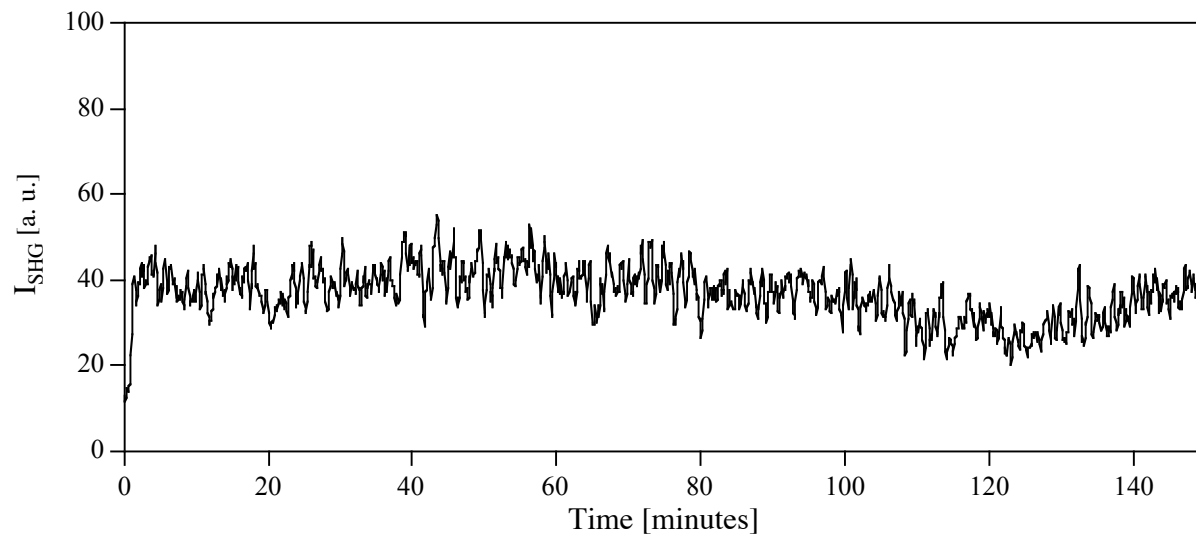


Figure 2.4

2.5 Summary

In this work, we use the experimental techniques and protocols outlined above to perform surface-specific studies of pollutants binding to environmentally relevant mineral oxide/water interfaces. The rest of this work will focus on how using SHG in combination with other complimentary techniques allows us to obtain thermodynamic and structural information for pollutants at the silica/water interface, and full thermodynamic state information for organic adlayers at the silica/water interface.

Chapter 3

Characterization of Carboxylic Acid Groups Tethered to Silica

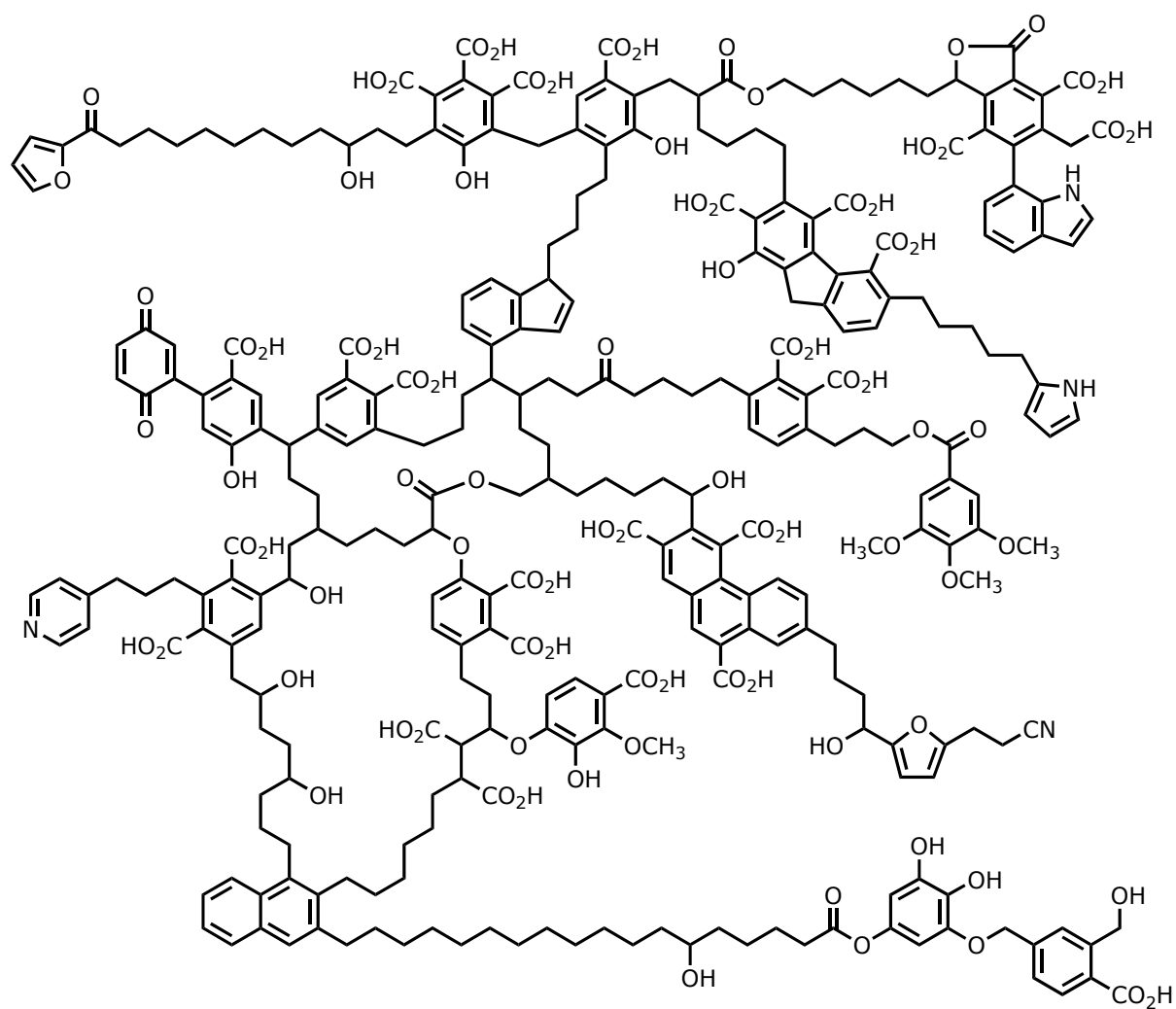
Portions of this chapter are reproduced in part with permission from:

Konek C.T.; Musorrafiti M.J.; Voges A.B.; Geiger F.M. “Tracking the interaction of transition metal ions with environmental interfaces using Second Harmonic Generation.” *Adsorption of Metals by Geomedia II* Ed. Mark Barnett and Douglass Kent. Elsevier series Developments in Earth and Environmental Sciences. Copyright 2007, Elsevier.

3.1 Introduction to Organics in the Environment

In the environment, reactions and binding processes which occur at interfaces can control the speciation, transport and ultimate fate of a wide range of organic and inorganic pollutants in the environment.¹ Pollutants dissolved in groundwater can bind at the surface of soil particulate matter. Although soil consists of a wide range of substances, the most common constituent is the mineral oxide silica, SiO_2 .² The polar nature of the surface of silica allows a wide variety of molecules to bind to it, including organic compounds with polar functional groups.^{2,3} Organic compounds are known to strongly bind to soil particles. While at the mineral oxide/water interface, they can participate in and control the interaction between pollutant molecules and the mineral oxide.^{4,5}

Natural organic matter (NOM) in the environment originates from microbial degradation of the products released during the cell death of plants, animals and bacteria which exist in soil. NOM is thought to be an intermediate step in the creation of fossil fuels from organic matter. NOM in the environment can be loosely divided into three categories.² Humic is a black, carbonaceous substance which is not soluble in water. Fulvic acid is a yellow-brown substance which is soluble in water for all pH values. Humic acid is a dark brown substance only soluble in water above a pH value of 2. Since humin is insoluble, the primary organic molecules found adsorbed to mineral oxides are humic and fulvic acids. Humic and fulvic acids consist of complex molecules with a wide variety of functional groups, including carboxylic acids, amines, quinones, and esters. The structure of these molecules is complex, and still a matter of discussion.⁶ A ChemDraw structure of a possible model building block is shown in Figure 3.1, adapted from reference 6. Note the large number of carboxylic acid groups shown in this structure. While humic acid was thought to consist of long biopolymers with large molecular

**Figure 3.1**

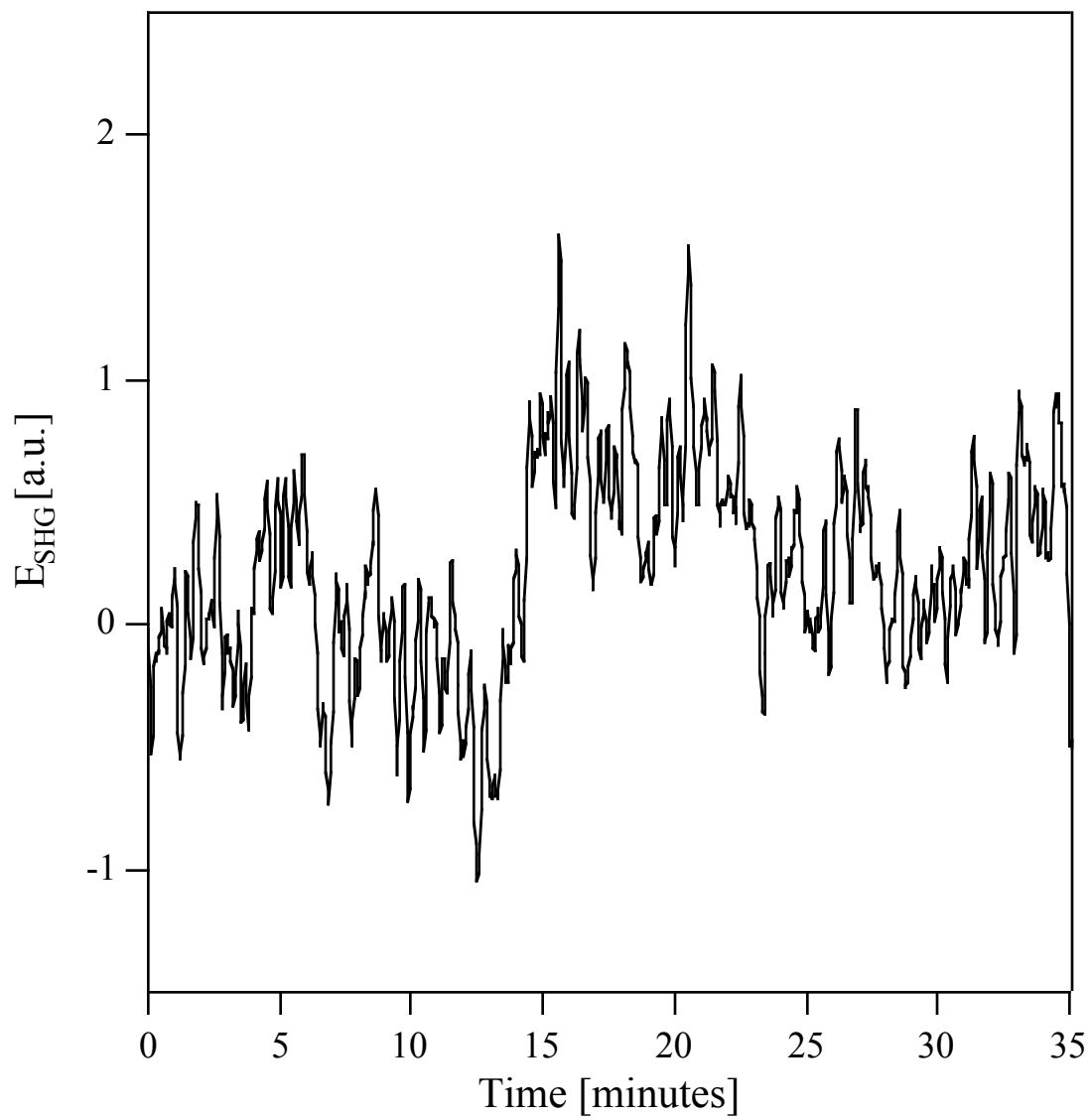


Figure 3.2

weights (as shown in Fig. 3.1), a new molecular view of humic acids is now emerging which describes these substances as agglomerations of low molecular weight compounds that aggregate based on shared properties, such as hydrophobicity or hydrophilicity.

3.2 Model Systems

It is possible to study the complicated humic acid molecule with SHG, according to the well-known UV-vis transition and brown color associated with humic acid dissolved in water. Figure 3.2 shows an SHG time trace of humic acid (Aldrich) binding to the silica/water interface. After flowing water over the interface, at approximately $t=13$ minutes humic acid flow is switched on at a concentration of 25 mg/L and a pH of 7.5, resulting in an increase in signal consistent with humic acid binding. At approximately $t=22$ minutes, the humic acid flow is turned off, and water flow is resumed. On the timescale of this experiment, the signal appears to remain at approximately the same level, indicating that humic acid binding is irreversible.

Although an adsorption experiment can be performed, it is challenging to perform further experiments to extract more information about the binding. Therefore, to understand the interaction of different pollutants with organic compounds in the environment, we focused on functional groups which are likely to control the behavior of organic compounds. The first functional group we focused on is the carboxylic acid because of its aforementioned prevalence in humic acid, as well as its ability to chelate aqueous metal cations. Depositing a scaffold terminated with a specific functional group with good surface coverage allows us to study the properties of a group of those functional groups, and study the interaction of a pollutant with that functional group. However, we have developed a general scaffold method based on a robust

connectivity to the silica surface which can be modified to study a wide range of organic functional groups. This work will focus on the carboxylic acid group.

To build a model system for studying pollutants interacting with organic molecules at the mineral oxide/water interface, we collaborated with Professor SonBinh Nguyen's group at Northwestern University. Using siloxane chemistry originally developed by Sagiv^{7,8} and Whitesides,⁹⁻¹¹ we prepared a methyl ester-terminated silane. We subsequently hydrolyzed the methyl ester into a carboxylic acid to yield a carboxylic acid-functionalized silica/water interface.

Other methodologies exist for functionalizing surfaces with organic molecules, including alkanethiols adsorbed to gold. While these methods can be attractive, we chose siloxane chemistry for a few specific reasons. Firstly, the silicon-oxygen bond is robust and stable under a wide range of environmentally relevant conditions. Secondly, siloxane adlayers are chemically tethered to the silica and allow us to study the binding of pollutants to the organic adlayer without concerns that the adlayer is undergoing an adsorption/desorption process over the course of the experiment. Thirdly, silica is the most abundant mineral oxide. It is often a primary constituent of the solid core which organic adlayers coat. Employing siloxane chemistry allows us to attach environmentally relevant organic scaffolds to the flat side of silica substrates, enabling us to perform these studies with minimal modification to the experimental setups used in our earlier work.¹²⁻¹⁴

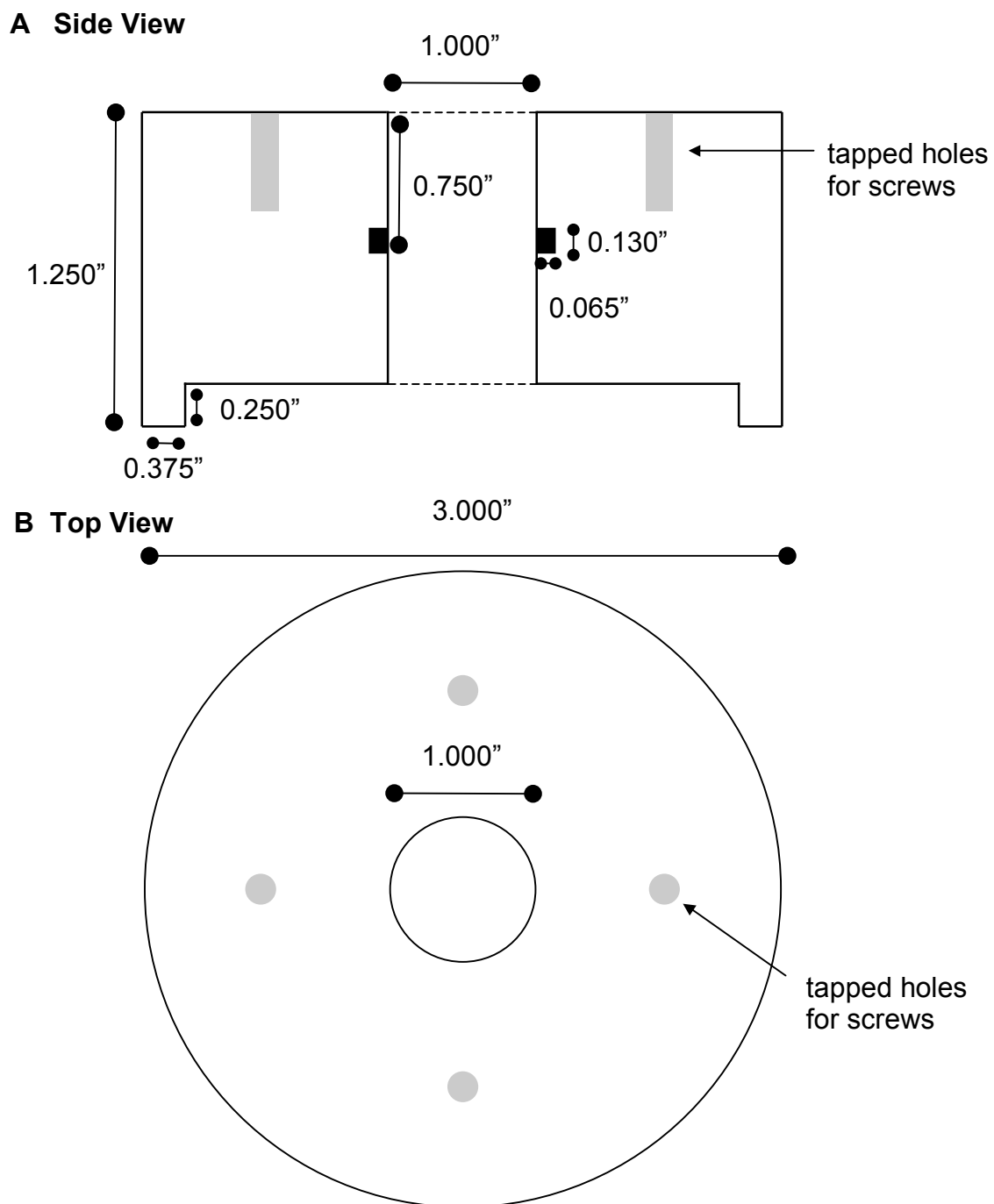


Figure 3.3

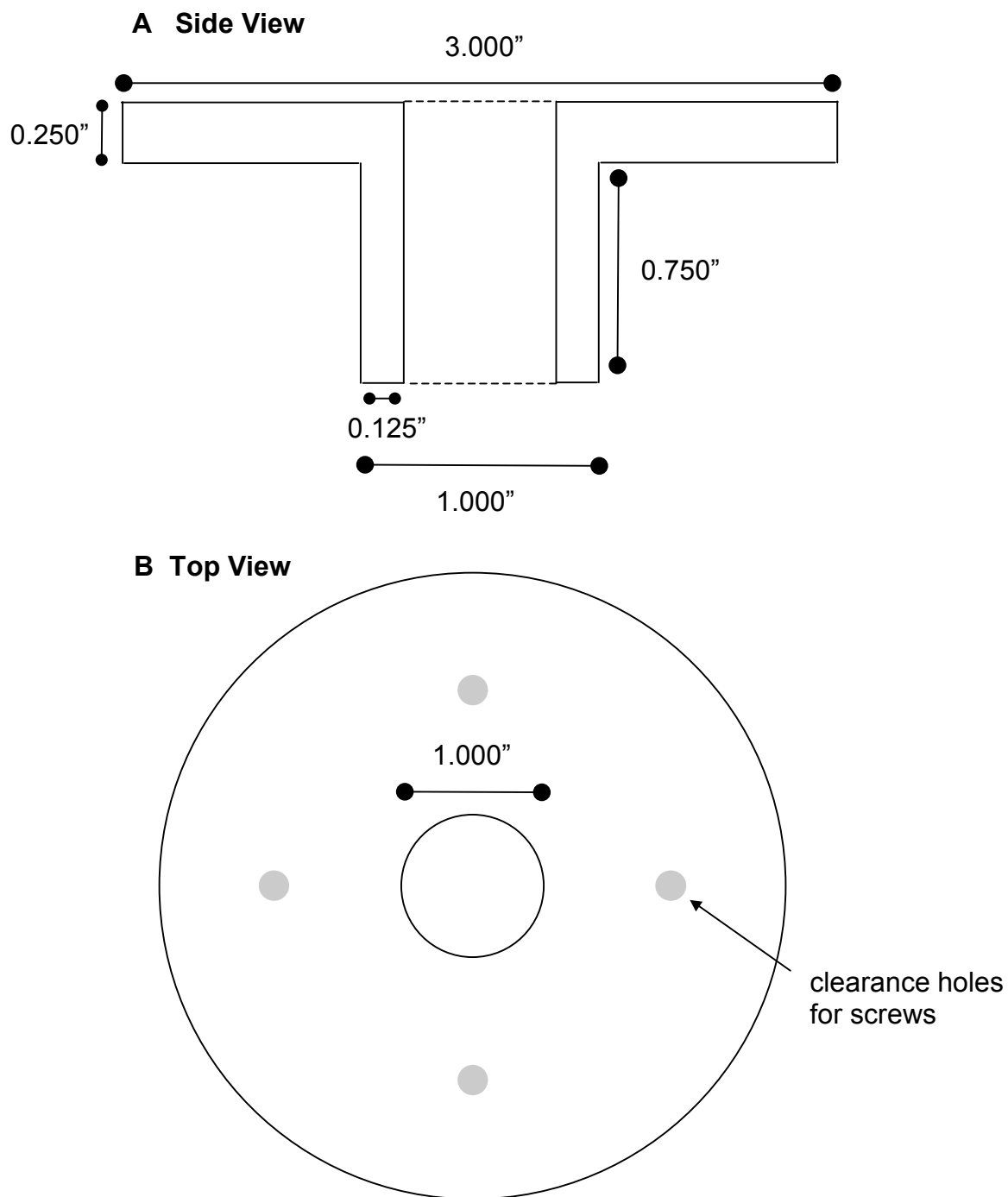


Figure 3.4

3.3 Deposition of Organic Adlayers

The deposition is performed following literature procedures.¹¹ The lens is cleaned by sonication in methanol for 6 minutes. The lens is subsequently dried by blowing with a house nitrogen stream and placed in an oven for 5 minutes at 100°C. Next, the lens is placed in a Harrick plasma cleaner (PDC-32G, 110V) on its highest setting for approximately 30 seconds. The lens is then covered, immediately placed in a custom-built Teflon chamber (Figure 3.3 and Figure 3.4), and taken into a nitrogen atmosphere glovebox. The trichlorosilane is diluted in dry toluene to 1% v/v, and placed in contact with the flat side of the lens. The deposition time is one hour, at which point the lens is rinsed six times with dry toluene in the glovebox. After removal from the glovebox, further rinsing is performed with toluene and then methanol. We place the lens in an oven at 100°C for one hour to anneal the sample and promote cross-linking at the surface. To hydrolyze the methyl ester terminal group, the lens is placed into 2.4 M HCl set at 85°C in a hot oil bath (Dow Corning 550 fluid (phenylmethyl siloxane)) for two hours. After rinsing with copious amounts of water, the lens is stored in slightly acidic water (~pH 5.5) in a beaker until the experiment. A summary of the deposition procedure is shown in Figure 3.5.

To investigate whether our experiments primarily probe the carboxylic acid groups or exposed patches of silica, a variety of surface analysis techniques are used to characterize the adlayers. Direct characterization of the hemispherical lenses was performed when possible, and on substrates with similar surface chemistry (glass slides, silicon wafers with a native oxide layer) in situations where the hemispherical lens is either too bulky for the instrument or the technique required different optical properties.¹⁵ In all cases, the deposition protocols are maintained. Silicon samples are first cleaned in HF, and subsequently left in the oven at 100°C for an hour to ensure a small, but present, native oxide layer.

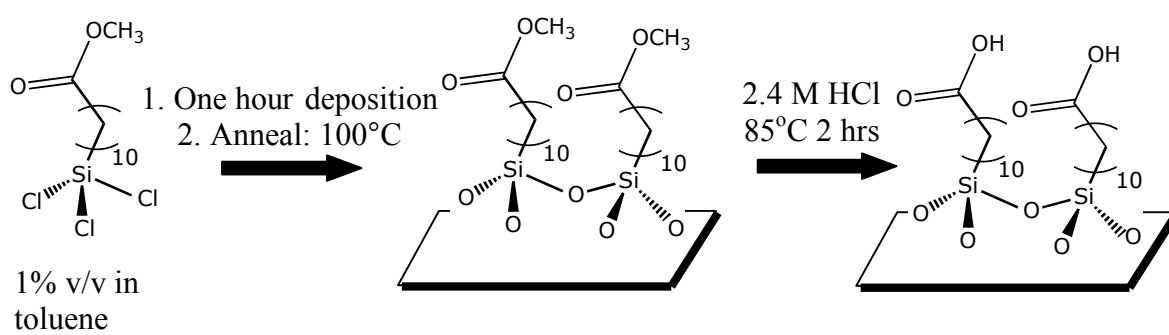


Figure 3.5

3.4 Contact Angle Measurements

As a qualitative measure of hydrophobicity or hydrophilicity, water contact angle measurements are used to characterize the silica surfaces of the silica lens after the preparation of the adlayer. Contact angle measurements (Tantec CamMicro) sample only the exposed surface. Since the water contact angle varies with hydrophobicity, it is an appropriate method for distinguishing between the surfaces discussed in this work. Twelve measurements for each surface are averaged together, resulting in static contact angles of $32^\circ(4)$ for clean silica lenses, $67^\circ(6)$ for methyl ester siloxanes, and $46^\circ(4)$ for carboxylic acid siloxanes. These measurements are consistent with an increase in hydrophobicity from the silica lenses to the methyl ester adlayers, and with a subsequent increase in hydrophilicity upon conversion to the carboxylic acid adlayer. The contact angles agree well with literature data on ester- and acid-terminated siloxanes.¹¹

3.5 Atomic Force Microscopy

In the AFM studies, the ester-silane deposition is carried out on a silicon wafer with a native oxide layer. The images are taken on a Nanoscope IIIa (Digital Instruments, Santa Barbara, CA). Phase mode AFM images indicate a high degree of surface functionalization. Fig. 3.6a shows that the degree of surface functionalization approaches 95%. A line scan shows that the surface is largely uniform, which is consistent with a high density adlayer. A line scan (Fig. 3.6b) across a hole in the adlayer indicates an adlayer height of 10 Angstroms, which is consistent with results from ellipsometry measurements presented in the following section.

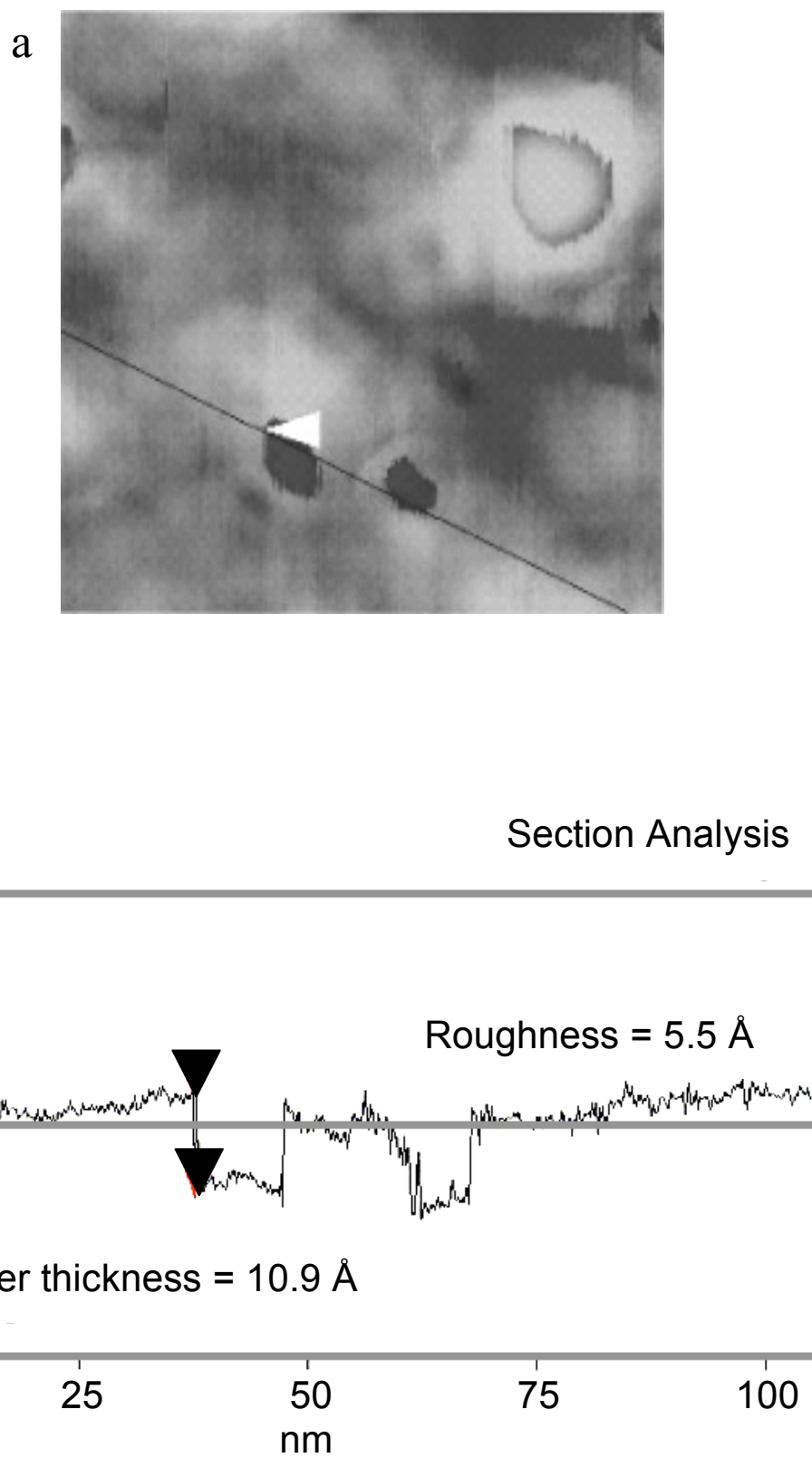


Figure 3.6

3.6 Ellipsometry

To further investigate the adlayer thickness, we carried out ellipsometry measurements (Gaernter Scientific, Model L116SF300) for two different ester-functionalized silicon wafers with a native oxide layer rather than perform the measurements on silica to ensure a significant difference in refractive index between the substrate and the organic adlayer. We average seven data points taken at different locations on each sample with two different probe wavelengths (544 and 632 nm) and used a refractive index of 1.55 for the organic adlayer, which is a typical bulk value for many organic compounds.^{16,17} Ellipsometry showed the thickness of the organic adlayer to be approximately 10-13 Angstroms, which is consistent with the presence of a slightly tilted 10-carbon atom long chain at the interface.¹¹

3.7 Time of Flight – Secondary Ion Mass Spectrometry (ToF-SIMS)

A ToF-SIMS (Phi Trift III, Physical Electronics) study is performed to investigate adlayer coverage and extent of conversion to the carboxylic acid on a glass slide using Ga atoms at 25keV. First, to track the ester group, a trichlorosilane molecule is synthesized by Paul Bertin that contained fluorine atoms instead of hydrogen atoms on the terminal methyl ester.¹⁸ The ester coverage is tracked by imaging fluorine when the trifluoro methyl ester is deposited. After the hydrolysis of the ester, a high degree of conversion implies that very few fluorine atoms would appear on an image of the surface. These data are shown in Fig. 3.7 and are consistent with both a high degree of surface functionalization and an efficient conversion of the ester group to a carboxylic acid group.

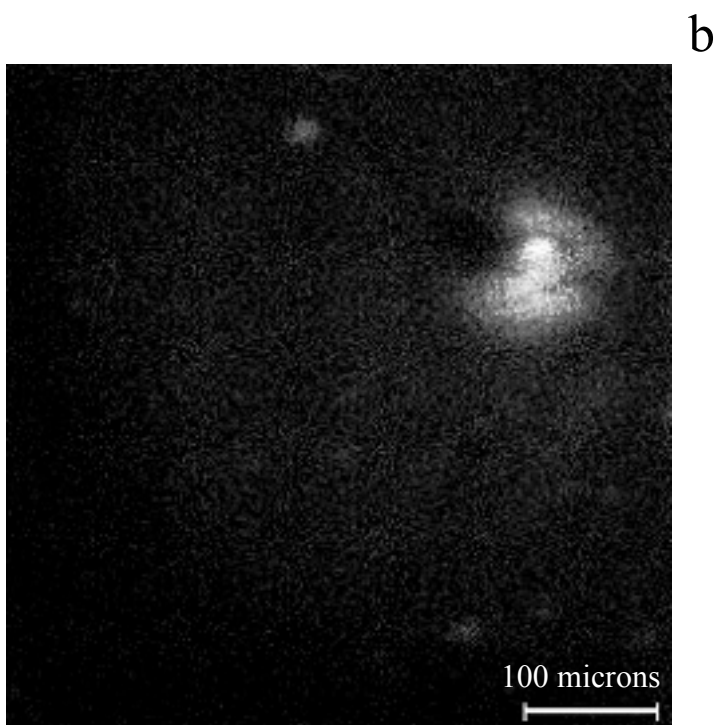
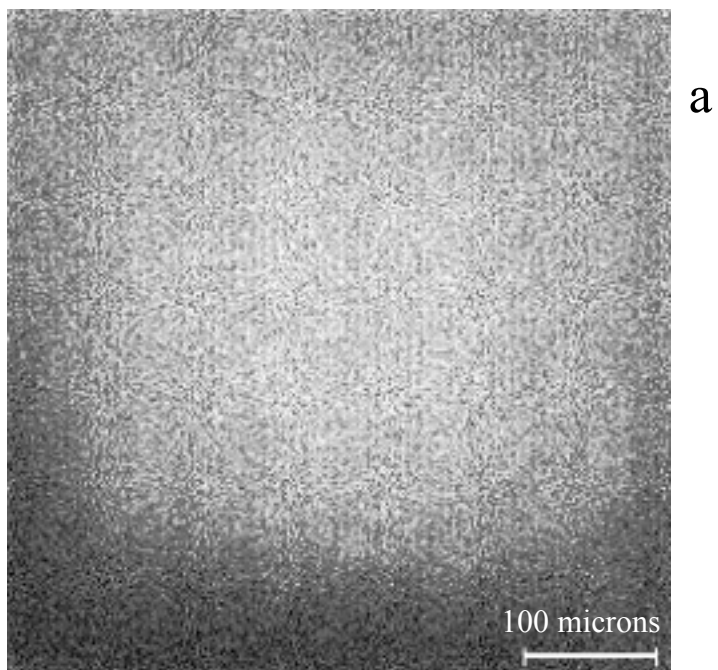


Figure 3.7

3.8 Vibrational Sum Frequency Generation

To further investigate the extent of ester conversion to the acid during hydrolysis, vibrational sum frequency generation (SFG) studies are carried out using broadband infrared radiation (140 cm^{-1} bandwidth at 3 mm) with signal upconversion at the sample surface using a psec visible (800 nm) pump beam in external reflection.^{3,18} The SFG experiments are carried out on functionalized glass microscope slides and probe infrared modes containing a component perpendicular to the interface by using the appropriate light field polarizations. Vibrational SFG measurements, shown in Fig. 3.8,¹⁸ demonstrate that the conversion from the methyl ester to the acid is high. The SFG spectrum of the methyl ester siloxane shows the methylene symmetric ($\sim 2850\text{ cm}^{-1}$) and asymmetric stretches ($\sim 2930\text{ cm}^{-1}$) of the carbon chain in the methyl ester as well as the CH_3 symmetric stretch of the methoxy group (R-O-CH_3) at 2975 cm^{-1} . After hydrolysis of the ester, this band is absent in the vibrational SFG spectrum. The disappearance of this methoxy CH stretch at 2975 cm^{-1} is consistent with a high efficiency of the hydrolysis of the methyl ester. This is consistent with the ToF-SIMS experiments presented in the previous section. Additionally, SFG spectra of both the methyl ester and carboxylic acid groups are well-defined with high signal-to-noise ratios, consistent with a well-packed organic adlayer.

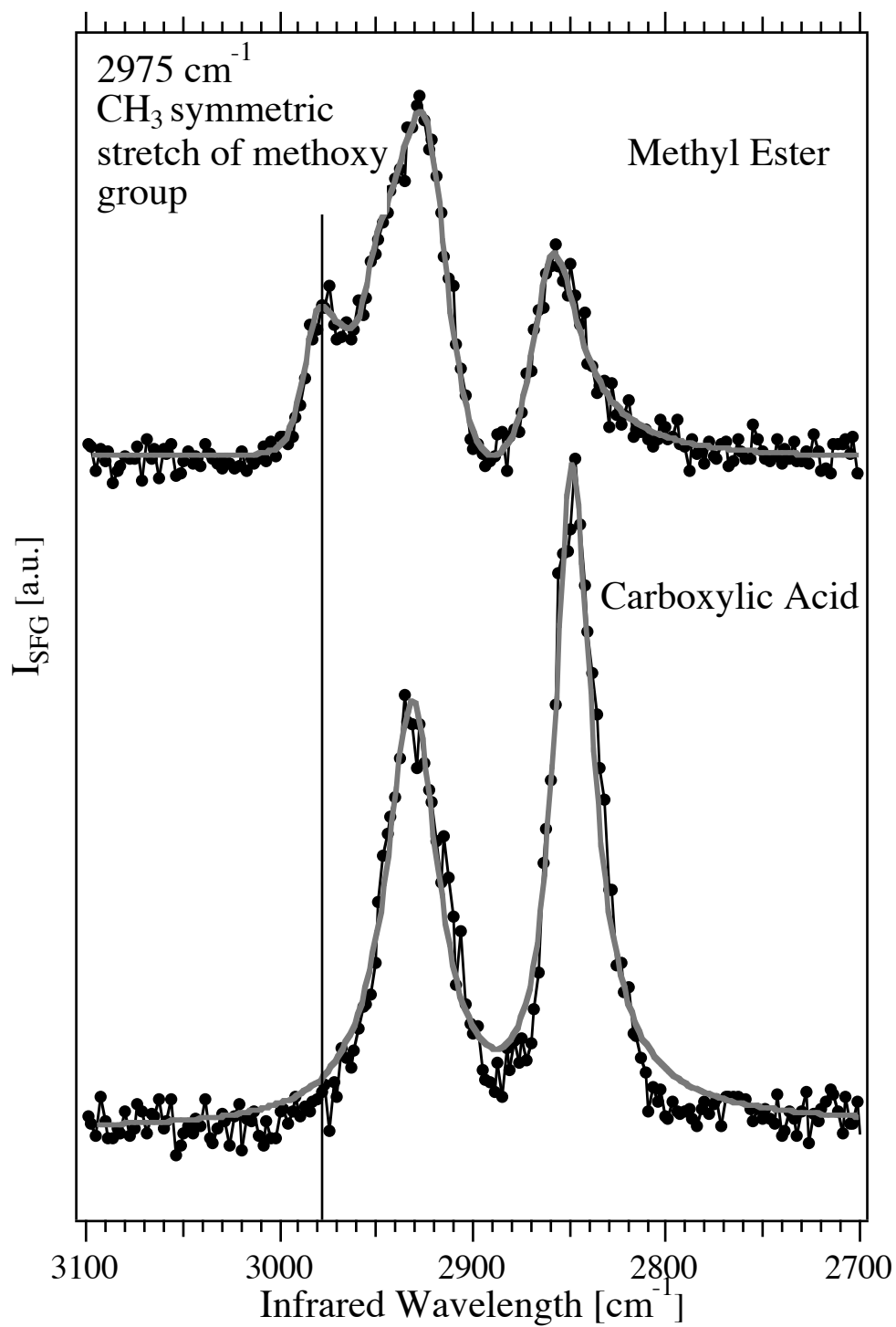


Figure 3.8

3.9 Conclusions

In this chapter, we discussed the characterization of carboxylic acid adlayers on silica. These measurements are complimentary to the second harmonic experiments that are outlined in chapters 4 and 5. Our results show a high degree of surface coverage during the deposition step and a high degree of conversion from the methyl ester to the carboxylic acid. AFM and SIMS imaging indicate a high degree of surface coverage. Adlayer thickness measurements from AFM and ellipsometry are consistent with a slightly tilted adlayer, which is expected for these systems. SIMS imaging and SFG both indicate that the methyl group disappears after hydrolysis, consistent with a high degree of conversion for the surface reaction. We now proceed to using second harmonic generation to probe these organic adlayers.

Chapter 4

Acid-Base Chemistry at the Carboxylic Acid-Functionalized Silica/Water Interface

Portions of this work are reproduced in part with permission from:

Konek C.T.; Musorrafiti M.J.; Al-Abadleh H.A.; Bertin P.A.; Nguyen S.T.; Geiger F.M. “Interfacial acidities, charge densities, potentials, and energies of carboxylic acid-functionalized silica/water interfaces determined by second harmonic generation.” *Journal of the American Chemical Society* **2004**, 126 (38), 11754-11755. Copyright 2004, American Chemical Society.

Konek C.T.; Musorrafiti M.J.; Voges A.B.; Geiger F.M. “Tracking the interaction of transition metal ions with environmental interfaces using second Harmonic Generation.” *Adsorption of Metals by Geomedia II* Ed. Mark Barnett and Douglass Kent. Elsevier series Developments in Earth and Environmental Sciences. Copyright 2007, Elsevier.

4.1 Carboxylic Acids in the Environment

Natural organic matter (NOM) is a class of complex organic molecules,¹ including humic and fulvic acid, which originate from biological degradation processes occurring in soils. NOM in the environment can bind to surfaces, chelate dissolved metal ions, and participate in many of the redox reactions which control the speciation, transport and ultimate fate of pollutants in the environment. The involvement of NOM in these key environmental processes suggest that the organic components in NOM may heavily influence geochemical processes. NMR studies have shown that NOM contains a wide variety of organic functional groups, including carboxylic acids, quinones, methyl esters, amines and others.² The most important functional group in environmental organic matter are carboxylic acids, which are major constituents of both humic and fulvic acids.² The importance of carboxylic acid groups stems from their two critical roles in the environment: (1) oxidation of carboxylic acids easily converts them into a thermodynamic sink, CO₂ (2) chelation by carboxylic acid groups provides a key step in controlling the mobility and oxidation state of metals in the environment.

Understanding the behavior of carboxylic acid groups at interfaces remains an important open question in environmental molecular science, and many surface studies of acid groups have been undertaken recently. Table 4.1 shows selected pK_a values for carboxylic acid functionalized interfaces reported in the literature. The results of these studies underscore the fact that interfaces are substantially different chemical environments from bulk solution, so properties of carboxylic acid groups at interfaces, including the pK_a, can vary widely from properties determined via bulk phase measurements. Since the acid-base behavior of carboxylic acid groups at interfaces can control the charge state of soil surfaces in the environment, a complete understanding of pollutant binding to soil surfaces and pollutant transport in the

Acid	Interface	Technique	pK _a value	Reference
CH ₃ (CH ₂) ₄ (CH=CH-CH ₂) ₂ (CH ₂) ₆ COOH	Ge/water	ATR	8.5	24
>Si(CH ₂) ₁₄ COOH	Si/D ₂ O	ATR	4.9, 9.3	22
SH(CH ₂) ₁₀ COOH	gold/water	AFM	4.84, 6.30	25
HS(CH ₂) ₁₃ COOH	gold/water	QCM	9.0	26
HS(CH ₂) ₂ COOH	gold/water	AFM	8.0	16
HS(CH ₂) ₁₀ COOH	gold/water	CFM	5.5	27
HS(CH ₂) ₁₄ COOH	gold/water	QCM	6.4, 4.3	28

Table 4.1

environment must be informed by surface-specific studies of carboxylic acids. In order to better predict the effect that carboxylic acids in the environment will have on pollutant binding, we performed a series of SHG experiments on the carboxylic acid-functionalized silica/water interfaces that were described in Chapter 3.

4.2 Interfacial Charge Screening Experiments

First, we perform an interfacial charge screening experiment to determine the interfacial charge density for carboxylic acid adlayers at the silica/water interface via the experimental strategy described in Chapter 2. In charge screening experiments, we determine the bulk ion concentration via off-line conductance measurements (VWR Extended Range Conductivity Meter). The conductivity is converted into ion concentration via a calibration curve constructed prior to the experiment with stock solutions. As the experiment progresses, the bulk ion concentration is increased by adding stock solutions of NaCl (Fisher) in Millipore water to the reservoir, and subsequently flowing the solution over the interface. It is critical to characterize the change in signal for very low ion concentrations, so prior to each experiment the tubing is flushed with 18.2 M Ω Millipore water for over two hours with the peristaltic pumps (Fisher) on the purge setting. The flow system is considered flushed when the conductivity probe consistently reads near its detection limit, 0.1 μ S. The first data point taken is at the lowest concentration and the ion concentration is gradually increased over the course of the experiment.

As described in Chapter 2, SHG directly samples the interfacial potential.³⁻⁵ When a carboxylic acid group is deprotonated, the resulting negatively charged species creates a static potential at the interface. If changing experimental parameters modulates the potential, the resulting change can be tracked via the second harmonic signal. A model must then be applied

to the SHG data to obtain quantitative information about the interfacial potential from the experimental measurable, namely, the number of photons produced at the second harmonic frequency per unit time. The Gouy-Chapman model, which describes the behavior of liquid interfaces in the presence of an electric potential, is an appropriate and straight-forward expression.^{6,7} The Gouy-Chapman model is not chemically specific, but rather treats all ions as point charges. The surface is described as a rigid sheet of charge; counter ions dissolved in the bulk are attracted to the surface, and form a diffuse layer next to the surface. In the mathematical derivation of the Gouy-Chapman model,⁸ it is assumed that the gradient of counter ions in the diffuse layer follows a Boltzman distribution according to:

$$C_o = C \exp\left(\frac{ze\Phi}{kT}\right) \quad 4.1$$

where C_o is the ion concentration near the surface, C is the bulk ion concentration, z is the charge on each counter ion, e is the charge on an electron, Φ is the potential, k is the Boltzman constant, and T is the temperature. The Gouy-Chapman expression for interfacial potential^{9,10} is as follows:

$$\Phi = \frac{2kT}{ze} \operatorname{arcsinh}\left(\sigma \sqrt{\frac{\pi}{2\epsilon kTC}}\right) \quad 4.2$$

where Φ is the potential at the interface, k is the Boltzman constant, T is the temperature, z is the charge on each counter ion, e is the elemental charge, σ is the surface charge density, ϵ is the permittivity of bulk water, and C is the bulk ion concentration. The governing equation for the $\chi^{(3)}$ technique (from Chapter 2) relates the second harmonic E-field to the potential at the interface:

$$E_{SHG} = \chi^{(2)} E_\omega E_\omega - \chi^{(3)} E_\omega E_\omega \Phi. \quad 4.3$$

Following Eisenthal and coworkers,¹¹⁻¹³ Eq. 4.3 is combined with the Gouy-Chapman model to yield the following equation:

$$E_{SHG} = \chi^{(2)} E_{\omega} E_{\omega} - \chi^{(3)} E_{\omega} E_{\omega} \frac{2kT}{ze} \operatorname{arcsinh} \left(\sigma \sqrt{\frac{\pi}{2\epsilon kTC}} \right) = A - B \frac{2kT}{ze} \operatorname{arcsinh} \left(\sigma \sqrt{\frac{\pi}{2\epsilon kTC}} \right) \quad 4.4$$

Equation 4.4 relates the second harmonic E-field to the bulk ion concentration, C , and the surface charge density, σ . During a charge screening experiment, we track the second harmonic E-field as a function of bulk ion concentration. To find the interfacial charge density the data is subsequently fit with Eq. 4.4 with A , B and σ as fit parameters. Although the fitting equation contains a product of two fitting parameters (B and σ), values for interfacial potential determined by the $\chi^{(3)}$ technique have been found to be in good agreement with ζ -potential measurements,^{4,14} and the results presented in this work are in good agreement with atomic force microscopy measurements¹⁵ (vide infra).

Fig. 4.1 shows that as the bulk ion concentration increases, the second harmonic signal decreases due to charge screening. This experiment is performed at a pH of 6.4 and the data shown are an average of two separate runs. The data is fit using Eq. 4.4, and the fit indicates a charge density of $2.8(6) \times 10^{-4} \text{ C/m}^2$. A similar experiment is performed at a pH of 11.2 (inset, Fig. 4.1) to determine the interfacial charge density under very basic conditions, resulting in a charge density of $4.2(2) \times 10^{-2} \text{ C/m}^2$. The interfacial charge density experiments indicate that for a bulk solution pH of 7, neutral carboxylic acid groups exceed the number of ionized carboxylate groups by two orders of magnitude. These experiments are performed at pH 11.2 and pH 6.5, and the results will be used in fitting the titration experiments discussed in the next section.

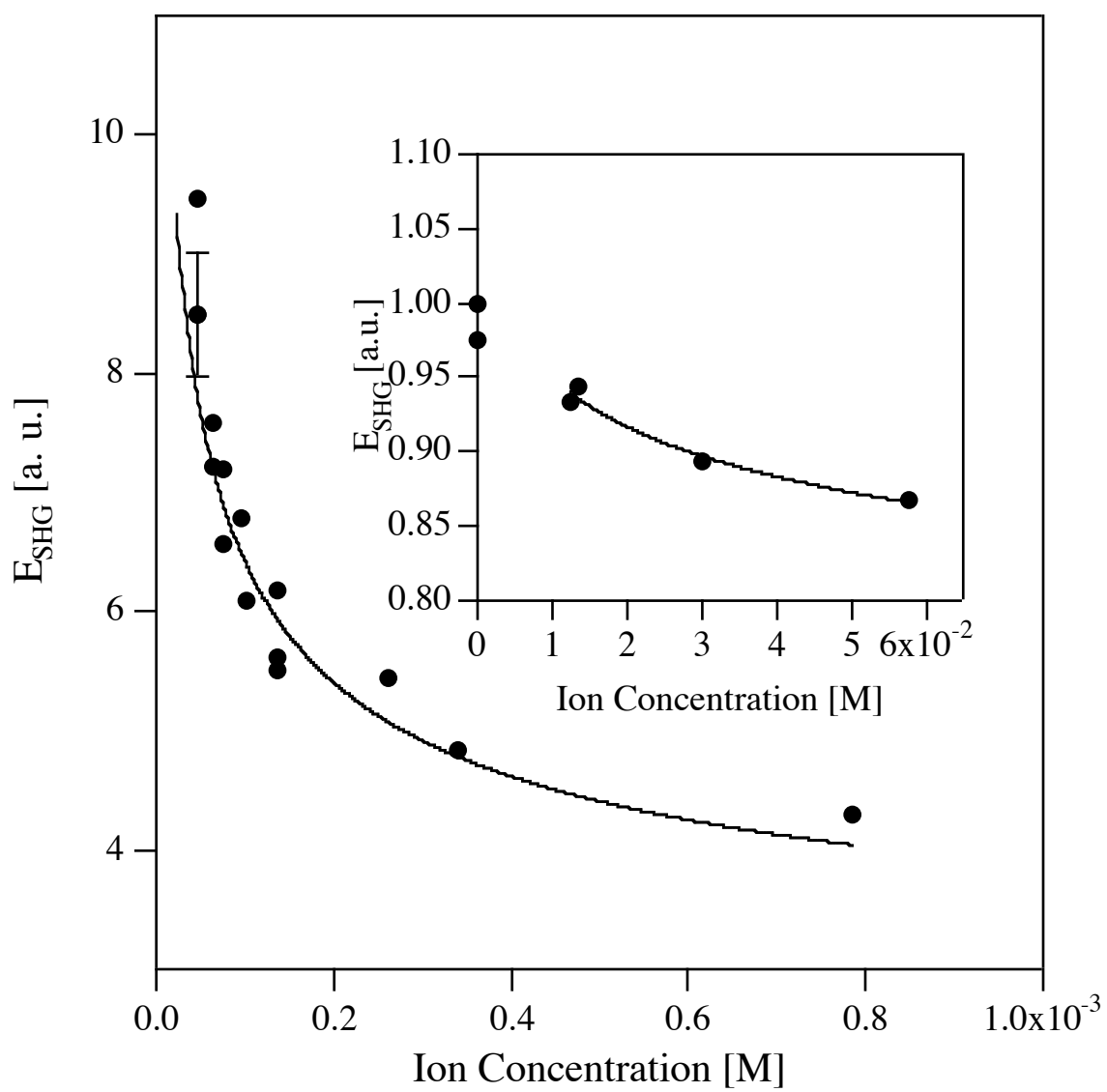


Figure 4.1

4.3 Titration of Carboxylic Acids at the Silica/Water Interface

To further understand the acid-base chemistry of the carboxylic acid groups, a titration is performed while probing the interface with second harmonic generation. In this experiment the deprotonation of the carboxylic acid groups directly changes the potential at the interface, modulating the SHG E-field via the relationship shown in Eq. 4.3. As carboxylic acid groups at the interface deprotonate, the negatively charged oxygen atoms increase the static interfacial potential. The degree of deprotonation and thus the potential can be controlled by changing the pH of the bulk solution flowing across the interface. Therefore, the titration and resultant change in potential can be tracked using SHG. Fig. 4.2 shows the results of these measurements.^{15,16}

During these experiments, we control the effect of bulk ionic strength on the interface potential by including a background electrolyte concentration of 0.5 M NaCl as described in section 2.4.2. The pH range is slightly below pH 2 to slightly above pH 12. Adjusting the pH from 7 to a value of either 2 or 12 causes an increase of ionic strength of approximately 10^{-2} M. The background electrolyte concentration is chosen conservatively to be two orders of magnitude greater than 10^{-2} to prevent a significant effect on the second harmonic signal due to variation in the ionic strength due to pH adjustments over the course of the experiment.

The titration data shown in Fig. 4.2 clearly show two inflection points in the interfacial titration curve, which is consistent with the presence of two acid-base equilibria for the carboxylic acid. To obtain quantitative pK_a information, it is necessary to fit the data using the information obtained in the previously mentioned charge screening experiments. The fitting procedure is summarized below, and more detail can be found in the published literature.^{3,4,10}

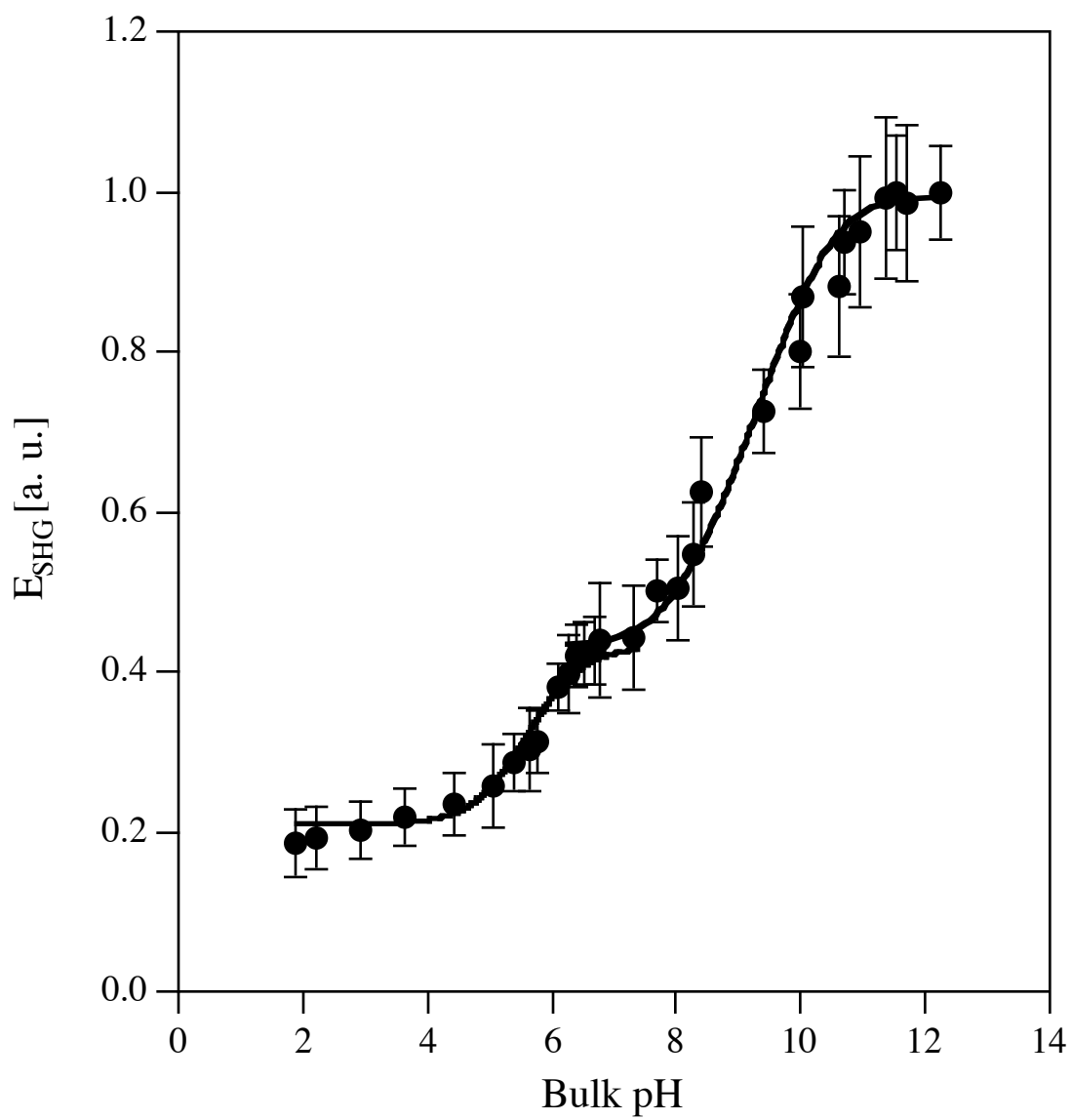


Figure 4.2

The two pK_a values apparent in Fig. 4.2 are separated by about 3 pH units, which allows them to be treated as separate entities.¹⁷ Since the second harmonic E-field increases monotonically with the number of deprotonated carboxylic acid groups, the fraction deprotonated (f) can be written in terms of the second harmonic E-field (vide infra, Eq. 4.4). Each titration step is characterized by an initial static region, where changing the bulk pH has little effect on the second harmonic signal because the bulk solution does not significantly deprotonate the carboxylic acid groups; the average value of the second harmonic signal in this static region is referred to as $E_{2\omega}^{\text{pH Low}}$. As the bulk pH approaches the pK_a value for the carboxylic acid, the protonation state is very sensitive to the bulk pH, and the SHG E-field depends strongly on bulk pH. When the bulk pH is much more basic than the pK_a , the signal intensity as a function of bulk pH is again static since the vast majority of carboxylic acid groups are already deprotonated. The average value of the second harmonic signal in this region is referred to as $E_{2\omega}^{\text{pH High}}$.

Using $E_{2\omega}^{\text{pH High}}$ and $E_{2\omega}^{\text{pH Low}}$ as reference points for the fully deprotonated and fully protonated regions, respectively, the value of the electromagnetic field for all data points is converted into a fraction of deprotonated carboxylic acid groups for every data point along the titration curve according to:

$$f = \left(\frac{E_{2\omega} - E_{2\omega}^{\text{pH Low}}}{E_{2\omega}^{\text{pH High}} - E_{2\omega}^{\text{pH Low}}} \right) \quad 4.4$$

where $E_{2\omega}$ is the SHG E-field for each data point. Again, it should be noted that this fitting methodology is applied separately to the curve associated with each inflection point.

The fit equation for interfacial titration data can then be written in terms of the fraction deprotonated (f), the interfacial charge density at pH 6.4 or pH 11.2 (σ_{max}) and the bulk pH. By

fitting the following equation to each acid-base equilibrium, values for the pK_a are determined.

$$pH = pK_a + \log \left(f \left(\left(f \sigma_{\max} \sqrt{\frac{\pi}{2C\epsilon kT}} \right) + \sqrt{1 + \left(f \sigma_{\max} \sqrt{\frac{\pi}{2C\epsilon kT}} \right)^2} \right) / (1 - f) \right) \quad 4.5$$

Fitting Eq. 4.5 to the data shown in Fig. 4.2 results in pK_a values of 5.6(2) and 9(1). The environmental significance and nature of the interaction which gives rise to two acid-base equilibria for a monoprotic acid at the silica/water interface will be discussed in more detail in section 4.5.

4.4 Full Thermodynamic State Information

Data obtained with the $\chi^{(3)}$ technique can be used to track the interfacial charge density, the interfacial potential, and the interfacial free energy density with high sensitivity and with a wide dynamic range. These parameters provide important information for understanding the driving forces for pollutant binding in the environment.

Combining the charge densities obtained for pH 6.4 and pH 11.2 with Eq. 4.5 for the fraction of carboxylic acid groups deprotonated at each pH allows the charge density to be determined for the entire experimental bulk pH range. Dividing the interfacial charge density by the charge on an electron (e) gives the absolute number of deprotonated carboxylic acid groups per cm^2 at the silica/water interface as a function of bulk pH. Fig. 4.3 shows that there are at least 3×10^{13} carboxylate groups per cm^2 at the interface at pH 12. Comparatively, at pH 7, the carboxylate density is only $\sim 10^{11}$ carboxylate groups per cm^2 , indicating that the vast majority of carboxylate groups remain protonated at pH 7. This is consistent with the charge density

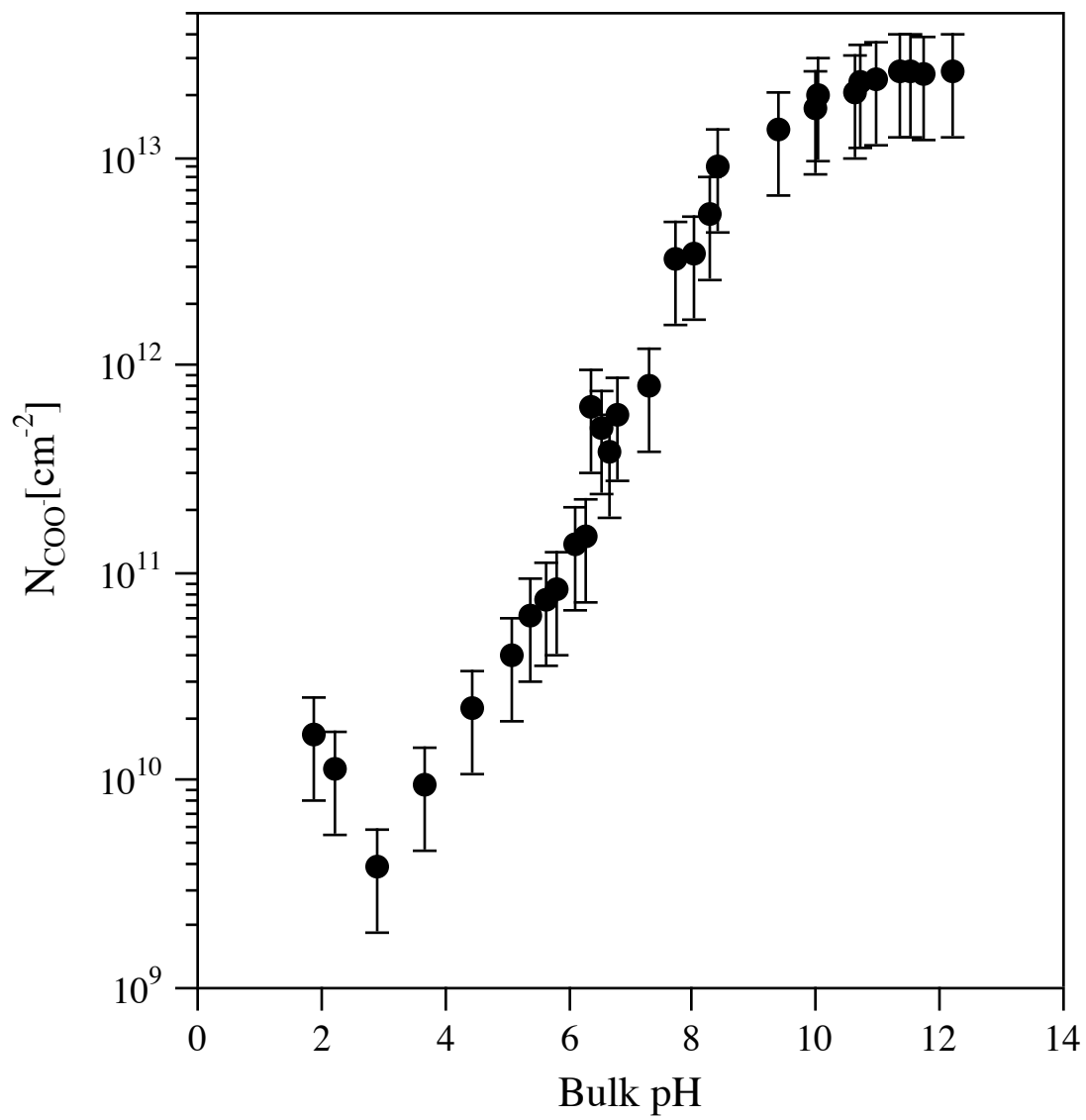


Figure 4.3

experiments, which showed that the charge density at pH 6.5 is two orders of magnitude lower than the charge density at pH 11.2. Therefore, approximately 1% of the carboxylic acid groups are deprotonated around neutral pH.

Additionally, since the $\chi^{(3)}$ technique samples the interfacial potential, Φ can be determined as a function of bulk pH (Fig. 4.4). In this plot, $\Delta\Phi$ is plotted relative to the average of the data points for low bulk pH, where a potential close to zero would be expected. Note the wide dynamic range of the second harmonic measurements; scatter in the data becomes evident below 10^{-4} V. As a point of comparison, Hu and Bard used atomic force microscopy (AFM) to study a similar system of carboxylic adlayers, and determined the interfacial potential.¹⁶ There is good quantitative agreement between our work and the AFM measurements. However, the dynamic range of SHG is much greater than AFM, as evidenced by the fact that in their work the first non-zero data point for potential is at 10 mV, which is two orders of magnitude greater than the observed sensitivity limit for SHG.

Although it is very useful to understand interfacial properties such as charge state and pK_a values, a key goal of these studies is to quantitatively determine the driving force for adsorption - the interfacial free energy, γ , which is also the surface tension. The Lippmann equation^{8,18} relates the interfacial free energy density to the potential and interfacial charge density according to:

$$\gamma = |\Delta\Phi|\sigma \quad 4.6$$

This relationship stems from the attraction of ions to the oppositely charged static field at the interface in the adjacent diffuse double layer. However, these ions, all the same charge, laterally repel one another at the interface, increasing the interfacial free energy. This physical

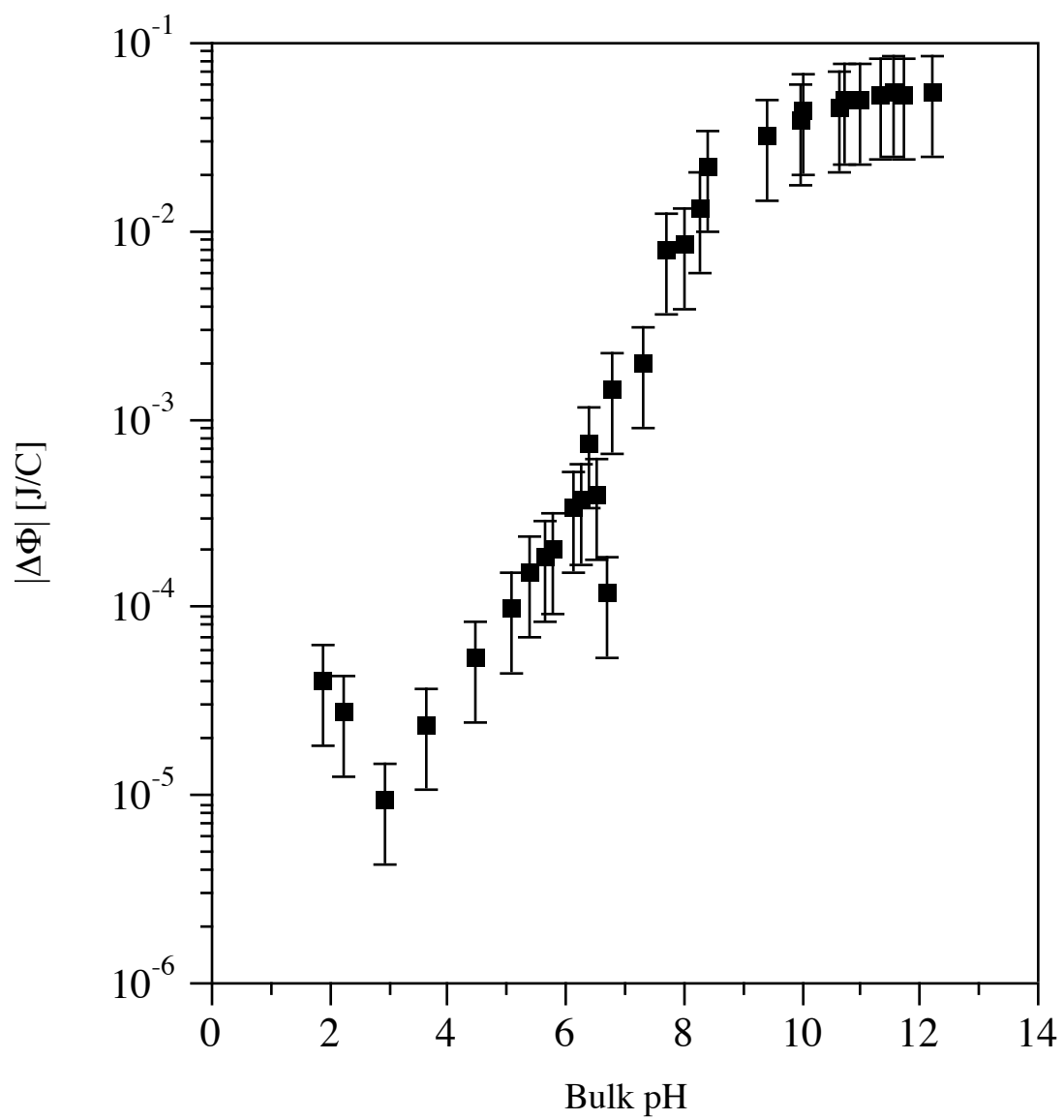


Figure 4.4

model has been shown to be useful in surface science as well as biology¹⁹ despite the fact that it ignores solvation spheres and sterics.

Since SHG allows the quantitative determination of both interfacial charge density (σ) and interfacial potential (Φ_0), applying the Lippmann equation to our SHG results gives the interfacial free energy density as a function of bulk pH (Fig. 4.5). For the carboxylic acid samples studied here, the interfacial free energy density ranges from 10^{-10} J/m² for low pH values to 10^{-2} J/m² for basic conditions. The wide dynamic range of SHG is again evident in the data. Since adsorbate binding to interfaces is driven by the minimization of free energy, quantitatively determining the thermodynamic parameter which drives binding at environmentally relevant interfaces is important for a complete understanding of pollutant binding processes in the environment.

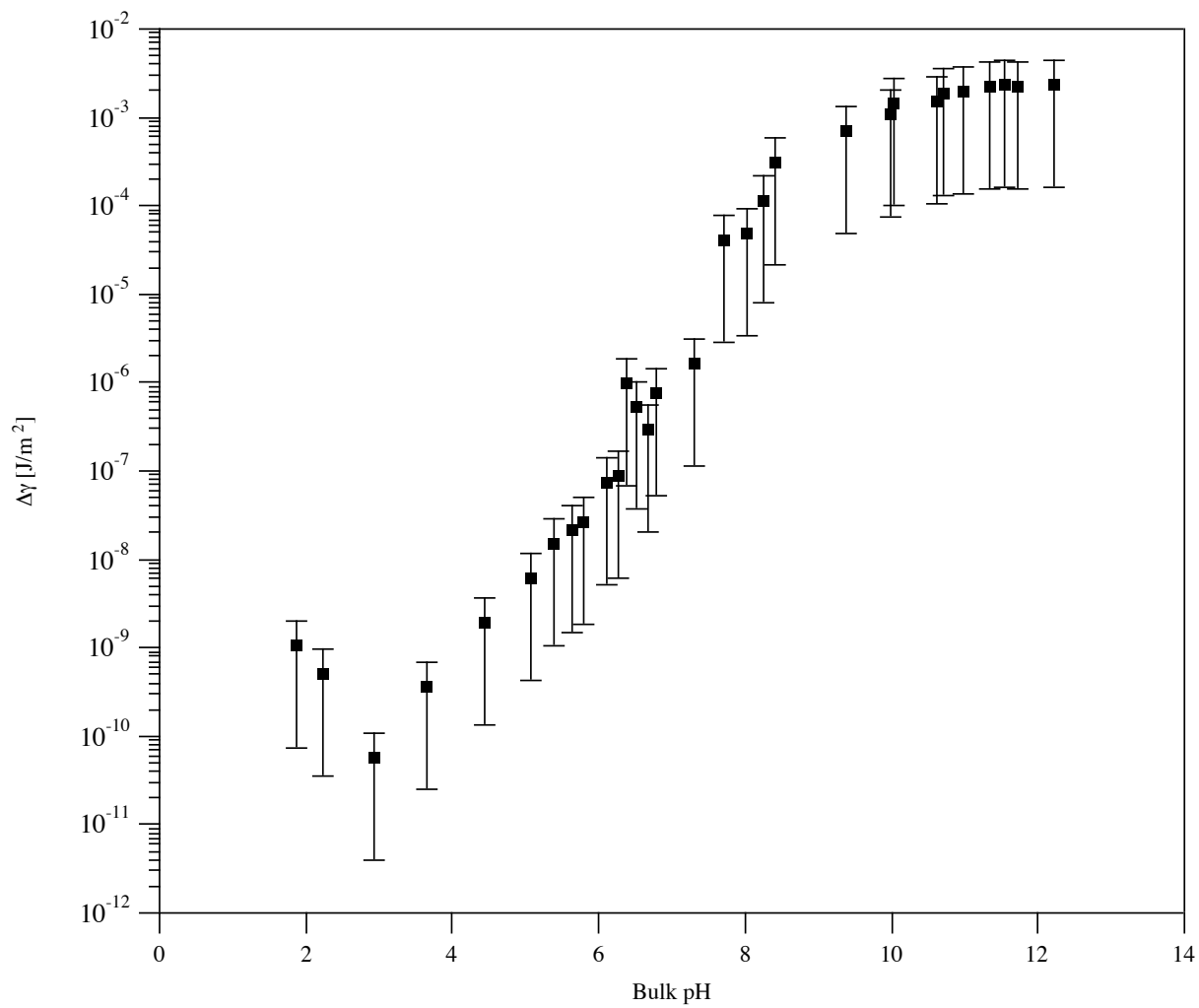


Figure 4.5

4.5 Environmental Implications and Conclusions

In this work, the $\chi^{(3)}$ technique has been shown to be a powerful and sensitive technique for probing environmentally relevant systems. The detailed data derived from SHG measurements guide the development of a physical picture of the carboxylic acid-functionalized silica/water interface (Figure 4.6), incorporating the observation of two acid-base equilibria for a monoprotic acid. Carboxylic acid groups at defect sites such as grain boundaries or adlayer holes, where the ionizable carboxyl groups are solvated by water in a manner similar to bulk aqueous solution²⁰ are associated with the lower pK_a value (5.6). This value is close to a pK_a of 5, approximately the pK_a value for monoprotic carboxylic acid groups in dilute aqueous solutions.²⁰ The higher pK_a value (9) is consistent with the presence of lateral hydrogen-bonding networks within the interfacial plane. The hydrogen-bonding network stabilizes the protons at the interface, therefore deprotonation of these carboxylic acid groups is energetically unfavorable¹⁵ and the carboxylic acid groups remain protonated until the aqueous phase is sufficiently alkaline.

The concept of a hydrogen bonding network affecting the ionization of carboxylic acid groups is consistent with previous work performed by Whitesides²¹ and Gershevitc and Sukenik.²² Whitesides and coworkers used contact angle measurements to show a shift in the pK_a of self-assembled monolayers terminated with carboxylic acid groups as compared to bulk values. However, they observed a single pK_a value, indicating that they likely studied very ordered monolayers and did not have the sensitivity to detect the lower pK_a value. More recent work by Gershevitc and Sukenik observed two pK_a values for carboxylic acid terminated adlayers on silicon with a native oxide layer, as determined by attenuated total reflection infrared spectroscopy. These two scenarios are consistent with the observation that glacial (pure)

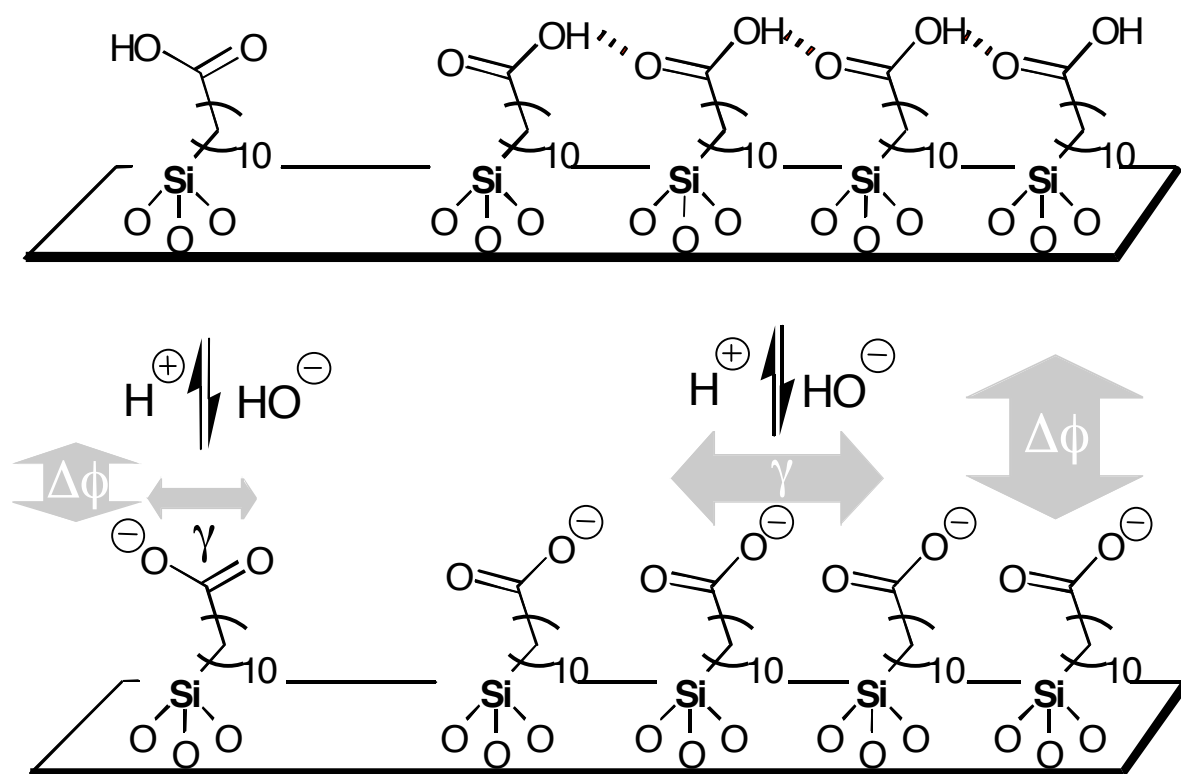


Figure 4.6

acetic acid does not conduct electricity because all of the acetic acid molecules remain protonated, stabilized by a hydrogen bonding network. When water is added to acetic acid, it disrupts the hydrogen bonding network, causing some of the acetic acid molecules to ionize. Once ionized, acetic acid with added water acts as an efficient conductor.²³

Due to the observed dual pK_a behavior, this work has important implications for computer modeling of pollutant transport in environmental systems. When modeling the organic groups contained in humic and fulvic acids at the surface of a mineral oxide particle, it is critical to use pK_a values determined by surface specific measurements. For example, this work demonstrates that simply assuming that the pK_a value of the surface-bound carboxylic acid group is the same as the bulk pK_a value underestimates the complexity of the system. Models based on the bulk pK_a , therefore, may not properly predict pollutant binding. The pK_a at the interface could be very different from the value observed in the bulk, and there may be multiple pK_a values for a monoprotic acid. In keeping with the idea of natural organic matter as groups of associated hydrophilic moieties presented by Sutton and Sposito,² it is likely that carboxylic acid groups in NOM are involved in hydrogen bonded networks, and thus remain neutral near pH 7. However, there could also be regimes where the carboxylic acid groups are disordered, thus not involved in hydrogen bonded network, and therefore deprotonated near pH 7. This work indicates that a pollutant molecule which approaches carboxylic acid groups adsorbed to different areas of a mineral oxide particle may encounter very different surface chemistry, even though the bulk pH and local pH is constant (Fig. 4.7).

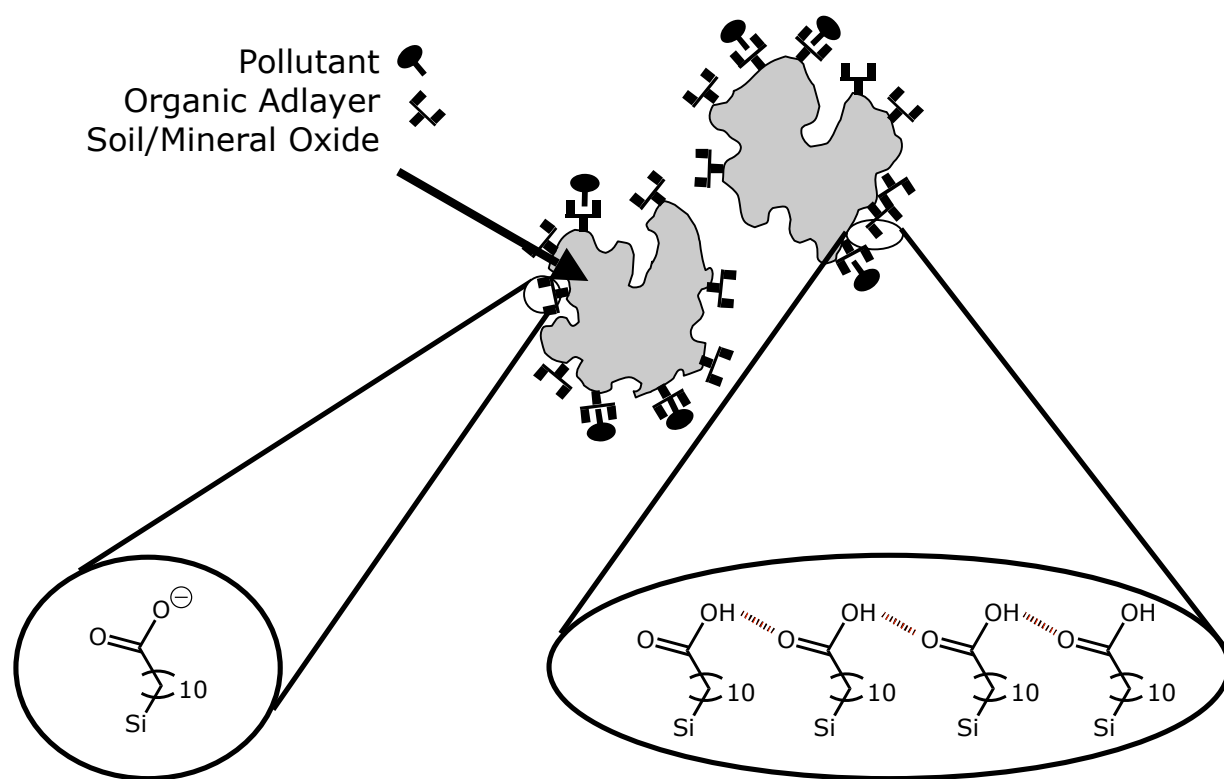


Figure 4.7

Chapter 5

Manganese Interacting with Carboxylic Acid Groups at the Silica/Water Interface

Portions of this chapter are reproduced in part with permission from:

Konek C.T.; Musorrafiti M.J.; Voges A.B.; Geiger F.M. “Tracking the interaction of transition metal ions with environmental interfaces using second harmonic generation.” *Adsorption of Metals by Geomedia II* Ed. Mark Barnett and Douglass Kent. Elsevier series Developments in Earth and Environmental Sciences. **2007**. Copyright 2007, Elsevier.

5.1 Manganese in the Environment

Manganese is a critical trace element important for both plants and humans, but in excess concentrations it is considered a pollutant and is toxic to life. In plants, manganese is an essential component of many enzymes. However, under conditions of excess manganese concentration, the plant can no longer regulate these enzymes, resulting in cell death.¹ In humans, manganese is responsible for the miner's disease manganism, which is associated with symptoms similar to Parkinson's disease.^{1,2} When manganese enters the bloodstream, it is able to pass the blood-brain barrier, and is preferentially retained in the brain relative to other organs.² Chronic manganese exposure generally results in neurodegenerative diseases with long latency periods. This delay in the onset of symptoms makes it difficult to assess what role, if any, manganese plays in the onset of diseases associated with advancing years.²

Manganese is ubiquitous in the environment – it is the twelfth most abundant element and fifth most abundant metal in the earth's crust.² Manganese is most commonly found in minerals as pyrolusite (MnO_2). It is also found in groundwater as the aqueous Mn(II) ion at an approximate background concentration of 4 ppb.¹ Although the United States Environmental Protection Agency only specifies a secondary, non-enforceable standard of 0.05 mg/L,¹ states such as Minnesota have adopted 100 ppb as a contamination limit.³ Nevertheless, manganese is often found in concentrations of 1000 ppm (18.2 mM) in groundwater near igneous rocks.³ Anthropogenic sources of manganese include acid mine drainage, industrial waste, and fertilizer. Over 70% of industrial manganese is used in making steel as a deoxidizing and desulfurizing agent.¹ Additional industrial uses for manganese include textiles, dry-cell batteries, and chemical manufacturing.¹ Manganese contamination in groundwater is expected to be a continuing problem in countries such as China and India.^{4,5}

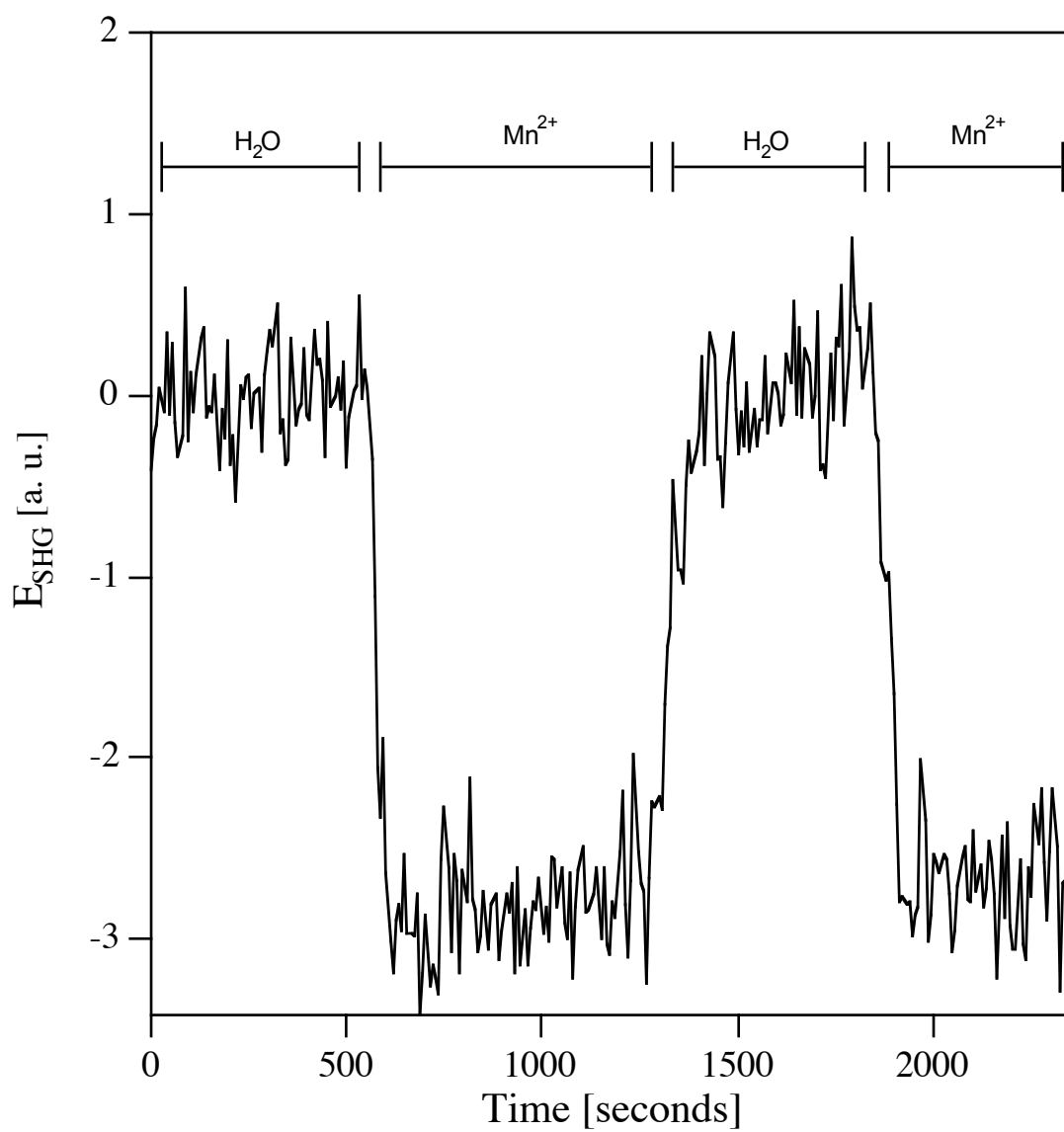
As pointed out earlier, processes which control the speciation, transport and ultimate fate of manganese in the environment occur at mineral/water interfaces. The chelation of manganese by carboxylic acid groups may play a role in the biogenic oxidation of manganese (II) to the solid Mn (IV)⁶⁻¹⁰ and also in the geochemical transport of manganese.¹¹

5.2. Manganese Mobility

In Chapter 4, we ascertained the charge state of the carboxylic acid-functionalized silica/water interfaces used in this work. At pH 7 they are mainly neutral, but contain approximately 1% deprotonated carboxylic acid groups. We proceeded to expose this interface to a solution containing divalent manganese ions to determine the nature of the interaction between manganese and carboxylic acid groups covalently bound to the silica/water interface. All manganese experiments are performed by dissolving MnSO₄ in Millipore water and subsequently adjusting the solution to pH 7. All solutions are exposed to atmosphere overnight to allow dissolved CO₂ concentrations to equilibrate. Dilute basic solutions are used to adjust the bulk solution pH to ensure that local regions of high pH did not cause the formation of solid manganese oxide. Additionally, UV-vis spectra show no formation of manganese carbonate solid over the timescale of the experiment. During the experiment, we take aliquots of the manganese solution from the effluent to perform off-line analysis of the manganese concentration using an ICP-MS with a Varian ICP Spectrometer. Until the measurement, samples are stored in clean fused quartz vials which had been thoroughly rinsed with the effluent solution.

To probe the interaction of manganese with carboxylic acids bound to a mineral oxide surface, we prepare organic adlayer samples as outlined in our previous studies.¹² Using second harmonic light at 310 nm, we first performed an adsorption trace to determine the mobility of

manganese across our carboxylic acid functionalized surface. Fig. 5.1 shows a decrease in the SHG E-field as manganese ions at a bulk solution concentration of 1.2 mM are passed across the interface at pH 7. This E-field decrease is consistent with a $\chi^{(3)}$ effect resulting from manganese cations binding to the carboxylic acid groups at the interface, leading to a decrease in the (negative) interfacial charge density and thus a smaller SHG E-field. Fig. 5.1 shows that when the manganese flow is stopped, and the water flow turned back on, the SHG E-field increases again to the original level. This experiment indicates that the interaction between the Mn(II) ion and the surface is fully reversible. This result suggests that a strong, irreversible chelation effect is not controlling the binding. Considering the well-known ability of carboxylic acid groups to chelate metal cations and the favorable Coulombic interaction between a dissolved cation and a negatively charged surface, it may be surprising a strong chelation effect is not observed. To more clearly understand the nature of the Mn(II) carboxylic acid interaction, we perform isotherm experiments to obtain quantitative thermodynamic information.

**Figure 5.1**

5.3 Manganese Isotherm

To quantify the thermodynamics of the manganese interaction with interfacial carboxylic acid groups, the dependence of the second harmonic E-field on manganese concentration is determined (Fig. 5.2) for pH 7. We gradually increased the concentration of manganese flowing across the interface while maintaining constant electrolyte concentration (NaCl) in the bulk solution. Since the SHG E-field depends on the interfacial charge density and thus the amount of manganese adsorbed to the interface, an isotherm can be constructed by tracking the SHG E-field decrease as a function of bulk manganese concentration. This methodology follows the $\chi^{(3)}$ experiments by Eienthal and Salafsky¹³ probing cytochrome *c*, which has a +9 charge, adsorbing to silica at neutral pH. To obtain thermodynamic information, we need to relate the Mn surface coverage to the second harmonic E-field via the surface charge density. The Langmuir model allows us to relate the bulk concentration to surface coverage according to:

$$\theta = \frac{KC}{1 + KC} \quad 5.1$$

where θ is the relative surface coverage of the transition metal at the interface, K is the equilibrium binding constant, and C is the manganese ion concentration in bulk solution.¹⁴ Eq. 5.1 directly relates the surface coverage to the interfacial charge density. The Gouy-Chapman model allows us to relate the charge density to the interfacial potential, which modulates the second harmonic signal. Equation 5.2 shows the combined Langmuir/Gouy-Chapman equation.

$$E_{SHG} = A - B \sinh \left[\left(\sigma - \sigma_{\max} \left(\frac{KC}{1 - KC} \right) \right) \sqrt{\frac{\pi}{2\epsilon kTC}} \right] \quad 5.2$$

where E_{SHG} is the square root of the observed number of photons, A and B are constants which

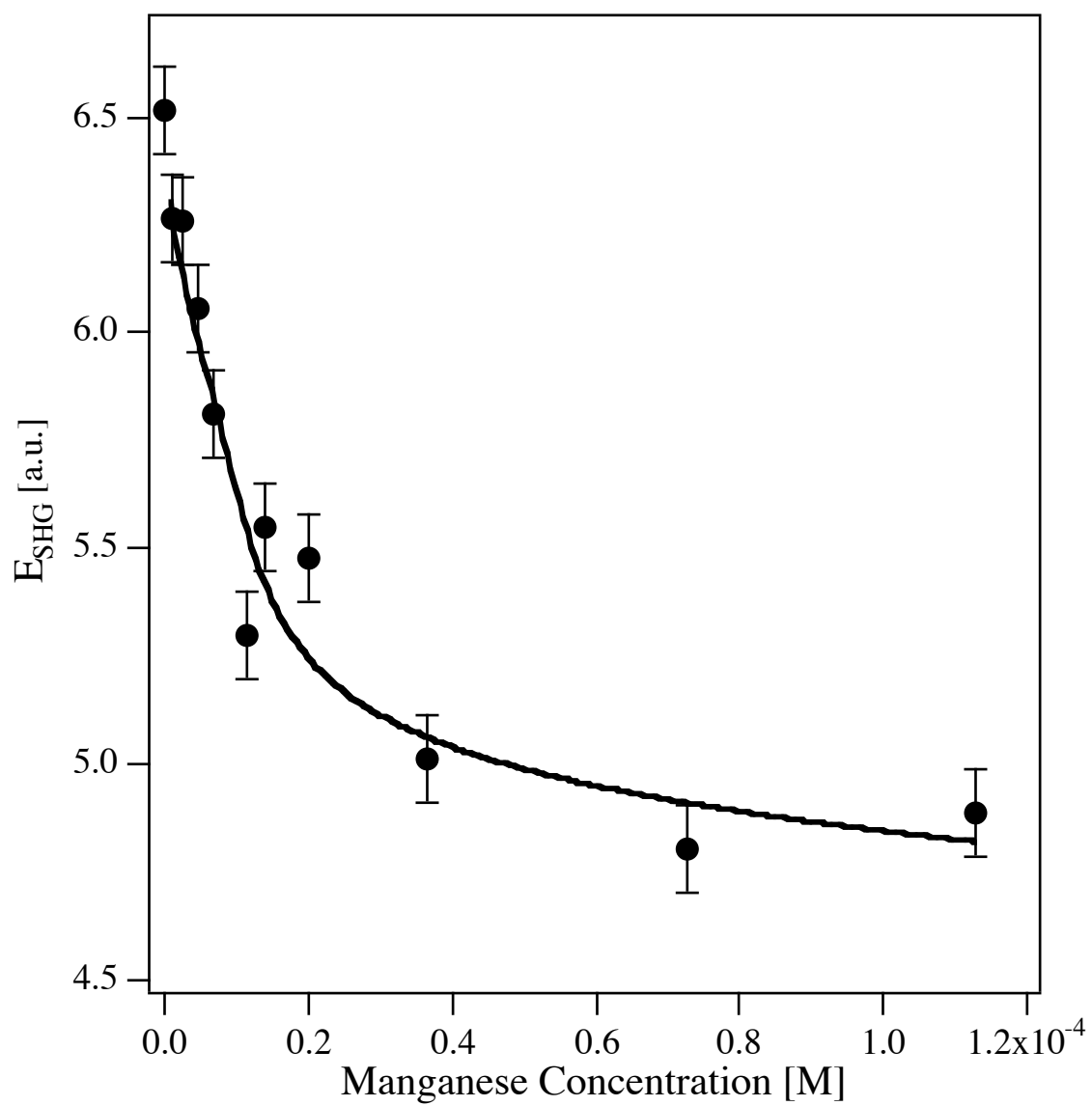


Figure 5.2

depend on the $\chi^{(2)}$ and the $\chi^{(3)}$ tensors respectively, σ is the interfacial charge density due to adsorbed Mn^{2+} , σ_{max} is the maximum interfacial charge density due to adsorbed Mn^{2+} , ϵ is the dielectric constant of bulk water, and T is the temperature. By fitting Eq. 5.2 to the isotherm data shown in Fig. 5.2, we obtain an equilibrium constant (K) of 1250 M^{-1} ($\pm 150 \text{ M}^{-1}$). The equilibrium constant is related to the free energy of adsorption, ΔG via:

$$\Delta G = -RT \ln(K * M_{\text{ref}}) \quad 5.3$$

Here, R is the universal gas constant, T is the experimental temperature (300K), and M_{ref} is the molarity of water (55.5M) chosen as the reference state.¹⁵ We calculate a free energy of adsorption of -27.8(3) kJ/mol. In the fitting, we used an initial interfacial charge density of $2.8 \times 10^{-4} \text{ C/m}^2$ to describe the interfacial carboxylate groups at pH 6.5.¹² The free energy of adsorption is consistent with approximately one hydrogen bond, and surface saturation occurs at about $40 \mu\text{M}$. If a direct Coulombic interaction is controlling the interaction between the Mn(II) and the carboxylic acid group, a much larger free energy of adsorption would be expected. These results support the idea that manganese binding is controlled by the solvation sphere via an outer-sphere mechanism. Assuming the manganese cations are binding at the interface as Mn^{2+} cations, the fit of the data shown in Fig. 5.2 with Eq. 5.2 results in a maximum interfacial charge density of $2.0(2) \times 10^{-2} \text{ C/m}^2$. With two positive charges on each manganese cation, this charge density corresponds to $6.2(6) \times 10^{12}$ adsorbed cations per cm^2 . This relatively low number density of adsorbed manganese ions can be reconciled by Coulombic repulsion and the size of the hydrated cations limiting the coverage at which the surface is saturated.

5.4 Interfacial Charge Screening Experiment

As discussed in Chapter 4, it is possible to perform an interfacial charge screening experiment to determine the interfacial charge density. In Fig. 5.2, we observe that the Mn ions decrease the charge density as more 2+ manganese ions adsorb to the interface, resulting in a decrease in SHG E-field. At surface saturation of Mn(II) and pH 7, the 2+ charge from each manganese ion should overwhelm the negative charge from the carboxylic acid groups, resulting in a net positive charge at the interface. An ion screening experiment allows us to test this theory. By keeping a constant flow of manganese ions flowing over the interface, while changing the background concentration of NaCl, a positive interfacial charge will show an increase in signal for increasing NaCl concentration. According to the governing equation for the $\chi^{(3)}$ technique, the second harmonic signal is produced from both the $\chi^{(2)}$ term and the $\chi^{(3)}$ term according to:

$$E_{2\omega} \propto \chi^{(2)} E_{\omega} E_{\omega} - \chi^{(3)} E_{\omega} E_{\omega} \Phi_0. \quad 5.4$$

In the absence of manganese, the potential (Φ_0) at the carboxylic acid functionalized surface is negative and Eq. 5.4 demonstrates that there is a constructive interference between the $\chi^{(3)}$ term and the $\chi^{(2)}$ term. This additive relationship is consistent with the fact that as the potential at the surface becomes more negative, we observe an increase in second harmonic E-field (see Chapter 4). Therefore, in the manganese isotherm experiments outlined above we observe a decrease in signal when we decrease the potential by using bulk ions to decrease the charge density. However, if the sign of the interfacial charge flips to a net positive, then we expect to see an increase in signal during a charge screening experiment. We can exploit this property to determine if, in fact, the manganese adsorption to the interface does cause a net positive charge

under saturation conditions for the manganese adsorbed to the interface. Additionally, this experiment will allow us to further test the charge density found from the data in Fig. 5.2.

As mentioned previously, at pH 7 the carboxylic acid surface has approximately 1% of the carboxylic acid groups deprotonated. As the Mn^{2+} cation adsorbs to the interface, the charge density is reduced until the net effect is of a positively charged interface. This polarity-switch is indeed observed in experiments where the manganese concentration in the aqueous solution is kept constant at 1.0 mM, and the NaCl concentration is increased over the course of the experiment. Fig. 5.3 shows that the SHG E-field gradually increases with increasing bulk ion concentration, which is consistent with screening a positively charged interface. Additionally, this experiment allows us to test the surface charge density determined from the data in Fig. 5.2. Using the interfacial charge density of $2.0 \times 10^{-2} \text{ C/m}^2$ in the Gouy-Chapman model yields a reasonable fit to the data.

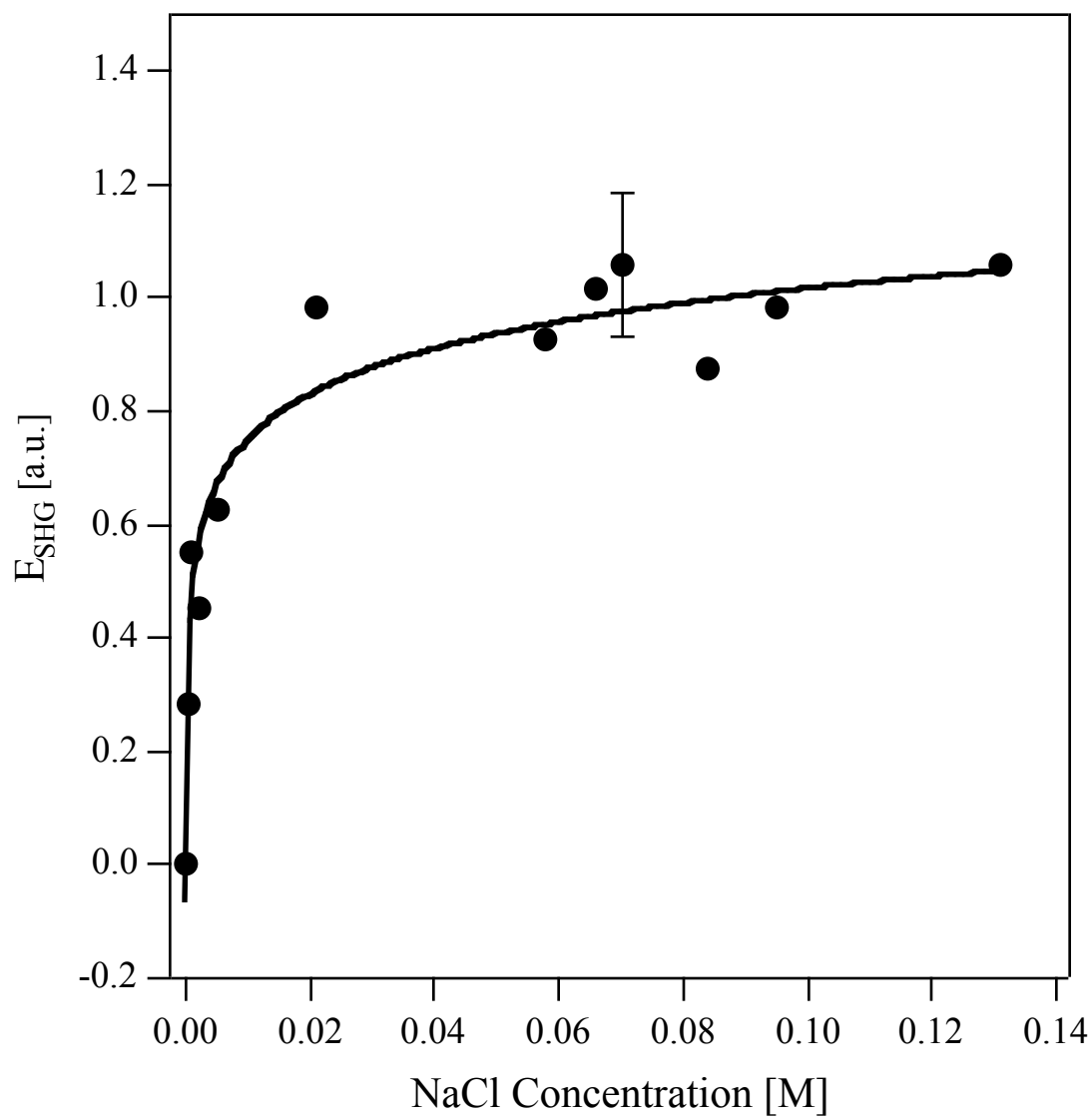


Figure 5.3

5.5 Conclusions

The results from this work demonstrate the versatility of second harmonic generation for studying pollutants at environmentally relevant interfaces. Past work in our group has focused on using resonantly enhanced second harmonic generation to track pollutants with electronic transitions located in the UV-visible region of the spectrum. These experiments probe thermodynamic, kinetic and structural information¹⁶⁻¹⁹ of pollutants in real time and in situ at environmentally relevant concentrations. However, many environmental pollutants do not contain suitable UV-vis transitions, and this work demonstrates the feasibility of using second harmonic generation to study ions that cannot be probed via resonantly enhanced SHG, while yielding important chemical information. These experiments exploit charge as an intrinsic label which allows us to track the populations of ions at the interface, and thus are applicable to a wide range of charged, environmentally relevant species.

Chapter 6

The Agricultural Antibiotic Morantel at the Silica/Water Interface

Portions of this chapter are reproduced in part with permission from:

Konek C.T.; Illg K.D.; Al-Abadleh H.A.; Voges A.B.; Yin G.; Musorrafiti M.J.; Schmidt C.M.; Geiger F.M. "Nonlinear optical studies of the agricultural antibiotic morantel interacting with silica/water interfaces." *Journal of the American Chemical Society*, **2005**, 127 (45), 15771-15777. Copyright 2005, American Chemical Society.

6.1 Morantel in the Environment

Previous chapters demonstrated how SHG can be used to provide molecular-level insight into the acid-base properties of carboxylic acid groups at the silica/water interface and information on the binding of manganese to carboxylic acid groups. In addition to understanding the interactions between pollutants and organic adlayers, it is important to understand the interactions between pollutants and the underlying mineral oxide itself. This chapter focuses on the agricultural antibiotic morantel interacting with the most abundant mineral oxide, SiO₂ or silica.¹

In 2007, the release of agricultural antibiotics and chemicals into the environment has recently received much attention.^{2,3} Approximately 70% of all antibiotic use in the United States occurs on animal farms,⁴ much of which is not used for therapy but instead to promote growth. Discharges of veterinary antibiotics can lead to increased drug resistance in biota. Understanding the transport and mobility of antibiotics in the environment^{5,6} is necessary to identify which bacteria are likely to come in contact with antibiotics, and thus develop resistance. These issues represent a major emerging problem for chemistry, biology, and engineering because of the increase in agribusiness over the past 50 years, which is anticipated to continue,⁷ and increase stresses on freshwater supplies.⁸

This work presents nonlinear optical studies that examine how morantel, a widely used agricultural antibiotic, interacts with a highly simplified mineral/water interface. Morantel (1,4,5,6-tetrahydro-1-methyl-2-(2-(3-methyl-2-thienyl)ethenyl) pyrimidine, see inset to Fig. 6.1) is a member of the tetrahydropyrimidine group that is used in the cattle industry as an antinematodal, or deworming, antibiotic.⁹ The interaction of this antihelmintic compound with acetylcholine receptors of the parasites is used to control and remove mature gastrointestinal

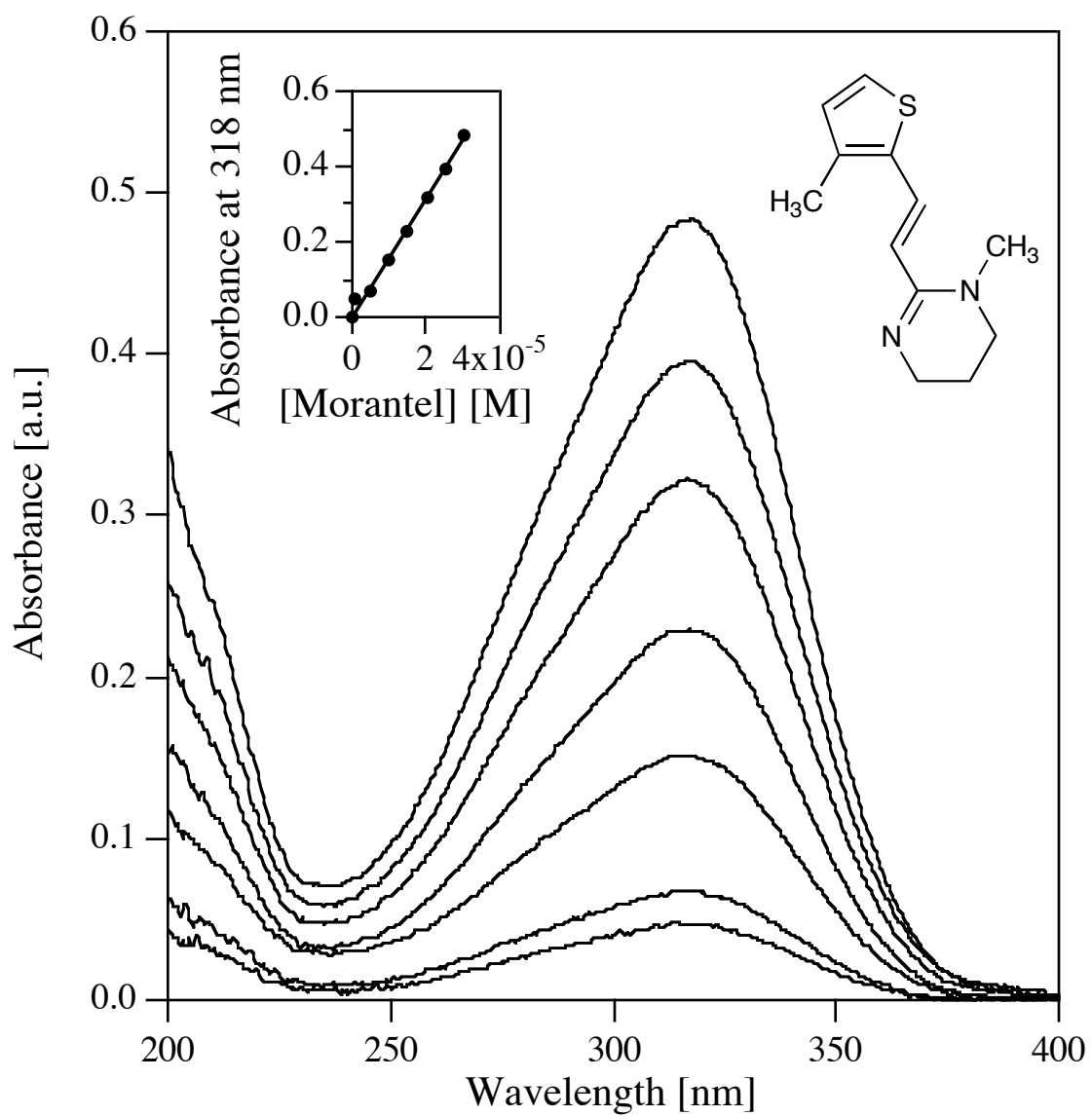


Figure 6.1

nematode infections in cattle and goats.⁹ Morantel is readily soluble in water¹⁰ and has a high potential for entering the environment.¹¹ It has been available in the United States since 1982, with average dosing levels of 4.4 mg/lb body weight of the animal.⁹ Only about one quarter of this amount is metabolized by the animal, with the remainder being excreted essentially unchanged.¹² On average 6600 kg of morantel are introduced into the environment every year in the United States.⁹

In addition to the environmental implications that morantel has for bacterial resistance, morantel can also be converted into the toxic chemical acrylic acid. Alkaline hydrolysis can yield *N*-methyl-1,3-propane diamine and 3-methyl-2-thianyl acrylic acid.^{9,13} Acrylic acid is listed in the EPA's toxic release inventory and is subject to several regulations, including the Clean Air Act, the Emergency Planning and Community Right-to-Know Act, and the Resource Conservation and Recovery Act.¹⁴ Given the possibility for acrylic acid formation and the development of drug resistance in parasites exposed to morantel present in farm runoff, determining the mobility of morantel in the environment is necessary in order to assess its potential for leaching into the ground water and its subsequent environmental fate.

In contrast to inorganic metal contaminants and many halogenated organic compounds, surprisingly little is known about the environmental fate of veterinary pharmaceuticals¹⁵ and their molecular-level interactions with mineral/water interfaces. This work seeks to fill this void while addressing important fundamental problems in studying environmental interfaces from a molecular perspective. While chemical binding and surface speciation in soils are generally governed by mechanisms operating at interfaces, chemical transport models commonly rely on pollutant-to-soil binding constants that are derived from bulk measurements.^{1,11,16-18} This chapter

will demonstrate how our surface-specific measurements yield data which can be included in the EPA's K_d model, a simple model used to estimate pollutant transport in the environment.

The K_d parameter is widely used to predict contaminant transport in the form of retardation factors,^{17,18} but the bulk measurements frequently used for obtaining K_d parameters from the initial slope of adsorption isotherms can overlook important molecular-level processes which may control binding events and often average over redox, pore diffusion and transport processes.¹⁹ Retardation factors derived from interface-specific binding studies may lead to improved predictions of contaminant transport in soils.¹⁹ Surface-specific approaches are complicated by the fact that many experimental techniques used for studying liquid/solid interfaces are limited by long signal integration times and low surface sensitivities.²⁰ This low sensitivity is especially important when considering the nonlinear relationship between aqueous phase concentration and surface coverage^{1,21-24} for small aqueous phase concentrations,^{22,23} which makes the extrapolation of data obtained with high bulk concentrations to environmentally representative concentrations problematic. Frequently used techniques for studying environmental interfaces include X-ray based techniques. X-ray absorption near-edge structure (XANES) and extended X-ray absorption fine structure (EXAFS) are extremely useful for identifying and characterizing metal-containing adsorbates.^{20,25-31} However, organic compounds are difficult to characterize, and even when studying metal-containing compounds, sensitivity issues can make the experiments challenging and real-time measurements of solute-surface binding processes difficult.³¹

6.2 UV-vis Spectroscopy

The morantel studies will utilize resonantly enhanced second harmonic generation (SHG), which is a surface specific technique, as outlined in Chapter 2. We first studied the UV-vis behavior of bulk aqueous morantel to identify electronic transitions in the molecule which we could exploit to obtain resonantly enhanced second harmonic signal. Based on the conjugated system observed in the structure (Fig. 6.1, inset), morantel is expected to demonstrate electronic transitions in the ultraviolet-visible region of the spectrum. The UV-vis measurements are performed by dissolving morantel citrate (Sigma) in Millipore water, and placing that solution in a quartz cuvette probed by an OceanOptics spectrophotometer. Fig. 6.1 shows the electronic transitions in the UV-Vis spectral region that are centered at 285 and 318 nm for morantel. The lower energy transition can be attributed to an $n \rightarrow \pi^*$ transition of the tetrahydropyrimidine moiety,³² which exhibits electronic resonances near 320 nm.³³ By plotting the UV-vis absorbance as a function of bulk concentration, the extinction coefficient can be measured using Beer's Law.³⁴ Fig. 6.1 (inset) shows, at a pH of 7, the extinction coefficient at 318 nm is $15.8(3) \times 10^3 \text{ cm}^{-1}\text{M}^{-1}$.

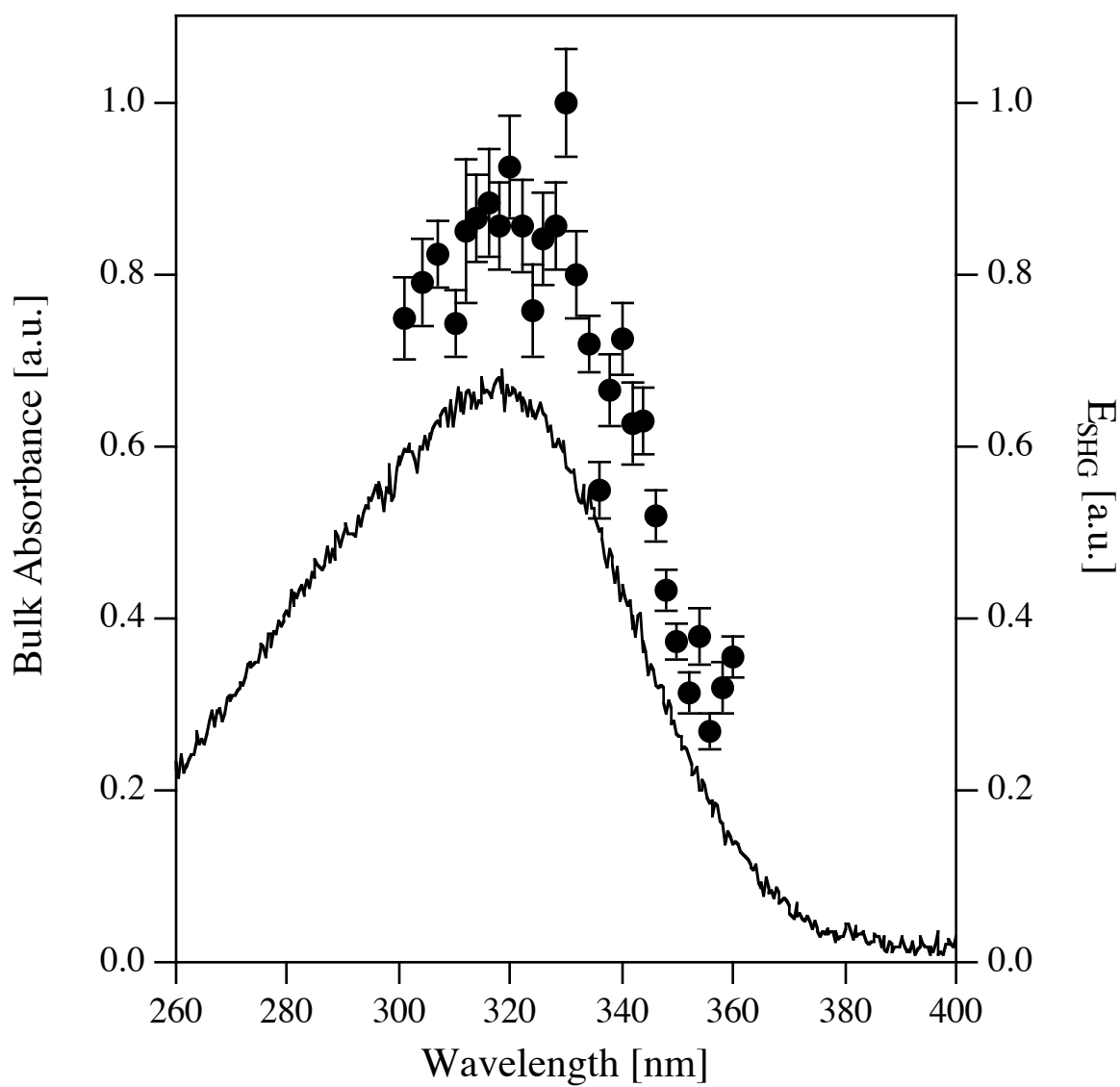


Figure 6.2

6.3 Second Harmonic Generation Spectroscopy

In resonantly enhanced SHG, the electronic transitions of the adsorbed species are studied by changing the probe wavelength and measuring the second harmonic signal, thereby effectively mapping out the UV-vis spectrum of morantel at the interface (for more detail, see Chapter 2). We subsequently compared the surface spectrum to the bulk UV-vis spectrum to understand how the electronic transitions might shift when morantel is adsorbed to the interface. Fig. 2 shows the SHG spectrum of morantel adsorbed at the silica/water interface (filled circles). The bulk solution is maintained at pH 7. The spectrum is taken at bulk concentrations resulting in surface adsorption saturation, as determined by adsorption isotherm measurements (vide infra). The spectral acquisition is carried out by recording the SHG intensity at a particular wavelength for five minutes. The probe wavelength is then changed by four nanometers and the data acquisition process is repeated. The total spectrum is recorded in increasing and decreasing SHG wavelength steps of two nanometers over a time period of six hours. Fig. 6.2 shows that the SHG spectrum of morantel tracks the bulk UV-Vis absorbance over the wavelength range investigated here, having a similar peak position as the bulk solution spectrum. This suggests that the $n-\pi^*$ transitions, which are presumably responsible for the SHG signal resonance enhancement, are not significantly perturbed when morantel is adsorbed at the silica/water interface.

6.4 Mobility

The resonance enhancement demonstrated in the SHG spectroscopy can be utilized to track morantel in real time at the silica/water interface (Figure 6.3). A probe wavelength of 580 nm is used in these experiments, and morantel is tracked at an SHG wavelength of 290 nm. After recording the SHG background signal from the neat interface while flowing bulk water maintained at pH 7 across the interface (no morantel present), the analyte solution (pH 7) flow is turned on using a Teflon on-off valve. The SHG signal increases, consistent with morantel adsorption and SHG resonance enhancement, and remains at a constant level once steady state conditions with respect to adsorption and desorption are reached. This equilibrium SHG signal is then taken to represent the relative equilibrium surface coverage at the analyte concentration at which the experiment was carried out. The analyte solution flow is then turned off while maintaining the flow of bulk water at pH 7. The SHG signal decreases, consistent with morantel desorption from the interface. These experiments indicate that morantel binding is reproducible and reversible, which is consistent with a high degree of mobility for morantel in a silica-rich soil environment.

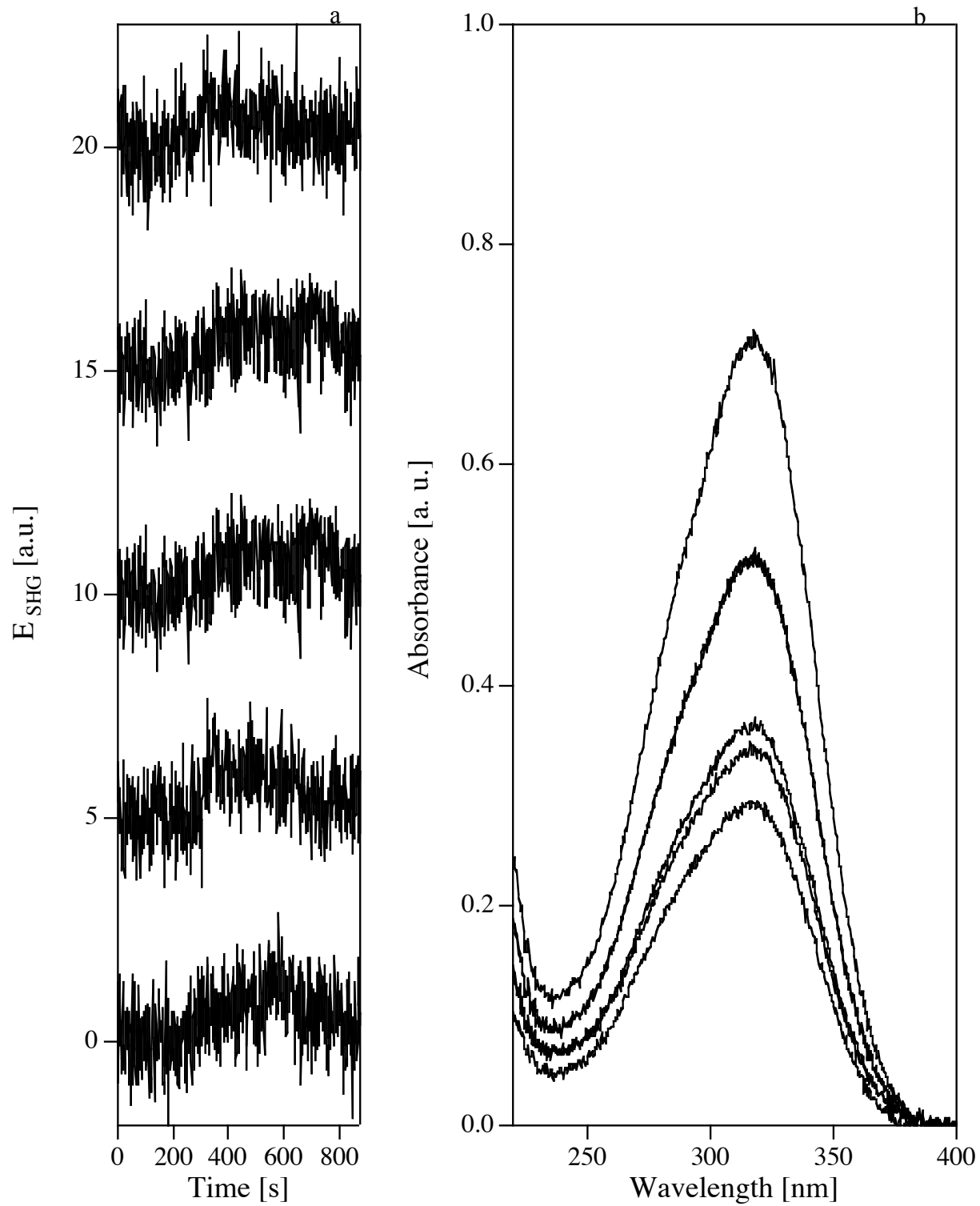


Figure 6.3

6.5 Adsorption Isotherm

To obtain quantitative thermodynamic information about the morantel/silica system, we perform an isotherm experiment that determines binding parameters from the plot of relative surface coverage versus bulk concentration. An isotherm is constructed by gradually increasing the bulk concentration of morantel flowing over the surface while tracking the amount of morantel adsorbed to the surface. Based on the increase in second harmonic E-field, we monitor the relative surface coverage in real time. By simultaneously tracking the bulk UV-vis spectrum in-line corresponding to each bulk morantel solution, we can calculate the concentration of morantel in the bulk. The morantel concentration in the reservoir is increased and the experiment is repeated. Morantel is flushed from the system by switching on the flow of water in between each data point, and observing the decrease in both bulk UV-vis and SHG E-field to background levels. The concentration of the analyte solution in a typical experiment ranged from 6×10^{-7} to 5×10^{-5} M, thereby covering the lowest detectable limit set by the United States Agricultural Administration Food Safety and Inspection Service (USDA FSIS), 0.25 ppm, or 1×10^{-6} M, referenced to 1L of water.³⁵ A series of adsorption traces and each corresponding UV-vis spectrum is shown in Fig. 6.3.

Figure 6.4 shows the adsorption isotherm of morantel citrate at the silica/water interface at pH 7 and room temperature. It can be seen that the morantel surface coverage gradually levels out, indicating surface adsorption saturation at a bulk concentration of about 1×10^{-5} M, and that the isotherm appears to follow the Langmuir model. Fitting the model to the data results in an equilibrium binding constant, K , of $2.3(3) \times 10^7$, referenced to the molarity of water under standard conditions (55.5 M).¹⁹ At 300 K, the standard free energy of adsorption, $\Delta G^{\circ}_{\text{ads}}$, is found to be $-42(3)$ kJ/mol. This free energy is on the order of hydrogen bonding interactions between

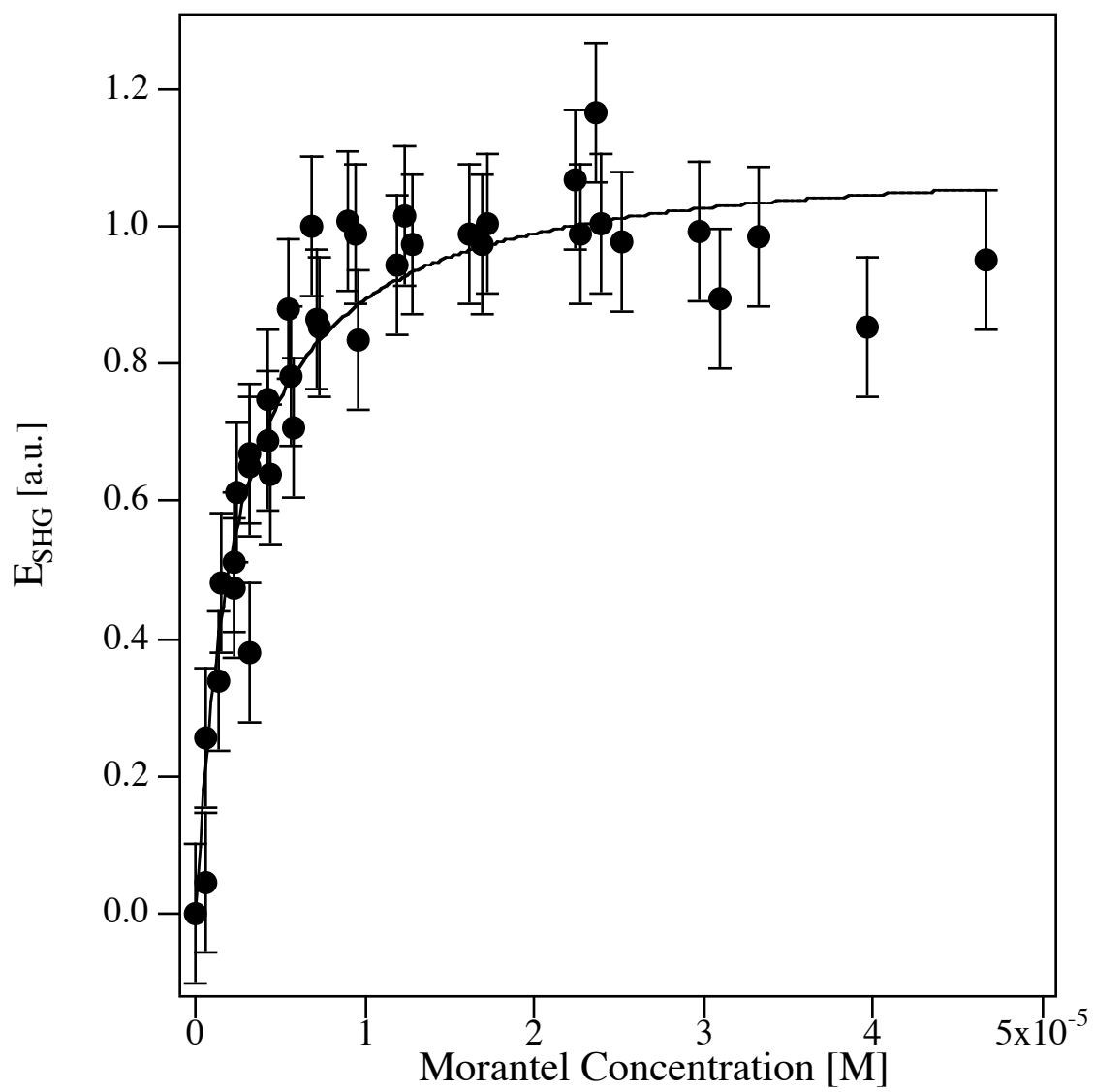


Figure 6.4

the morantel and the silica/water interface. This interaction is likely to be mediated by either the nitrogen centers or the sulfur center in morantel, or a combination of the two.

6.6 Orientation Studies

SHG studies aimed at tracking changes in the orientation of the adsorbed morantel species were carried out at surface saturation of adsorbed morantel and submonolayer surface coverages of morantel, as determined by the adsorption isotherm, which correlate to bulk concentrations of 5.2×10^{-5} M and 2.5×10^{-6} M, respectively. Specifically, two kinds of polarization studies are performed, by setting the polarization of the fundamental excitation frequency at 640 nm at a 0-degree angle (p-in), or a 45-degree angle (45-in) from the plane of incidence. In both sets of experiments, the SHG signal intensity is recorded at 320 nm as a function of the polarizer-analyzer angle on the output side.

The results of these polarization measurements are shown in Figure 6.5 for a saturated surface of adsorbed morantel. As expected, second harmonic signal is strongest for the p-in/p-out polarization combination. The p-in/s-out polarization response, which is allowed for chiral systems but not for achiral interfaces,³⁶ exhibits a zero-intensity SHG response within experimental error, which is expected for morantel citrate. The submonolayer surface coverage also displays similar polarization dependence.

When probing a surface saturated with adsorbed morantel with the 45-in polarization, the SHG response of the interface is lowest at a polarizer-analyzer angle near 120 degrees (the null angle). For this input polarization, the null angle³⁷ does not change for submonolayer surface coverages of morantel, indicating little or no orientational rearrangement of the adsorbate with changing surface coverage. In addition, the ratio of the SHG signal intensity for the 45-in/p-out

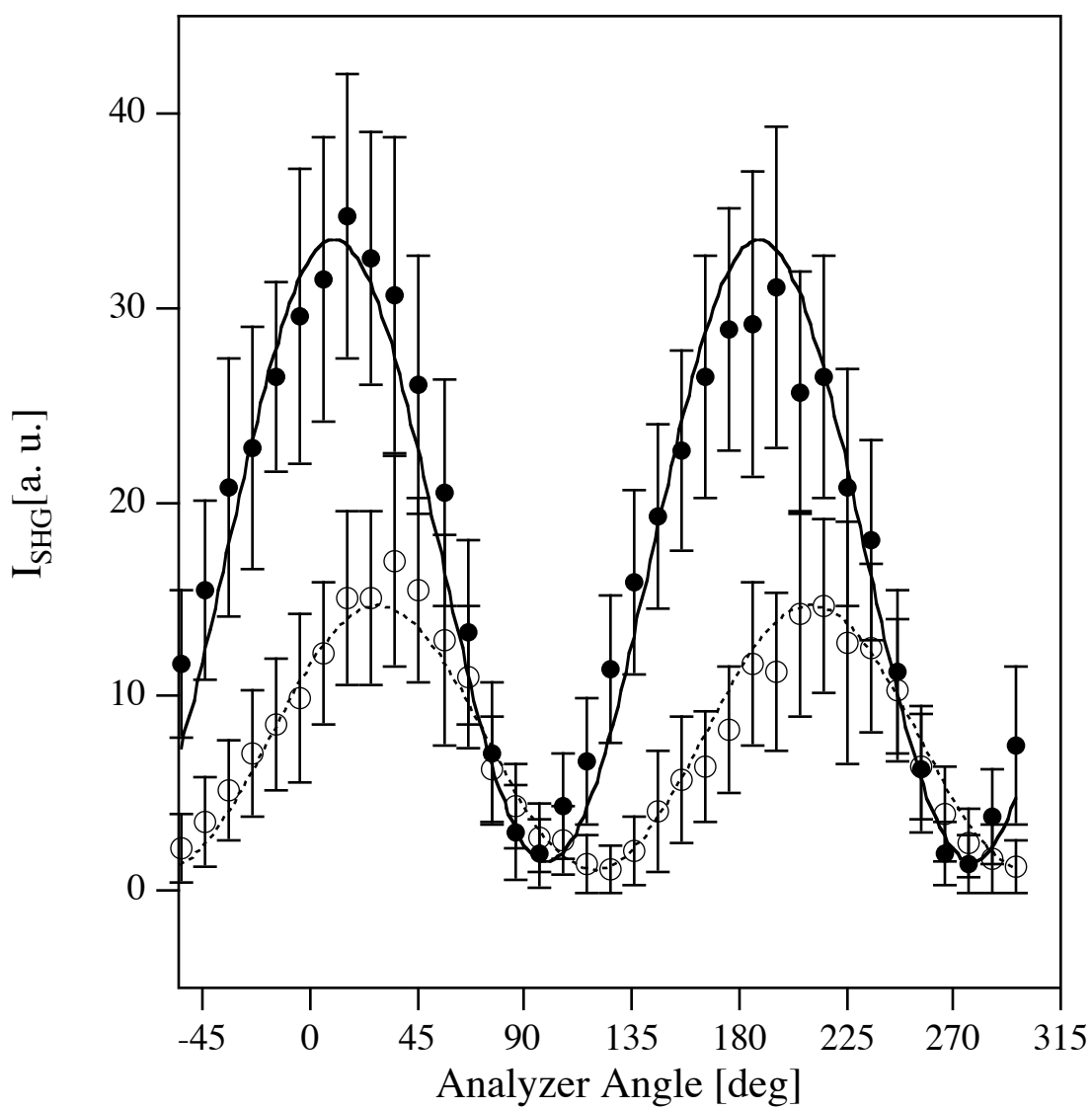


Figure 6.5

and the 45-in/s-out polarization combinations is approximately four, indicating an approximately four-fold stronger SHG response of morantel along the surface normal than along the interface. If the conjugated π -electron system in morantel can be viewed as the main pathway for movement of the electrons which give rise to the nonlinear optical response, then morantel can be considered a rod-like chromophore. The polarization measurements are consistent with the notion that the conjugated π -electron system in morantel is slightly tilted away from the surface normal when it is adsorbed at the silica/water interface. Following the literature,³⁶⁻⁴⁰ an orientation parameter D of 0.528 was calculated for this system. The orientation parameter can be related to the molecular tilt angle:

$$D = \frac{\langle \cos^3 \theta \rangle}{\langle \cos \theta \rangle} \quad 6.1$$

where the brackets indicate an orientational average, and θ is the molecular tilt angle with respect to the surface normal. Assuming a delta function – which is equivalent to assuming each adsorbed morantel has the exact same tilt angle - for the orientational distribution of the adsorbed morantel would result in a tilt angle of 43 degrees. However, the angle distribution is likely to be broader than a delta function. We performed simulations to understand what tilt angles are possible if the distribution of molecular tilt angle was not a delta function. Figure 6.6 shows these simulations plotted in a polar graph. In Fig. 6.6, the radial axis is the D parameter, and the angle is the molecular tilt angle. The D parameter, as calculated from the experimental values, is the dark line at 0.528, and the possible D parameters for each distribution of molecular tilt angles is shown in gray. Note that for all distributions calculated, the lines describing possible D values only intersect with 0.528 for angles greater than 43° . Therefore, we can conclude that the ensemble average tilt

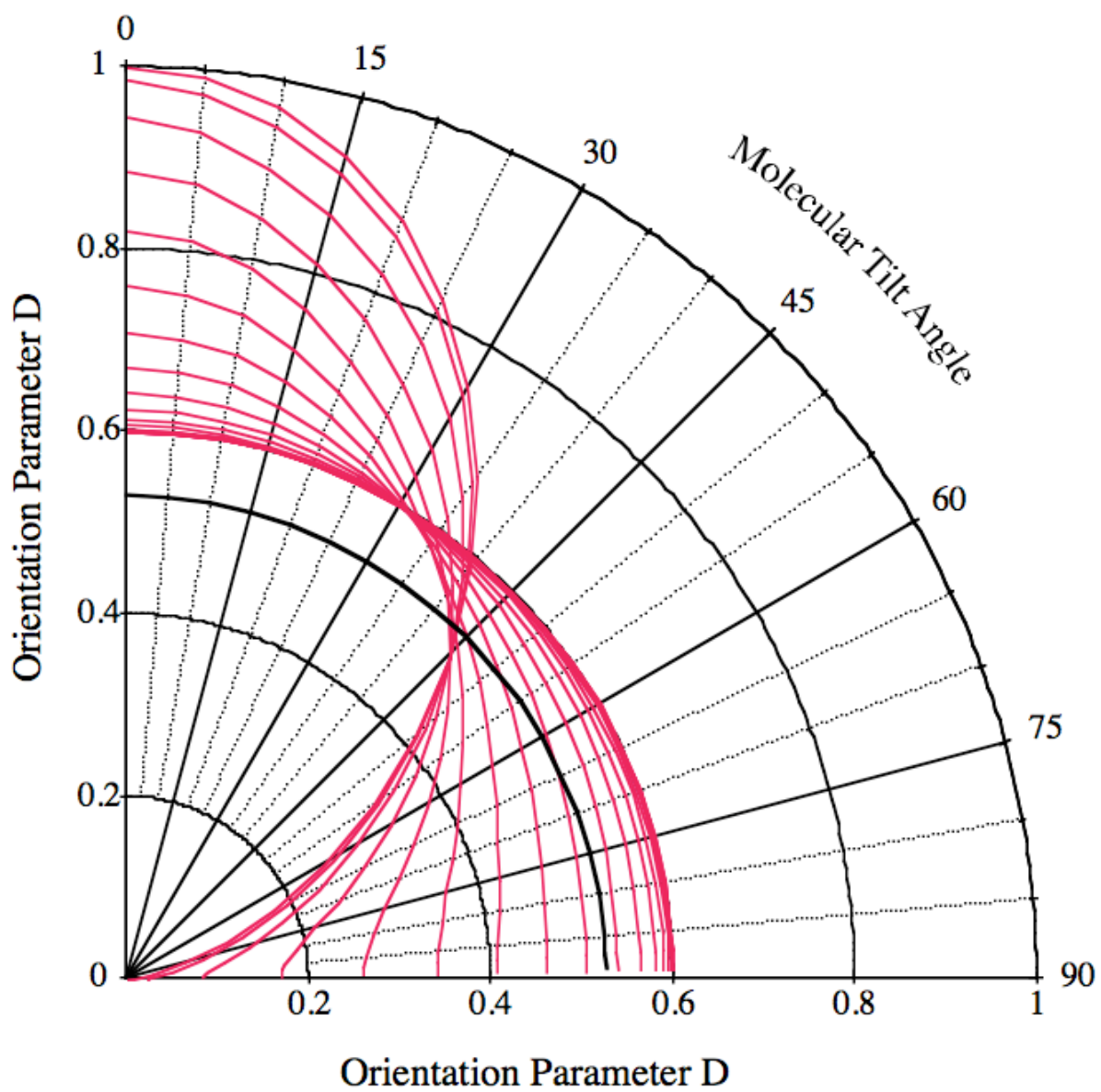


Figure 6.6

angle for morantel is 43° or greater from normal. Details of these calculations are published elsewhere.⁴¹

6.7 Environmental Implications

The equilibrium binding constant derived from our SHG adsorption isotherm measurements can be used to assess the mobility of morantel in silica-rich soil environments. To this end, we applied the K_d model to our data.¹⁷ The K_d model is frequently used to predict the degree to which pollutant transport is slowed down due to heterogeneous binding events occurring at mineral/water interfaces. The retardation factor, R , is given by

$$R=1+(\rho/n)K_d \quad 6.2$$

where ρ is the soil density, n is the soil porosity, and the K_d parameter is related to the binding constants calculated from our isotherm data. After appropriate variable transformation of the equilibrium constant to the K_d parameter,^{19,42} the retardation of morantel is calculated to be 2-5% with respect to ground water flowing through soils when using typical ρ/n ratios between 4 and 10.¹ This value agrees with our reversibility traces which also indicate that morantel is expected to be highly mobile in a silica-rich soil environment.

Given the low retardation factor calculated from the measured adsorption isotherms, it is highly likely that morantel and related pharmaceuticals can leach into the ground water during raining events and possibly into municipal water systems. At low concentrations, it is difficult to remove these compounds in water treatment plants, which suggests a low but constant background concentration of pharmaceuticals in municipal water systems. Daily intake of such water over long periods of time could thus lead to adverse health effects in humans, especially in farming communities. Additionally, the high mobility of morantel indicates that it is likely to

come into contact with a wide range of bacteria, increasing the likelihood that strains of bacteria will develop resistance to antibiotics.

6.8 Conclusion

The results presented in this chapter are the first direct, interface-specific studies that address the mobility of a widely used agricultural pharmaceutical, morantel, which is commonly present in farm runoff. The measurements are carried out using nonlinear optical laser spectroscopy and allow us to study the interaction of morantel with silica/water interfaces in the mM to μ M concentration regime. We identified the adsorbed compound via its $n-\pi^*$ transition and measured a free energy of adsorption to the silica/water interface of $-42(3)$ kJ/mol at pH 7. This work shows that the ability to track monolayer and submonolayer coverages of pharmaceuticals at solid/liquid interfaces is key to assessing their mobility in the environment. While such surface-specific studies are in principle possible with ATR-FTIR or Raman-based spectroscopies, SHG provides the sensitivity and the real-time capability necessary for making such assessments. We find that the interaction of morantel with silica/water interfaces is fully reversible, indicating a high mobility in silica-rich soil environments. This high mobility could lead to increased interaction of morantel with target organisms, which could respond by increasing their drug resistance. Furthermore, this work indicates that pharmaceuticals discharged into the environment could readily enter the ground water supply of municipal water systems, at which point their removal is challenging.

Chapter 7

Conclusions and Future Directions

7.1 Conclusions

This work demonstrates the utility of second harmonic generation for studying the interactions between environmentally relevant interfaces and a wide array of pollutants, and for obtaining fundamental thermodynamic information about the interface itself. The thermodynamics of the pollutant/interface interaction drive adsorption processes which are critical to regulating pollutant transport, speciation and fate in the environment. Quantitatively describing pollutant binding to environmentally relevant interfaces at appropriate bulk concentrations, under representative flow conditions, and for submonolayer coverages is an important outstanding problem in environmental molecular science. This work addresses that problem, and elucidates how SHG can be used to provide quantitative information for the binding of both metal cations and organic pharmaceutical compounds.

The following sections will present conclusions and environmental implications from each of the specific systems we focused on in this work. To address the scientific question of the behavior of carboxylic acid groups when tethered to a surface, we performed second harmonic studies of organic adlayers at the silica/water interface. We then examined the interaction of the manganese (II) cation and carboxylic acid groups at the silica/water interface to address the interaction between aqueous pollutants and organic adlayers at mineral oxide/water interfaces. Lastly, we studied the interaction between the agricultural antibiotic, morantel, and the bare silica/water interface to address how pollutants bind to the mineral oxide core of many colloidal soil particles.

7.2 Environmental Implications: Carboxylic Acid Groups at the Silica/Water Interface

This work exploited the $\chi^{(3)}$ technique of second harmonic generation to study carboxylic acid groups chemically tethered to the silica/water interface. Changing the pH of the bulk solution flowing past the interface allowed us to titrate the carboxylic acid at the silica/water interface, which showed two pK_a values for the monoprotic acid at the interface, 5.6(2) and 9(1). The molecular origin of the phenomenon is thought to be a hydrogen bonding network which forms at the interface. Carboxylic acid groups involved in the hydrogen bonding network have their protons stabilized by the hydrogen bond, causing the protons to be removed at a higher (more basic) pH. Carboxylic acid groups not involved in a hydrogen bonding interaction, either at edges or defect sites, deprotonate at pH values similar to that of bulk carboxylic acid groups.

The fact that carboxylic acid groups can have pK_a values which shift dramatically compared to pK_a values determined for bulk measurements demonstrates the importance of surface-specific measurements in determining parameters used in modeling environmental systems. Our work shows that for our system, about 99% of the carboxylic acid groups which deprotonate at high pH remain protonated at pH 7. Using pK_a values of bulk carboxylic acids in a pollutant transport model would cause the model to mischaracterize the charge state of the surface in the environment. Additionally, our data show that it is possible for two different carboxylic acid sites to exist at a surface. At a constant bulk pH, it is possible that a soil particle will contain ordered regions of protonated, hydrogen bonded carboxylic acid groups and disordered regions of deprotonated carboxylic acid groups. Therefore, a pollutant which approaches the soil particle may behave differently when interacting with different regions of the surface, depending on the ordering of the local environment.

Additionally, in this work we demonstrate the ability of second harmonic generation to quantitatively determine, with wide dynamic range, thermodynamic and charge state information

for environmentally relevant interfaces. Determining these parameters is important for a molecular view of how and under what bulk conditions binding events happen. Additionally, to understand binding processes at interfaces, it is critical to understand the driving force for adsorption processes, which is the lowering of the interfacial free energy density. Charge screening experiments were used to determine interfacial charge densities for carboxylic acid groups at the silica/water interface which showed that at pH 6.5, approximately 1% of the carboxylic acid groups at the interface were deprotonated. Since SHG has direct access to the interfacial potential, Φ was plotted as a function of bulk pH over 3 orders of magnitude. By using the Lippmann equation, we relate charge density and potential to the free energy density, and we quantitatively determined the free energy over eight orders of magnitude.

7.3 Environmental Implications: Manganese Interacting with Carboxylic Acids

The methods presented in this work for tracking manganese at the water/mineral oxide interface are general in scope. The $\chi^{(3)}$ technique allows us to study analytes using charge as an intrinsic label. We determined the free energy of adsorption (-27.8(3) kJ/mole) for Mn^{2+} binding to carboxylic acid groups at the silica/water interface. Additionally, since SHG allows us to quantitatively determine the interfacial charge density, we calculated the number of manganese ions per square centimeter ($6.2(6) \times 10^{12}$). The relatively low free energy of adsorption indicates that solvation sphere mediated hydrogen bonding interaction may control manganese binding, rather than a direct ion-ion interaction between the deprotonated carboxylic acid groups and the manganese cation.

7.4 Environmental Implications: Morantel

By tracking morantel adsorption to the silica/water interface under flow conditions and in real time, our work indicates that morantel is highly mobile in silica-rich soil environments. We spectroscopically identified morantel at the interface via the $n-\pi^*$ transition. Comparison of the surface spectrum with bulk UV-vis spectroscopy suggests that the electronic transition which gives rise to the resonantly enhanced signal is not affected by sorption to the silica/water interface. By performing isotherm experiments, we determined a free energy of adsorption for morantel of $-42(3)$ kJ/mole, which is consistent with a hydrogen bonding interaction at the interface. Additionally, by varying the polarization of the input laser beam, we calculated an orientation parameter which results in a tilt angle of 43° or greater for morantel adsorbed to the silica/water interface.

7.5 Future directions

This work has outlined the broad scope of SHG for studying environmentally relevant interfaces. Possible future directions include varying the adsorbate, the mineral oxide substrate, or the organic functional group studied. Recent work in the Geiger group is addressing all three of these possible directions; however, current studies are limited because the current experimental geometry requires an optically transparent solid substrate (See Figure 2.3). The fundamental wavelength and the second harmonic pass through the transparent silica substrate. This drawback is significant given that opaque substrates comprise a large segment of environmental interfaces, including iron oxides, calcium phosphates, and manganese oxides.

To perform experiments with an opaque substrate, the experimental setup described previously would need to be modified as shown in Figure 7.1. The laser light will pass through the aqueous phase and reflect off of the substrate. Second harmonic signal is collected and

analyzed similarly to the methods presented in previous chapters. The aqueous solution will be held in a quartz dome sealed to a custom-built Teflon support via a Viton O-ring. The substrate of interest is placed on the Teflon support in the middle of the dome. Aqueous solution can flow in through a hole in the top of the dome, and out through an outlet in the Teflon support. The dome has been constructed by Master Glassblower Earl Morris (ret.) of Georgetown. It is necessary to make the dome from quartz so that the second harmonic signal in the UV is not absorbed.

By using SHG with this experimental setup, it would be possible to study a wide range of analytes on opaque substrates. Although a brief survey of soil will indicate that the vast majority of soil is opaque, a brief list is included here. Opaque silicates, which make up the vast majority of soil, include pyrope ($\text{Mg}_3\text{Al}_2\text{Si}_3\text{O}_{12}$), almandine ($\text{Fe}_3\text{Al}_2\text{Si}_3\text{O}_{12}$), spessartite ($\text{Mn}_3\text{Al}_2\text{Si}_3\text{O}_{12}$). Some of the important non-silica opaque minerals include hematite (Fe_2O_3), barite (BaSO_4), spinel (MgAl_2O_4), dolomite ($\text{CaMg}(\text{CO}_3)_2$), siderite (FeCO_3). Additionally, many clays which consists of alluminasilicates are opaque, including montmorillonite, kaolinite, illite and chlorites. By polishing these substrates until optically flat, and placing them in the middle of the experimental setup outlined above, SHG can be used to probe the interactions between pollutants and opaque environmentally relevant substrates.

This future direction, by complimenting and extending the work outlined previously in this document, will increase the molecular-level understanding of the critical aspects of geochemical systems and address the scientific questions outlined previously. Specifically, this work will increase the accuracy of environmental modeling from the simple K_d model, to more complex models like MUSIC, by informing the parameters they use with surface-specific measurements.

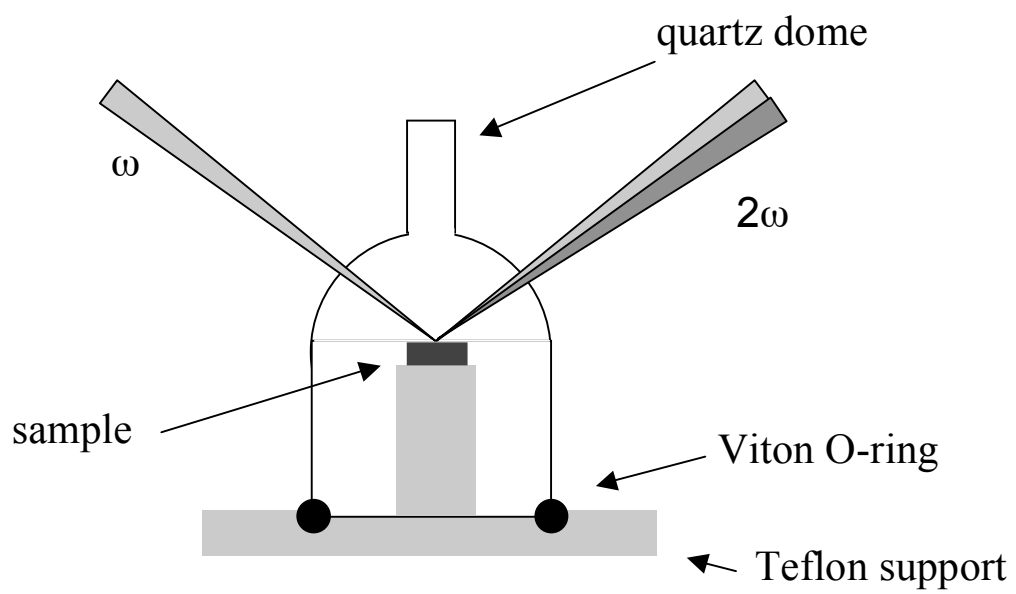


Figure 7.1

The $\chi^{(3)}$ technique provides a method by which opaque substrates can be studied because we can tune the input wavelength so that bulk solution absorption of either the fundamental or second harmonic laser light is not a concern. For example, studying chromate absorption on iron oxide would be challenging with the experimental setup outlined in Chapter 2. Instead of passing the fundamental light through the solid phase it would be necessary to pass the laser light through the aqueous phase because iron oxide is not transparent. Chromate at the silica/water interface has a resonance at 290 nm. Thus, to obtain a resonantly enhanced second harmonic signal, we would tune the input laser light to 580 nm, and collect the second harmonic signal at 290 nm. However, the bulk chromate solution would absorb light at 290 nm, so the SH signal collected would have to be adjusted for the absorption that occurs as the SHG signal passes through the bulk solution. Since chromate is a divalent ion, the $\chi^{(3)}$ technique can be applied to track chromate adsorption to non-transparent substrates similarly to the techniques used for manganese. This approach would allow us to track chromate while tuning the input and second harmonic signal far from any absorbance peaks.

Since the $\chi^{(3)}$ technique allows to study analytes without an electronic transition in the UV-vis region of the spectrum, we can now study any charged species from the periodic table. This allows us to study other d-block elements, including copper, cadmium, nickel, cobalt, or iron. Many radioactive waste products are also known to be charged, so the $\chi^{(3)}$ technique could be used to explore how they interact with environmentally relevant surfaces and help identify their mobility and transport in the environment. Additionally, many of the most redox active mineral oxides in the environment are opaque, including iron and manganese oxides. The experimental geometry in Figure 7.1 allows us to track the interaction between environmental pollutants and many redox-active substrates. Many of the ions of d-block elements have a rich

redox chemistry which we can now track with the $\chi^{(3)}$ technique, allowing for many future studies. Accomplishing this work will move us towards our ultimate goal of understanding how interactions at interfaces control the speciation, transport and ultimate fate of contaminants in the environment by probing chemical reactions at environmentally relevant interfaces.

Chapter 1 References

1. Stumm, W.; Morgan, J. J. *Aquatic Chemistry*. 3rd ed.; Wiley-Interscience: New York, 1996.
2. Finlayson-Pitts, B. J.; Pitts Jr., J. N. *Chemistry of the Upper and Lower Atmosphere*. Academic Press: New York, 2000.
3. Boxall, A. B. A.; Kolpin, D. W.; Halling-Sorensen, B.; Tolls, J. Are veterinary medicines causing environmental risks? *Env. Sci. Technol. A-Pages* **2003**, 286-294.
4. Tolls, J. Sorption of veterinary pharmaceuticals in soils: a review. *Env. Sci. Technol.* **2001**, 35, 3397-3406.
5. Understanding Variation in Partition Coefficient, K_d , Values: Introduction. www.epa.gov/radiation/cleanup/partition.htm (August 18, 2003).
6. Understanding Variation in Partition Coefficient, K_d , Values: Appendix E, Partition Coefficients for Chromium (VI). www.epa.gov/radiation/cleanup/partition.htm
7. Langmuir, D. *Aqueous Environmental Geochemistry*. Prentice-Hall, Inc: New Jersey, 1997.
8. Brown, G. E.; Henrich, V. E.; Casey, W. H.; Clark, D. L.; Eggleston, C.; Felmy, A.; Goodman, D. W.; Graetzel, M.; Maciel, G.; McCarthy, M. I.; Nealson, K. H.; Sverjensky, D. A.; Toney, M. F.; Zachara, J. M. Metal oxide surface and their interactions with aqueous solutions and microbial organisms. *Chem. Rev.* **1999**, 99, 77-174.
9. Bostick, B. C.; Fendorf, S.; Manning, B. A. Arsenite adsorption on galena (PbS) and sphalerite (ZnS). *Geochim. Cosmochim. Acta* **2003**, 67, 895-907.

10. Farquhar, M. L.; Charnock, J. M.; Livens, F. R.; Vaughan, D. J. Mechanisms of arsenic uptake from aqueous solution by interaction with goethite, lepidocrocite, mackinawite, and pyrite: An X-ray absorption spectroscopy study. *Env. Sci. Technol.* **2002**, *36*, 1757-1762.
11. Foster, A. L.; Brown, G. E.; Parks, G. A. X-ray absorption fine structure study of As(V) and Se(IV) sorption complexes on hydrous Mn oxides. *Geochim. Cosmochim. Acta* **2003**, *67*, 1937-1953.
12. Paktunc, D.; Foster, A.; Laflamme, G. Speciation and characterization of arsenic in Ketzka River mine tailings using x-ray absorption spectroscopy. *Environmental Science & Technology* **2003**, *37*, 2067-2074.
13. Smith, P. G.; Koch, I.; Gordon, R. A.; Mandoli, D. F.; Chapman, B. D.; Reimer, K. J. X-ray absorption near-edge structure analysis of arsenic species for application to biological environmental samples. *Environmental Science & Technology* **2005**, *39*, 248-254.
14. Takahashi, Y.; Ohtaku, N.; Mitsunobu, S.; Yuita, K.; Nomura, M. Determination of the As(III)/As(V) ratio in soil by X-ray absorption near-edge structure (XANES) and its application to the arsenic distribution between soil and water. *Analytical Sciences* **2003**, *19*, 891-896.
15. Weckhuysen, B. M.; Wachs, I. E.; Schoonheydt, R. A. Surface chemistry and spectroscopy of chromium in inorganic oxides. *Chemical Reviews* **1996**, *96*, 3327-3349.
16. Nishiyama, K.; Tanaka, Y.; Harada, H.; Yamada, T.; Niwa, D.; Inoue, T.; Homma, T.; Osaka, T.; Taniguchi, I. Adsorption of organic molecules by photochemical reaction on Cl : Si(111) and H : Si(111) evaluated by HREELS. *Surface Science* **2006**, *600*, 1965-1972.
17. Shaikhutdinov, S.; Ritter, M.; Weiss, W. Hexagonal heterolayers on a square lattice: A combined STM and LEED study of FeO(111) on Pt(100). *Physical Review B* **2000**, *62*, 7535-7541.

18. Haes, A. J.; Van Duyne, R. P. A nanoscale optical biosensor: Sensitivity and selectivity of an approach based on the localized surface plasmon resonance spectroscopy of triangular silver nanoparticles. *Journal of the American Chemical Society* **2002**, 124, 10596-10604.
19. Jensen, T. R.; Schatz, G. C.; Van Duyne, R. P. Nanosphere lithography: Surface plasmon resonance spectrum of a periodic array of silver nanoparticles by ultraviolet-visible extinction spectroscopy and electrodynamic modeling. *Journal of Physical Chemistry B* **1999**, 103, 2394-2401.
20. Usher, C. R.; Cleveland, C. A.; Strongin, D. R.; Schoonen, M. A. Origin of oxygen in sulfate during pyrite oxidation with water and dissolved oxygen: An in situ horizontal attenuated total reflectance infrared spectroscopy isotope study. *Environmental Science & Technology* **2004**, 38, 5604-5606.
21. Dubowski, Y.; Vieceli, J.; Tobias, D. J.; Gomez, A.; Lin, A.; Nizkorodov, S. A.; McIntire, T. M.; Finlayson-Pitts, B. J. Interaction of gas-phase ozone at 296 K with unsaturated self-assembled monolayers: A new look at an old system. *Journal of Physical Chemistry A* **2004**, 108, 10473-10485.
22. Gershevit, O.; Sukenik, C. N. In Situ FTIR-ATR Analysis and Titration of Carboxylic Acid-Terminated SAMs. *J. Am. Chem. Soc.* **2004**, 126, 482-483.
23. Chung, Y. W. *Practical Guide to Surface Science and Spectroscopy*. Academic Press: San Diego, 2001.
24. Grassian, V. H. *Environmental Catalysis*. CRC Press: Boca Raton, 2005.
25. Masel, R. I. *Principles of Adsorption and Reaction on Solid Surfaces*. John Wiley and Sons: New York, 1996.

26. Somorjai, G. A. *Introduction to Surface Chemistry and Catalysis*. John Wiley and Sons: New York, 1994.
27. Sposito, G. *The Surface Chemistry of Soils*. Oxford University Press: New York, 1984.
28. Adamson, A. W. *Physical Chemistry of Surfaces*. 5th ed.; John Wiley & Sons: New York, 1990.

Chapter 2 References

1. Boyd, R. W. *Nonlinear Optics*. Academic Press: New York, 1992.
2. Shen, Y. R. *The Principles of Nonlinear Optics*. John Wiley & Sons: New York, 1984.
3. Eienthal, K. B. Liquid interfaces probed by second-harmonic and sum-frequency spectroscopy. *Chem. Rev.* **1996**, 96, 1343-1360.
4. Eienthal, K. B. Second harmonic spectroscopy of aqueous nano- and microparticle interfaces. *Chemical Reviews* **2006**, 106, 1462-1477.
5. Boyd, R. W. *Nonlinear Optics*. second ed.; Academic Press: New York, 2003; p 578.
6. Milonni, P. W. a. E., Joseph H. *Lasers*. Wiley: New York, 1988; p 731.
7. Shen, Y. R. *Principles of Nonlinear Optics*. second ed.; Wiley: New York, 2003; p 563.
8. Moad, A. J.; Simpson, G. J. A unified treatment of selection rules and symmetry relations for sum-frequency and second harmonic spectroscopies. *Journal of Physical Chemistry B* **2004**, 108, 3548-3562.
9. Miranda, P. B.; Du, Q.; Shen, Y. R. Interaction of water with a fatty acid Langmuir film. *Chemical Physics Letters* **1998**, 286, 1-8.
10. Ong, S.; Zhao, X.; Eienthal, K. B. Polarization of water molecules at a charged interface; second harmonic studies of the silica/water interface. *Chem. Phys. Lett.* **1992**, 191, 327-335.
11. Eienthal, K. B.; Liu, Y.; Yan, E.; Zimdars, D.; Dadap, J.; Srivistava, A.; Zhao, X.; Ong, S.; Wang, H. Molecules and charges at the aqueous interface of microscopic particles: Polymer beads, emulsions, semiconductors, and liposomes. *Abstracts of Papers of the American Chemical Society* **1999**, 217, U304-U304.

12. Eiseenthal, K. B. Liquid interfaces probed by second-harmonic and sum-frequency spectroscopy. *Chemical Reviews* **1996**, 96, 1343-1360.
13. Corn, R. M.; Higgins, D. A. Optical 2nd-Harmonic Generation as a Probe of Surface-Chemistry. *Chemical Reviews* **1994**, 94, 107-125.
14. Shen, Y. R. A few selected applications of surface nonlinear optical spectroscopy. *Proceedings of the National Academy of Sciences of the United States of America* **1996**, 93, 12104-12111.
15. Konek, C. T.; Illg, K. D.; Al-Abadleh, H. A.; Voges, A. B.; Yin, G.; Musorrafiti, M. J.; Schmidt, C. M.; Geiger, F. M. Nonlinear Optical Studies of the Agricultural Antibiotic Morantel Interacting with Silica/Water Interfaces. *Journal of the American Chemical Society* **2005**, 127, 15771-15777.
16. Mifflin, A. L.; Gerth, K. A.; Geiger, F. M. Kinetics of chromate adsorption and desorption at fused quartz/water interfaces studied by second harmonic generation. *J. Phys. Chem. A* **2003**, 107, 9620-9627.
17. Higgins, S. R., Stack, A.G., Knauss, K.G., Eggleston, C.M., Jordan, G. Probing molecular-scale adsorption and dissolution-growth processes using nonlinear optical and scanning probe methods suitable for hydrothermal applications. *Geochemical Society* **2002**, Special Publication No. 7, 111.
18. Higgins, S. R.; Stack, A.; Eggleston, C. M. Proton and ligand adsorption at silica- and alumina-water interfaces studied by optical second harmonic generation (SHG). *Mineral. Mag.* **1998**, 62A, 616-617.
19. Stack, A. G.; Higgins, S. R.; Eggleston, C. M. Point of zero charge of a corundum-water interface probed with optical second harmonic generation (SHG) and atomic force microscopy

- (AFM): New approaches to oxide surface charge. *Geochimica Et Cosmochimica Acta* **2001**, 65, 3055-3063.
20. Konek, C. T.; Musorrafiti, M. J.; Al-Abadleh, H. A.; Bertin, P. A.; Nguyen, S. T.; Geiger, F. M. Interfacial Acidities, Charge Densities, Potentials, and Energies of Carboxylic Acid-Functionalized Silica/Water Interfaces Determined by Second Harmonic Generation. *Journal of the American Chemical Society* **2004**, 126, 11754-11755.
21. Mifflin, A. L.; Gerth, K. A.; Weiss, B. M.; Geiger, F. M. Surface studies of chromate binding to fused quartz/water interfaces. *J. Phys. Chem. A* **2003**, 107, 6212-6217.
22. Mifflin, A. L.; Musorrafiti, M. J.; Konek, C. T.; Geiger, F. M. Second Harmonic Generation Phase Measurements of Cr(VI) at a Buried Interface. *Journal of Physical Chemistry B* **2005**, 109, 24386-24390.
23. Petersen, P. B.; Saykally, R. J. Probing the interfacial structure of aqueous electrolytes with femtosecond second harmonic generation spectroscopy. *Journal of Physical Chemistry B* **2006**, 110, 14060-14073.
24. Petersen, P. B.; Saykally, R. J. On the nature of ions at the liquid water surface. *Annual Review of Physical Chemistry* **2006**, 57, 333-364.
25. Petersen, P. B.; Saykally, R. J. Adsorption of ions to the surface of dilute electrolyte solutions: The Jones-Ray effect revisited. *Journal of the American Chemical Society* **2005**, 127, 15446-15452.
26. Benderskii, A. V.; Eissenthal, K. B. Aqueous solvation dynamics at the anionic surfactant air/water interface. *J. Phys. Chem. B* **2001**, 105, 6698-6703.

27. Benderskii, A. V.; Eissenthal, K. B. Dynamical time scales of aqueous solvation at negatively charged lipid/water interfaces. *Journal of Physical Chemistry A* **2002**, 106, 7482-7490.
28. Shang, X.; Benderskii, A. V.; Eissenthal, K. B. Ultrafast Solvation Dynamics at Silica/Liquid Interfaces Probed by Time-Resolved Second Harmonic Generation. *J. Phys. Chem. B* **2001**, 105, 11578-11585.
29. Voges, A. B.; Al-Abadleh, H. A.; Musorrafiti, M. J.; Bertin, P. A.; Nguyen, S. T.; Geiger, F. M. Carboxylic Acid- and Ester-Functionalized Siloxane Scaffolds on Glass Studied by Broadband Sum Frequency Generation. *J. Phys. Chem. B.* **2004**, 108, 18675-18682.
30. Voges, A. B.; Al-Abadleh, H. A.; Geiger, F. M. Development of Nonlinear Optical Spectroscopies for Studying Heterogeneous Environmental Catalytic Processes. In *Environmental Catalysis*, Grassian, V. H., Ed. CRC Press: Boca Raton, FL, 2005.
31. Al-Abadleh, H. A.; Mifflin, A. L.; Bertin, P. A.; Nguyen, S. T.; Geiger, F. M. Control of Carboxylic Acid and Ester Groups on Chromium (VI) Binding to Functionalized Fused Silica/Water Interfaces Studied by Second Harmonic Generation. *J. Phys. Chem. B.* **2005**, 109, 9691-9702.
32. Al-Abadleh, H. A.; Mifflin, A. L.; Musorrafiti, M. J.; Geiger, F. M. Kinetic Studies of Chromium (VI) Binding to Carboxylic acid- and Methyl Ester- Functionalized Silica/Water Interfaces Important in Geochemistry. *J. Phys. Chem. B., in press* **2005**.
33. Al-Abadleh, H. A.; Voges, A. B.; Bertin, P. A.; Nguyen, S. T.; Geiger, F. M. Chromium(VI) Binding to Functionalized Silica/Water Interfaces Studied by Nonlinear Optical Spectroscopy. *J. Am. Chem. Soc.* **2004**, 126, 11126-11127.

34. Wasserman, S. R.; Tao, Y. T.; Whitesides, G. M. Structure and Reactivity of Alkylsiloxane Monolayers Formed by Reaction of Alkyltrichlorosilanes on Silicon Substrates. *Langmuir* **1989**, 5, 1074-1087.

Chapter 3 References

1. Brown, G. E.; Foster, A. L.; Ostergren, J. D. Mineral surfaces and bioavailability of heavy metals: A molecular-scale perspective. *Proceedings of the National Academy of Sciences of the United States of America* **1999**, 96, 3388-3395.
2. Evangelou, V. P. *Environmental Soil and Water Chemistry*. John Wiley & Sons: New York, 1998.
3. Voges, A. B.; Al-Abadleh, H. A.; Geiger, F. M. Applications of nonlinear optical techniques for studying heterogeneous systems relevant in the natural environment. *Environmental Catalysis* **2005**, 83-128.
4. Brown, G. E. Surface science - How minerals react with water. *Science* **2001**, 294, 67-69.
5. Brown Jr., G. E.; Foster, A. L.; Ostergren, J. D. Mineral surfaces and bioavailability of heavy metals: a molecular-scale perspective. *Proc. Natl. Acad. Sci. USA* **1999**, 96, 3388-3395.
6. Sutton, R.; Sposito, G. Molecular structure in soil humic substances: The new view. *Environmental Science & Technology* **2005**, 39, 9009-9015.
7. Sagiv, J. ORGANIZED MONOLAYERS BY ADSORPTION .1. FORMATION AND STRUCTURE OF OLEOPHOBIC MIXED MONOLAYERS ON SOLID-SURFACES. *Journal of the American Chemical Society* **1980**, 102, 92-98.
8. Polymeropoulos, E. E.; Sagiv, J. ELECTRICAL-CONDUCTION THROUGH ADSORBED MONOLAYERS. *Journal of Chemical Physics* **1978**, 69, 1836-1847.
9. Holmesfarley, S. R.; Reamey, R. H.; McCarthy, T. J.; Deutch, J.; Whitesides, G. M. Acid-Base Behaviour of Carboxylic-Acid Groups Covalently Attached at the Surface of Polyethylene - the Usefulness of Contact-Angle in Following the Ionization of Surface Functionality. *Langmuir* **1985**, 1, 725-740.

10. Troughton, E. B.; Bain, C. D.; Whitesides, G. M.; Nuzzo, R. G.; Allara, D. L.; Porter, M. D. Monolayer Films Prepared by the Spontaneous Self-Assembly of Symmetrical and Unsymmetrical Dialkyl Sulfides from Solution onto Gold Substrates - Structure, Properties, and Reactivity of Constituent Functional Groups. *Langmuir* **1988**, 4, 365-385.
11. Wasserman, S. R.; Tao, Y. T.; Whitesides, G. M. Structure and Reactivity of Alkylsiloxane Monolayers Formed by Reaction of Alkyltrichlorosilanes on Silicon Substrates. *Langmuir* **1989**, 5, 1074-1087.
12. Mifflin, A. L.; Gerth, K. A.; Geiger, F. M. Kinetics of chromate adsorption and desorption at fused quartz/water interfaces studied by second harmonic generation. *J. Phys. Chem. A* **2003**, 107, 9620-9627.
13. Mifflin, A. L.; Gerth, K. A.; Weiss, B. M.; Geiger, F. M. Surface studies of chromate binding to fused quartz/water interfaces. *J. Phys. Chem. A* **2003**, 107, 6212-6217.
14. Mifflin, A. L.; Musorrafiti, M. J.; Konek, C. T.; Geiger, F. M. Second Harmonic Generation Phase Measurements of Cr(VI) at a Buried Interface. *Journal of Physical Chemistry B* **2005**, 109, 24386-24390.
15. Al-Abadleh, H. A.; Voges, A. B.; Bertin, P. A.; Nguyen, S. T.; Geiger, F. M. Chromium(VI) binding to functionalized silica/water interfaces studied by nonlinear optical spectroscopy. *J. Am. Chem. Soc.* **2004**, 126, 11126-11127.
16. Lide, D. R. *CRC Handbook of Chemistry and Physics*. CRC Press: Boca Raton, 1996.
17. *CRC Handbook of Chemistry and Physics*. 71st ed.; CRC Press: Boston, 1990-1991.
18. Voges, A. B.; Al-Abadleh, H. A.; Musorrafiti, M. J.; Bertin, P. A.; Nguyen, S. T.; Geiger, F. M. Carboxylic Acid- and Ester-Functionalized Siloxane Scaffolds on Glass Studied by Broadband Sum Frequency Generation. *J. Phys. Chem. B* **2004**, 108, 18675-18682.

Chapter 4 References

1. Brown, G. E.; Henrich, V. E.; Casey, W. H.; Clark, D. L.; Eggleston, C.; Felmy, A.; Goodman, D. W.; Gratzel, M.; Maciel, G.; McCarthy, M. I.; Nealson, K. H.; Sverjensky, D. A.; Toney, M. F.; Zachara, J. M. Metal oxide surfaces and their interactions with aqueous solutions and microbial organisms. *Chemical Reviews* **1999**, *99*, 77-174.
2. Sutton, R.; Sposito, G. Molecular structure in soil humic substances: The new view. *Environmental Science & Technology* **2005**, *39*, 9009-9015.
3. Ong, S.; Zhao, X.; Eiseenthal, K. B. Polarization of water molecules at a charged interface; second harmonic studies of the silica/water interface. *Chem. Phys. Lett.* **1992**, *191*, 327-335.
4. Yan, E. C. Y.; Liu, Y.; Eiseenthal, K. B. New method for determination of surface potential of microscopic particles by second harmonic generation. *J. Phys. Chem. B* **1998**, *102*, 6331-6336.
5. Miranda, P. B.; Du, Q.; Shen, Y. R. Interaction of water with a fatty acid Langmuir film. *Chemical Physics Letters* **1998**, *286*, 1-8.
6. Chapman, D. L. A Contribution to the Theory of Electrocapillarity. *Philosophical Magazine* **1913**, *25*, 6.
7. Gouy, G. L. Constitution of the Electric Charge at the Surface of an Electrolyte. *Journal Physique* **1910**, *9*, 10.
8. Adamson, A. W. *Physical Chemistry of Surfaces*. 5th ed.; John Wiley & Sons: New York, 1990.

9. Zhao, X. L.; Ong, S. W.; Eisenthal, K. B. Polarization of Water-Molecules at a Charged Interface - 2nd Harmonic Studies of Charged Monolayers at the Air-Water-Interface. *Chemical Physics Letters* **1993**, 202, 513-520.
10. Zhao, X. L.; Ong, S. W.; Wang, H. F.; Eisenthal, K. B. New Method for Determination of Surface Pk(a) Using 2nd-Harmonic Generation. *Chemical Physics Letters* **1993**, 214, 203-207.
11. Zhao, X.; Ong, S.; Wang, H.; Eisenthal, K. B. New method for determination of surface pKa using second harmonic generation. *Chem. Phys. Lett.* **1993**, 214, 203-207.
12. Zhao, X.; Subrahmanyam, S.; Eisenthal, K. B. Determination of pKa at the air/water interface by second harmonic generation. *Chem. Phys. Lett.* **1990**, 171, 558-562.
13. Zhao, X. L.; Subrahmanyam, S.; Eisenthal, K. B. Determination of Pka at the Air-Water-Interface by 2nd Harmonic-Generation. *Chemical Physics Letters* **1990**, 171, 558-562.
14. Liu, Y.; Yan, C. Y.; Zhao, X. L.; Eisenthal, K. B. Surface potential of charged liposomes determined by second harmonic generation. *Langmuir* **2001**, 17, 2063-2066.
15. Konek, C. T.; Musorrafiti, M. J.; Al-Abadleh, H. A.; Bertin, P. A.; Nguyen, S. T.; Geiger, F. M. Interfacial Acidities, Charge Densities, Potentials, and Energies of Carboxylic Acid-Functionalized Silica/Water Interfaces Determined by Second Harmonic Generation. *Journal of the American Chemical Society* **2004**, 126, 11754-11755.
16. Hu, K.; Bard, A. J. Use of Atomic Force Microscopy for the Study of Surface Acid-Base Properties of Carboxylic Acid-Terminated Self-Assembled Monolayers. *Langmuir* **1997**, 13, 5114-5119.
17. Rick Van Duyne, personal communication
18. Lippmann, G. Relations Entre les Phenomenes Electriques et Capillaires. *Annales de Chimie (Physique)* **1875**, 5.

19. Zhang, P. C.; Keleshian, A. M.; Sachs, F. Voltage-induced membrane movement. *Nature* **2001**, 413, 428-432.
20. Ege, S. N. *Organic Chemistry: Structure and Reactivity. 4th Ed.* Houghton Mifflin Company: Boston, 1999; p 1148 pp.
21. Wasserman, S. R.; Tao, Y. T.; Whitesides, G. M. Structure and Reactivity of Alkylsiloxane Monolayers Formed by Reaction of Alkyltrichlorosilanes on Silicon Substrates. *Langmuir* **1989**, 5, 1074-1087.
22. Gershevit, O.; Sukenik, C. N. In Situ FTIR-ATR Analysis and Titration of Carboxylic Acid-Terminated SAMs. *J. Am. Chem. Soc.* **2004**, 126, 482-483.
23. Jacobsen, J. J.; Johnson, K.; Moore, J. W.; Trammell, G. Chemistry comes alive!, Volume 5 - Abstract of special issue 29, a CD-ROM for organic and biochemistry. *Journal of Chemical Education* **2001**, 78, 423-424.
24. Stefan, I. C.; Scherson, D. A. Attenuated total reflection infrared studies of bilayers self-assembled onto a germanium prism. *Langmuir* **2000**, 16, 5945-5948.
25. Kane, V.; Mulvaney, P. Double-Layer Interactions between Self-Assembled Monolayers of ω -Mercaptoalkanoic Acids on Gold Surfaces. *Langmuir* **1998**, 14, 3303-3311.
26. Wang, J.; Frostman, L. M.; Ward, M. D. Self-Assembled Thiol Monolayers with Carboxylic Acid Functionality: Measuring pH-Dependent Phase Transitions with the Quartz Crystal Microbalance. *J. Phys. Chem.* **1992**, 96, 5224-5228.
27. Vezenov, D. V.; Noy, A.; Rozsnyai, L. F.; Lieber, C. M. Force Titrations and Ionization State Sensitive Imaging of Functional Groups in Aqueous Solutions by Chemical Force Microscopy. *J. Am. Chem. Soc.* **1997**, 119, 2006-2015.

28. Sugihara, K.; Shimazu, K.; Uosaki, K. Electrode Potential Effect on the Surface pKa of a Self-Assembled 15-Mercaptohexadecanoic Acid Monolayer on Gold/Quartz Crystal Microbalance Electrode. *Langmuir* **2000**, 16, 7101-7105.

Chapter 5 References

1. Du, J. Health Effects Support Document for Manganese. In Environmental Protection Agency - Office of Water, H. a. E. C. D., Ed. Environmental Protection Agency: 2003.
2. Air Quality Guidelines for Europe. In Second ed.; Europe, W. H. O. R. O. f., Ed. World Health Organization: 2000; Vol. 91.
3. Manganese in Minnesota's Groundwater. In Agency, M. P. C., Ed. Minnesota Pollution Control Agency: 1999; p 2.
4. Ayoko, G. A.; Singh, K.; Balarea, S.; Kokot, S. Exploratory multivariate modeling and prediction of the physico-chemical properties of surface water and groundwater. *Journal of Hydrology* **2007**, 336, 115-124.
5. Upadhyay, A. K.; Gupta, K. K.; Sircar, J. K.; Deb, M. K.; Mundhara, G. L. Dominance of lithogenic effect for nickel, cobalt, chromium and mercury as found in freshly deposited sediments of the river Subernarekha, India. *Environmental Geology* **2007**, 51, 1447-1453.
6. Ridge, J. P.; Lin, M.; Larsen, E. I.; Fegan, M.; McEwan, A. G.; Sly, L. I. A multicopper oxidase is essential for manganese oxidation and laccase-like activity in *Pedomicrobium* sp ACM 3067. *Environmental Microbiology* **2007**, 9, 944-953.
7. Miyata, N.; Tani, Y.; Maruo, K.; Tsuno, H.; Sakata, M.; Iwahori, K. Manganese(IV) oxide production by *Acremonium* sp strain KR21-2 and extracellular Mn(II) oxidase activity. *Applied and Environmental Microbiology* **2006**, 72, 6467-6473.
8. Tebo, B. M.; Bargar, J. R.; Clement, B. G.; Dick, G. J.; Murray, K. J.; Parker, D.; Verity, R.; Webb, S. M. Biogenic manganese oxides: Properties and mechanisms of formation. *Annual Review of Earth and Planetary Sciences* **2004**, 32, 287-328.

9. Miyata, N.; Tani, Y.; Iwahori, K.; Soma, M. Enzymatic formation of manganese oxides by an Acremonium-like hyphomycete fungus, strain KR21-2. *Fems Microbiology Ecology* **2004**, *47*, 101-109.
10. Saratovsky, I.; Wightman, P. G.; Pasten, P. A.; Gaillard, J. F.; Poepelmeier, K. R. Manganese oxides: Parallels between abiotic and biotic structures. *Journal of the American Chemical Society* **2006**, *128*, 11188-11198.
11. Konek, C. T.; Musorrafiti, M. J.; Voges, A. B.; Geiger, F. M. Tracking the interaction of transition metal ions with environmental interfaces using second harmonic generation. In *Adsorption of Metals in Geomedia II*, Barnett, M. a. K., Douglass, Ed. Elsevier: New York, 2007; Vol. 2.
12. Konek, C. T.; Musorrafiti, M. J.; Al-Abadleh, H. A.; Bertin, P. A.; Nguyen, S. T.; Geiger, F. M. Interfacial Acidities, Charge Densities, Potentials, and Energies of Carboxylic Acid-Functionalized Silica/Water Interfaces Determined by Second Harmonic Generation. *Journal of the American Chemical Society* **2004**, *126*, 11754-11755.
13. Salafsky, J. S.; Eisenthal, K. B. Protein adsorption at interfaces detected by second harmonic generation. *J. Phys. Chem. B* **2000**, *104*, 7752-7755.
14. Atkins, P. W. *Physical Chemistry*. 6th ed.; Oxford University Press: 1998.
15. Adamson, A. W. *Physical Chemistry of Surfaces*. 5th ed.; John Wiley & Sons: New York, 1990.
16. Mifflin, A. L.; Gerth, K. A.; Geiger, F. M. Kinetics of chromate adsorption and desorption at fused quartz/water interfaces studied by second harmonic generation. *J. Phys. Chem. A* **2003**, *107*, 9620-9627.

17. Mifflin, A. L.; Gerth, K. A.; Weiss, B. M.; Geiger, F. M. Surface studies of chromate binding to fused quartz/water interfaces. *J. Phys. Chem. A* **2003**, 107, 6212-6217.
18. Mifflin, A. L.; Musorrafiti, M. J.; Konek, C. T.; Geiger, F. M. Second Harmonic Generation Phase Measurements of Cr(VI) at a Buried Interface. *Journal of Physical Chemistry B* **2005**, 109, 24386-24390.
19. Konek, C. T.; Illg, K. D.; Al-Abadleh, H. A.; Voges, A. B.; Yin, G.; Musorrafiti, M. J.; Schmidt, C. M.; Geiger, F. M. Nonlinear Optical Studies of the Agricultural Antibiotic Morantel Interacting with Silica/Water Interfaces. *Journal of the American Chemical Society* **2005**, 127, 15771-15777.

Chapter 6 References

1. Langmuir, D. *Aqueous Environmental Geochemistry*. Prentice-Hall, Inc: New Jersey, 1997.
2. Dean, C. Drugs Are in the Water. Does it Matter? *The New York Times* 2007.
3. Barringer, F. A Plan to Curb Farm-to-Watershed Pollution of Chesapeake Bay. *The New York Times* 2007.
4. Mellon, M.; Benbrook, C.; Benbrook, K. L. *Hogging it: Estimates of antimicrobial abuse in livestock*. Union of Concerned Scientists: Cambridge, MA, 2001.
5. Ferber, D. Superbugs on the Hoof? *Science* **2000**, 288, 792-794.
6. Molbak, K.; Baggesen, D. L.; Aarestrup, F. M.; Ebbesen, J. M.; Engberg, J.; Frydendahl, K.; Gerner-Smidt, P.; Petersen, A. M.; Wegener, H. C. An outbreak of multidrug-resistant, quinolone-resistant *Salmonella enterica* serotype typhimurium DT104. *New England Journal of Medicine* **1999**, 341, 1420-1425.
7. Matson, P. A.; Parton, W. J.; G., P. A.; Swift, M. J. Agricultural Intensification and Ecosystem Properties. *Science* **1997**, 277, 504-509.
8. Vorosmarty, C. J.; Green, P.; Salisbury, J.; Lammers, R. B. Global Water Resources: Vulnerability from Climate Change and Population Growth. *Science* **2000**, 289, 284-288.
9. *Environmental Impact Statement*; Pfizer Incorporated New York: Lee's Summit, MO, 1994; pp 1-93.
10. *Clarke's Analysis of Drugs and Poisons*. 3rd ed.; Pharmaceutical Press: London, 2003.
11. Boxall, A. B. A.; Kolpin, D. W.; Halling-Sorensen, B.; Tolls, J. Are veterinary medicines causing environmental risks? *Env. Sci. Technol. A-Pages* **2003**, 286-294.

12. Melancon, J. J. A Review of Morantel Citrate. http://us.merial.com/Pdf/page_pdf/A_Review_of_Morantel_Tartrate.pdf (March 1, 2005).
13. Tornoe, C.; Bai, D.; Holdendye, L.; Abramson, S. N.; Sattelle, D. B. ACTIONS OF NEUROTOXINS (BUNGAROTOXINS, NEOSURUGATOXIN AND LOPHOTOXINS) ON INSECT AND NEMATODE NICOTINIC ACETYLCHOLINE-RECEPTORS. *Toxicon* **1995**, 33, 411-424.
14. Acrylic Acid Hazard Summary. <http://www.epa.gov/ttn/atw/hlthef/acrylica.html>
15. Schmitt, H.; van Beelen, P.; Tolls, J.; van Leeuwen, C. L. Pollution-Induced Community Tolerance of Soil Microbial Communities Caused by the Antibiotic Sulfachloropyridazine. *Env. Sci. Technol.* **2004**, 38, 1148-1153.
16. Tolls, J. Sorption of veterinary pharmaceuticals in soils: a review. *Env. Sci. Technol.* **2001**, 35, 3397-3406.
17. Understanding Variation in Partition Coefficient, K_d , Values: Introduction. www.epa.gov/radiation/cleanup/partition.htm (August 18, 2003).
18. Understanding Variation in Partition Coefficient, K_d , Values: Appendix E, Partition Coefficients for Chromium (VI). www.epa.gov/radiation/cleanup/partition.htm
19. Al-Abadleh, H. A.; Mifflin, A. L.; Bertin, P. A.; Nguyen, S. T.; Geiger, F. M. Control of Carboxylic Acid and Ester Groups on Chromium (VI) Binding to Functionalized Fused Silica/Water Interfaces Studied by Second Harmonic Generation. *J. Phys. Chem. B.* **2005**, 109, 9691-9702.
20. Brown, G. E.; Henrich, V. E.; Casey, W. H.; Clark, D. L.; Eggleston, C.; Felmy, A.; Goodman, D. W.; Graetzel, M.; Maciel, G.; McCarthy, M. I.; Nealson, K. H.; Sverjensky, D. A.;

Toney, M. F.; Zachara, J. M. Metal oxide surface and their interactions with aqueous solutions and microbial organisms. *Chem. Rev.* **1999**, *99*, 77-174.

21. Stumm, W.; Morgan, J. J. *Aquatic Chemistry*. 3rd ed.; Wiley-Interscience: New York, 1996.

22. Sposito, G. *The Surface Chemistry of Soils*. Oxford University Press: New York, 1984.

23. Adamson, A. W. *Physical Chemistry of Surfaces*. 5th ed.; John Wiley & Sons: New York, 1990.

24. Masel, R. I. *Principles of adsorption and reaction on solid surfaces*. John Wiley & Sons: New York, 1996.

25. Bostick, B. C.; Fendorf, S.; Manning, B. A. Arsenite adsorption on galena (PbS) and sphalerite (ZnS). *Geochim. Cosmochim. Acta* **2003**, *67*, 895-907.

26. Farquhar, M. L.; Charnock, J. M.; Livens, F. R.; Vaughan, D. J. Mechanisms of arsenic uptake from aqueous solution by interaction with goethite, lepidocrocite, mackinawite, and pyrite: An X-ray absorption spectroscopy study. *Env. Sci. Technol.* **2002**, *36*, 1757-1762.

27. Foster, A. L.; Brown, G. E.; Parks, G. A. X-ray absorption fine structure study of As(V) and Se(IV) sorption complexes on hydrous Mn oxides. *Geochim. Cosmochim. Acta* **2003**, *67*, 1937-1953.

28. Paktunc, D.; Foster, A.; Laflamme, G. Speciation and characterization of arsenic in Ketza River mine tailings using x-ray absorption spectroscopy. *Environmental Science & Technology* **2003**, *37*, 2067-2074.

29. Smith, P. G.; Koch, I.; Gordon, R. A.; Mandoli, D. F.; Chapman, B. D.; Reimer, K. J. X-ray absorption near-edge structure analysis of arsenic species for application to biological environmental samples. *Environmental Science & Technology* **2005**, *39*, 248-254.

30. Takahashi, Y.; Ohtaku, N.; Mitsunobu, S.; Yuita, K.; Nomura, M. Determination of the As(III)/As(V) ratio in soil by X-ray absorption near-edge structure (XANES) and its application to the arsenic distribution between soil and water. *Analytical Sciences* **2003**, 19, 891-896.
31. Weckhuysen, B. M.; Wachs, I. E.; Schoonheydt, R. A. Surface chemistry and spectroscopy of chromium in inorganic oxides. *Chemical Reviews* **1996**, 96, 3327-3349.
32. Uray, G.; Verdino, P.; Belaj, F.; Kappe, C. O.; Fabian, W. M. F. Absolute Configuration in 4-Alkyl- and 4-Aryl-3,4-dihydro-2(1H)-pyrimidones: A Combined Theoretical and Experimental Investigation. *J. Org. Chem.* **2001**, 66, 6685-6694.
33. Jug, K.; Hahn, G. Properties of excited states of aromatic rings containing nitrogen. *J. Comp. Chem.* **1983**, 4, 410-418.
34. Skoog, D. A. *Principles of Instrumental Analysis*. Fifth ed.; Harcourt: Crawfordsville, MD, 1998.
35. *Morantel And Pyrantel Drug-Related Metabolites*. US Department of Agriculture Food Safety and Inspection Service: Athens, GA, 1991.
36. Heinz, T. F. Second-Order Nonlinear Optical Effects at Surfaces and Interfaces. In *Nonlinear Surface Electromagnetic Phenomena*, Ponath, H.-E.; Stegeman, G. I., Eds. Elsevier Publishers: 1991.
37. Hicks, J. M.; Kemnitz, K.; Eisenthal, K. B.; Heinz, T. F. Studies of liquid surfaces by second harmonic generation. *J. Phys. Chem.* **1986**, 90, 560-562.
38. Simpson, G. J.; Rowlen, K. L. Orientation-insensitive methodology for second harmonic generation. 1. theory. *Anal. Chem.* **2000**, 72, 3399-3406.

39. Simpson, G. J.; Rowlen, K. L. Orientation-insensitive methodology for second harmonic generation. 2. Application to adsorption isotherm and kinetics measurements. *Anal. Chem.* **2000**, *72*, 3407-3411.
40. Simpson, G. J.; Westerbuhr, S. G.; Rowlen, K. L. Molecular Orientation and Angular Distribution Probed by Angle-Resolved Absorbance and Second Harmonic Generation. *Analytical Chemistry* **2000**, *72*, 887-898.
41. Musorrafiti, M. Nonlinear optical studies of model environmental interfaces. Northwestern University, Evanston, IL, 2007.
42. Mifflin, A. L.; Gerth, K. A.; Geiger, F. M. Kinetics of chromate adsorption and desorption at fused quartz/water interfaces studied by second harmonic generation. *J. Phys. Chem. A* **2003**, *107*, 9620-9627.

About the Author

Christopher Konek was raised in Allentown, Pennsylvania, where he attended Allentown Central Catholic High School. Chris went on to study at Cornell University, earning a Bachelor of Science in Chemical Engineering in May 2002. His undergraduate work at Cornell included research in inorganic solid state chemistry with Professor Stephen Lee as part of a project to understand how the Fibonacci sequence might play a role in determining the stoichiometry of γ -brass phases. Chris' interest in the environmental chemistry led him to his work in studying pollutant binding with Dr. Franz Geiger at Northwestern University. Chris received the L. Carrol King award for his work as a teaching assistant. Throughout his years at Northwestern, Chris devoted time to teaching science lessons for young students in the Chicago Public School system and to serving as an executive board member for a local community service organization.